REPUBLIC OF TURKEY
YILDIZ TECHNICAL UNIVERSITY
GRADUATE SCHOOL OF NATURAL AND APPLIED SCIENCES

ANALYSES AND ASSESSMENTS OF THREE RENEWABLE ENERGY BASED INTEGRATED SYSTEMS FOR MULTIGENERATION

ARAS KARAPEKMEZ

MSc. THESIS
DEPARTMENT OF MECHANICAL ENGINEERING
PROGRAM OF THERMODYNAMICS AND HEAT TRANSFER

ADVISER
PROF. DR. IBRAHIM DINCER

ISTANBUL, 2018

REPUBLIC OF TURKEY
YILDIZ TECHNICAL UNIVERSITY
GRADUATE SCHOOL OF NATURAL AND APPLIED SCIENCES

ANALYSES AND ASSESSMENTS OF THREE RENEWABLE ENERGY BASED INTEGRATED SYSTEMS FOR MULTIGENERATION

A thesis submitted by ARAS KARAPEKMEZ in partial fulfillment of the requirements for the degree of **MASTER OF SCIENCE** is approved by the committee on 25/10/2018 in Department of Mechanical Engineering, Thermodynamics and Heat Transfer Program.

Thesis Adviser

Prof. Dr. Ibrahim Dincer

Yildiz Technical University

Approved by the Examining Committee

Prof. Dr. Ibrahim Dincer

Yildiz Technical University   _____

Dr. Nader Javani

Yildiz Technical University   _____

Prof. Dr. Adnan Midilli

Recep Tayyip Erdoğan University   _____

ACKNOWLEDGEMENTS

Firstly, I would like to express my sincerest gratitude to my advisor Prof. Dr. Ibrahim Dincer for the continuous support during my study and related research, for his patience, motivation, kind spirit and immense knowledge. Secondly, I would like to remark that I have significantly broaden my own horizon in the field of energy by means of his guidance. Therefore, I am grateful to my esteemed professor and supervisor.

Also, I would like to thank Assistant Prof. Nader Javani for his help in course studies and for his motivation and support. I feel myself lucky to have such an opportunity to work with them.

Furthermore, I would like to acknowledge the support provided by the Scientific Research Projects Council of Yildiz Technical University for the financial support which gave an opportunity to participate several conferences.

October 2018

Aras KARAPEKMEZ

TABLE OF CONTENTS

LIST OF SYMBOLS

α	Thermal diffusivity (m^2/s)
A_a	Collector aperture area (m^2)
A_s	Heat transfer surface area (m^2)
b	Distance between the charging and discharging pipes (m)
Bi	Biot number
C_p	Specific heat (kJ/kgK)
$C_{pl,av}$	Average specific heat of the liquid phase (kJ/kgK)
$C_{ps,av}$	Average specific heat of the solid phase (kJ/kgK)
c_{rock}	Specific heat of the packed rock (kJ/kgK)
D	Inner diameter of the pipe (m)
ex	Specific exergy (kJ/kg)
ex_{ch}	Chemical exergy (kJ/kmol)
ex^o_{ch}	Standard chemical exergy (kJ/kmol)
ex_{ph}	Physical exergy (kJ/kg)
$\dot{E}$	Energy transfer rate (kW)
$\dot{E}x_d$	Exergy destruction rate (kW)
f	Friction factor
g	Gravitational acceleration (m/s^2)
h	Specific enthalpy (kJ/kg)
h_c	Convection heat transfer coefficient of the charging period (W/m^2K)
h_d	Convection heat transfer coefficient of the discharging period (W/m^2K)
h_{na}	Natural heat transfer coefficient (W/m^2K)
$\bar{h}^o_f$	Enthalpy of formation (kJ/kmol)
H	Length of the packed bed system (m)
I_{av}	Average hourly solar radiation (MJ/m^2h)
J	Bessel function
k	Thermal conductivity (W/mK)
l_c	Aperture length (m)
L_c	Characteristic length (m)
LHV	Lower heating value (kJ/kg)
m	Mass (kg)
$\dot{m}$	Mass flow rate (kg/s)
$n_{collector}$	The number of collectors
$\dot{n}$	Molar flow rate (kmol/s)
Nu	Nusselt number
P	Pressure (kPa)
Pr	Prandtl number
r	Radius (m)

R	Radius of the packed bed system (m)
Ra	Rayleigh number
Re	Reynolds number
s	Specific entropy (kJ/kgK)
$\dot{S}_{gen}$	Entropy generation rate (kW/K)
$t_{charging}$	Charging period (h)
$t_{discharging}$	Discharging period (h)
$t_{storing}$	Storing period (h)
t	Time (hour)
T	Temperature (K)
v_{air}	Kinematic viscosity of air (m^2/s)
V	Volume (m^3)
Q	Thermal energy (kJ)
$\dot{Q}$	Heat transfer rate (kW)
χ	The constant of wood
$\dot{W}$	Work rate (kW)
w_c	Width of the collector (m)
z	Mass fraction

Greek letters

η	Energy efficiency
ψ	Exergy efficiency
γ$_c$	Reflection rate
β	Volume expansion coefficient (1/K)
ρ	Density (kg/m^3)
ꚍ	Dimensionless time

Subscripts

av	Average
b	Boundary
ch	Chemical
cs	Combustible substances
db	Dry biomass
in	Inlet
ir	Initial properties of the rock
out	Outlet
p	Product
ph	Physical
r	Reactant
s	Surface
wb	Wet biomass
wf	Wet fuel

Superscripts

Geo	Geothermal

LIST OF ABBREVIATIONS

A-CAES	Adiabatic compressed air energy storage
CAES	Compressed air energy storage
CCHP	Combined cooling, heating and power
CCS	Carbon capture and storage
CFB	Circulating fluidized bed
COP	The coefficient of performance
EES	Engineering equation solver
ER	Equivalence ratio
HHV	Higher heating value
HP	High pressure
HTH-CAES	High temperature hybrid compressed air energy storage
LHV	Lower heating value
LP	Low pressure
MEA	Membrane exchange assembly
NCG	Non condensable gases
ORC	Organic Rankine cycle
PBTES	Packed bed thermal energy storage
PCM	Phase change material
PEM	Proton exchange membrane
PHES	Pumped hydro energy storage
PTC	Parabolic trough collector
PV	Photovoltaic
RES	Renewable energy sources
S-CAES	Solar and compressed air energy storage
SEMS	Superconducting magnetic energy storage
SEACS	Single effect absorption cooling system
TES	Thermal energy storage

LIST OF FIGURES

LIST OF TABLES

ABSTRACT

ANALYSES AND ASSESSMENTS OF THREE RENEWABLE ENERGY BASED INTEGRATED SYSTEMS FOR MULTIGENERATION

Aras KARAPEKMEZ

Department of Mechanical Engineering

MSc. Thesis

Adviser: Prof. Dr. Ibrahim Dincer

The modern world depends on the fossil fuel consumption as a primary energy source, and this is especially obvious in all industrialized countries. Due to the resource depletion and non-sustainable resources, fossil fuels are not capable of compensating the growing energy needs. In addition, the easily extractable fossil fuels are facing an increase in their prices. It is worth mentioning that greenhouse gases (mainly CO_2) have been accumulated in the atmosphere by burning fossil fuels. Therefore, recently scientific research and academic studies as well as energy policies have been focused to find a permanent solution for the environmental issues by utilizing from the non-polluting resources such as renewable energy and hydrogen. Furthermore, one other way to reduce the greenhouse gases emissions is to design the energy systems in a more effective manner by producing multiple useful commodities from the system. Therefore, one of the main goals of the thesis is to design three different types of renewable based energy systems which provide higher energy and exergy efficiencies by producing electricity, heating, cooling, hot domestic water and hydrogen outputs, as useful outputs.

One of the most important enviromental issues related to the using geothermal operating fluids to generate electricity is non-condensable gases (NCG) emissions. Hydrogen sulfide (H_2S), which is one of these gases, has many adverse effects on the environment and human body. Therefore, another objective of the present study is to reduce the hydrogen sulfide emissions in the geothermal power plants. For this purpose, an AMIS (AMIS® - acronym for "Abatement of Mercury and Hydrogen Sulfide" in Italian language) unit and an electrolyzer system are integrated to the presently developed systems. In this way, not only the negative effects of hydrogen sulfide are reduced, but also hydrogen is generated as a clean fuel which has a vast potential to replace fossil fuels.

To accomplish the specific objectives and evaluate the newly developed systems and their performance both energetically and exergetically, a detailed thermodynamic analysis is performed by using Engineering Equation Solver (EES) software. The results show that overall energy and exergy efficiencies for the studied systems becomes 67.95% and 60.94%, respectively. In addition, hydrogen sulfide emissions are reduced by 738.8 g/s, while the inlet mass flow rate of geothermal fluid is 60 kg/s. Also 6.234 MW additional power can be produced through hydrogen fuel from the geothermal power plants.

Keywords: Biomass, Efficiency, Energy, Exergy, Geothermal, Hydrogen, Hydrogen Sulfide, Solar, Wind

YILDIZ TECHNICAL UNIVERSITY

GRADUATE SCHOOL OF NATURAL AND APPLIED SCIENCES

ÖZET

ÇOKLU ÜRETİM İÇİN YENİLENEBİLİR ENERJİ KAYNAKLI ÜÇ ENTEGRE SİSTEMİN ANALİZ VE DEĞERLENDİRİLMESİ

Aras KARAPEKMEZ

Makine Mühendisliği Anabilim Dalı

Yüksek Lisans Tezi

Tez Danışmanı: Prof. Dr. İbrahim Dinçer

Günümüzde dünya birincil enerji kaynağı olarak fosil yakıtların kullanımına bağımlıdır ve bu durum özellikle tüm sanayileşmiş ülkelerde gözlemlenmektedir. Fosil yakıtların sürdürülebilir olmaması ve rezervlerin tükeniyor olmasından dolayı, fosil kaynaklar büyüyen enerji ihtiyaçlarını dengeleyebilecek potansiyele sahip değildirler. Buna ilaveten, kolay çıkartılabilen fosil yakıtların fiyatlarında artış meydana gelmektedir. Fosil yakıtların yakılmasıyla sera gazlarının (özellikle CO_2) atmosferde biriktiğine değinmek dikkate değer bir konudur. Bu yüzden, son zamanlarda enerji politikalarının yanı sıra bilimsel araştırma ve akademik çalışmalar da, yenilenebilir enerji ve hidrojen gibi çevreyi kirletmeyen kaynakları kullanarak çevresel sorunlara kalıcı bir çözüm bulmaya odaklanmıştır. Ayrıca, sera gazı emisyonlarının azaltılması için izlenecek bir başka yol ise enerji sistemlerini, sistemlerden çeşitli sayıda faydalı ürünün elde edilebileceği daha verimli bir tutum ile tasarlamaktır. Bu yüzden, bu tezin ana amaçlarından bir tanesi elektrik, ısıtma, soğutma, sıcak kullanım suyu ve hidrojen çıktılarını üreterek daha yüksek enerji ve ekserji verimliliği sunan üç farklı tipte ki yenilenebilir kaynaklı enerji sistemini tasarlamaktır.

Jeotermal akışkanların kullanılarak güç üretilen sistemler ile ilgili en önemli çevresel sorunlardan bir tanesi yoğuşmayan gazların emisyonudur. Hidrojen sülfür (H_2S) bu gazlardan bir tanesidir ve hem çevre hemde insan bedeni üzerinde birçok zararlı etkiye sahiptir. Bu yüzden, mevcut çalışmanın bir başka hedefi ise jeotermal enerji santrallerinde hidrojen sülfürün emisyonunu azaltmaktır. Bu amaç doğrultusunda, AMIS (AMIS® - İtalyanca'da " Cıva ve Hidrojen Sülfürün azaltılması" anlamına gelen bir kısaltmadır.) ünitesi ve bir elektroliz sistemi geliştirilen sistemlere entegre edilmiştir. Böylelikle, sadece hidrojen sülfürün olumsuz etkileri azaltılmıyor, aynı zamanda temiz bir yakıt olarak hidrojen üretiliyor öyle ki hidrojen fosil yakıtların yerini alma konusunda büyük potansiyele sahiptir. Belirtilen amaçları yerine getirebilmek ve tasarlanan sistemlerin

performanslarını hem enerji hem de ekserji açısından değerlendirebilmek için Engineering Equation Solver (EES) programı kullanılarak detaylı bir termodinamik analiz gerçekleştirilmiştir. Elde edilen sonuçlara göre, enerji ve ekserji verimlerinin incelenen sistemler için %67,95 ve %60,94 değerlerine ulaşmıştır. Buna ilaveten, jeotermal akışkanın kütlesel debisi 60 kg/s iken, hidrojen sülfür emisyonları 738,8 g/s azaltılabilir ve ayrıca jeotermal enerji santrallerinden hidrojen aracılığıyla 6,234 MW ek güç üretilebilir.

Anahtar Kelimeler: Biyokütle, Enerji, Ekserji, Güneş, Hidrojen, Hidrojen Sülfür, Jeotermal, Rüzgar, Verim

---

INTRODUCTION

1.1 Literature Review

The recent era depends mainly on the deployment use of fossil fuel as a primary energy source. This is more pronounced in all industrialized countries. On the one hand, the reserves of fossil fuels have been decreasing day by day and it is predicted that they will be no longer available in the next century. On the other hand, the demand in energy production is rising depending on the population growth rate and developing industrial applications. Moreover, it is undeniable that fossil fuels have many adverse effects on the environment since they emit relatively higher amounts greenhouse gases (mainly CO_2) which trigger the global warming. Therefore, nowadays more and more scientists and politicians touch on the importance of renewable energy sources and hydrogen in order to create a sustainable energy future. Hydrogen, has no undesirable environmental effects and includes high energy density which makes it a highly valuable resource for the forthcoming energy needs [1]. In this section, the literature review is classified based on the type of resources, systems and technologies as follows:

1.1.1 Renewable Based Multigeneration Systems

Al-Ali et al. [2] suggested a solar and geothermal based system for multigeneration of electrical power, space heating, cooling, domestic hot water and heat for industrial applications. Detailed thermodynamic analyses were conducted for single generation, cogeneration, trigeneration and multigeneration systems through energy and exergy approaches in order to show the performance of each system and to compare the results. The energy and exergy efficiencies were determined to be 16.4% and 26.2% for single generation system, respectively. However, while various useful commodities are obtained

from the system, the energy and exergy efficiencies reached to 78% and 36.6%, respectively. Bicer et al. [3] suggested a novel solar and geothermal based combined system for hydrogen production. The system includes PV modules for the purpose of heating, water heating and also hydrogen production and benefited from geothermal energy sources in order to obtain electrical power, cooling and again hydrogen production. In order to calculate and evaluate the system performance, first and second laws of thermodynamics are implemented to each component of the proposed system. As a result, overall energy and exergy efficiencies of the multigeneration system were found to be 10.8% and 46.3%, respectively while geothermal water temperature is 210 °C. Akrami et al. [4] proposed a geothermal based multi-objective energy system in order to generate electrical power, heating, cooling and hydrogen, simultaneously. The system includes an Organic Rankine Cycle (ORC), domestic water heater, a single effect absorption cooling system and water electrolyzer. Detailed energy and exergy analyses of the system were made as well as exergoeconomic analyses. In addition, the effects of some design parameters and operating conditions such as inlet mass flow rate of geothermal steam and electrolyzer current density on the overall energy and exergy efficiencies were examined. Eventually, overall energy and exergy efficiencies of the studied system were determined as 34.98% and 49.17%, respectively.

Ozturk et al. [5] developed a geothermal based integrated system in order to obtain electricity, heating, cooling, domestic hot water as well as hydrogen fuel. Energy and exergy efficiencies and exergy destruction rates for the whole system and its subsystems were defined. The results showed that overall energy and exergy efficiencies of the designed system are 39.46% and 44.27%, respectively.

1.1.2 Renewable Based Energy Systems Equipped with Energy Storage Systems

Barbour et al. [6] made a detailed analysis of adiabatic compressed air energy storage (A-CAES) system with packed bed and developed a numerical model. They remarked that their system promises higher efficiencies than many of the previous studies and suggested that 70% efficiency is accessible. Also, they conducted a thermodynamic analyses for a single charge, storage and discharge cycle so as to examine where the main losses occur. They specified that main losses take place in expanders and compressors rather than in

the packed beds. High temperature hybrid compressed air energy storage (HTH-CAES) system was analyzed by Houssainy et al. [7]. The designed system includes a two-stage heating system with low-temperature and high-temperature thermal energy storage equipments. A detailed thermodynamic analyses of the HTH-CAES system is conducted coupled with parametric studies. The main goal of the study is to emphasize the importance of the thermal storage temperature and operating pressure on the performance of the storage system. The results show that the hybrid system is more efficient with higher energy density in comparison to an advanced adiabatic design, considering the equal power output. Zhao et al. [8] indicated that by adding the energy storage systems into the energy systems, the negative effects of renewable resources such as intermittency can be reduced. During the discharging period, exhaust gases which leave the low-pressure turbine should be used rather than leaving them to the atmosphere. For this reason, through the designed system, which contains a Kalina cycle and a compressed air energy storage system (CAES), this waste heat can be recovered. A detailed thermodynamic analysis of the integrated system is performed by creating a steady-state thermodynamic model and thermodynamics laws. The exergy efficiency of the designed system can be increased by nearly 4% in comparison to that of the single conventional compressed air energy storage system. Arabkoohsar et al. [9] performed a detailed thermodynamic analysis for a 100 MWp (megawatt peak) PV plant which is integrated with a compressed air energy storage system. By using the laws of thermodynamics, they wrote the balance equations for each component of the system and also benefited from the related formulations, PV and solar heating systems are investigated. Considering the actual operating conditions, the energy and exergy efficiencies of the designed system are examined for the whole year. According to the results, the energy and exergy efficiencies get very close values and change between 35% to 65%. Barbato et al. [10] suggest that by utilizing from a thermal energy storage system (TES) the performance of a CAES system can be improved considerably. Therefore, the thermal energy which is generated during the compression process is stored in a thermal energy storage system. Their results show that by integrating a packed bed thermal energy storage system with an Adiabatic-CAES cycle a remarkable increase is observed in the performance of the designed system. A thorough thermo-fluid dynamics model is developed, by taking into consideration the operating thermal energy storage units at changeable pressure values. Afterwards, the performance of the designed TES system for the both charging and discharging periods

are examined in a realistic manner. Finally, they express that high-potential of TES systems should be integrated with a CAES plant.

1.1.3 Decomposition of Hydrogen Sulfide

Different types of methods, materials and technologies have been investigated in order to obtain hydrogen from hydrogen sulfide (H_2S). Reverberi et al. [11] examined the new technologies as well as pre-existing strategies for hydrogen sulfide decomposing, touching on the importance of chemical methods that appear as the remarkable solutions. Thermocatalytic, photocatalytic and thermochemical methods are investigated, respectively and a comparative study is conducted by revealing the advantages and drawbacks of each process. Baykara et al. [12] studied the catalytic thermal splitting of hydrogen sulfide by using a wide range of perovskite type catalysts at changing temperature values from 600 °C to 950 °C for the purpose of generating hydrogen. From the lanthanide series, lanthanum is selected as an A-site element. Additionally, to create the perovskite structure as $La(M)O_3$, M: Ce,Co, Cr, Cu, Mo, Sr, V are selected as the B-site. By taking into consideration the catalyst characterization and catalyst activity tests, the effect of several metals (Co, Cr, Cu, Mo, V) on the catalyst structure and catalytic activity are examined. The results show that the most active catalyst is $LaCrO_3$ at 750 °C with a conversion value of 14%. Chakma et al. [13] conducted a detailed study about hydrogen sulfide splitting processes namely, thermal, thermochemical, electrochemical, photochemical and plasmochemical. Possibilities and limitations of the each method were remarked explicitly as well as chemical reactions and operation conditions. According to the authors, there is not a mature technology in the industry to decompose hydrogen sulfide into two valuable products, hydrogen and sulfur. Mbah [14] carried out an experimental study on hydrogen sulfide splitting in an electrolytic cell. Electrolysis is one the way to convert hydrogen sulfide into pure hydrogen and sulfur. The study suggested a novel apparatus and materials such that a membrane exchange assembly (MEA) made from a solid acid material, and cesium hydrogen sulfate ($CsHSO_4$) were chosen for the electrolysis process. Hydrogen sulfide feed content gas operating at 135 kPa and 150 °C. It can be clearly inferred that the performance of the overall system can decrease approximately 30% by using a thin (200 μm) $CsHSO_4$ electrolyte, which reduces the thickness of MEA from 2.3 mm to 500 μm.

1.2 Objectives of the Thesis

Fossil fuels have various adverse effects on the environment due to the combustion process they emit in larger amounts greenhouse gases (mainly CO_2) to the atmosphere which trigger the climate change. Therefore, recently, scientific researches, as well as energy policies, have been focused on to find a permanent solution for the environmental issues through utilizing the non-polluting resources such as renewable energy or hydrogen. In addition, another way to reduce the greenhouse gas emissions is to design the energy systems in a more effective manner by producing multiple useful commodities from the system. Therefore, the main goal of the thesis is to design three different types of renewable based energy system which provide higher energy and exergy efficiencies by producing electrical power, heating, cooling, domestic hot water and hydrogen outputs, simultaneously. Geothermal power plants emit relatively higher amounts of hydrogen sulfide which has many harmful effects on the environment and human body. Therefore, another objective of the present study is to produce hydrogen from hydrogen sulfide through the electrolysis process. In this manner, not only the negative effects of hydrogen sulfide are reduced, but also hydrogen is obtained as a clean energy resource which has a vast potential to replace fossil fuels. To reach the specified objectives and evaluate the designed systems performance both energetically and exergetically, a detailed thermodynamic analysis is performed by using Engineering Equation Solver (EES) software.

The specific objectives of the thesis can be listed as follows:

1. To design and develop four different systems using renewable energy sources for multigeneration.
2. To analyze these four systems thermodynamically through energy and exergy approaches.
3. To assess the performances of the presently developed systems through energy and exergy efficiencies and evaluate them comparatively.
4. To investigate the effects of some design parameters and operating conditions such as ambient temperature, equivalence ratio, and average hourly solar radiation on the system performance and illustrate them through graphs.
5. To integrate the energy storage systems to the designed systems in order to reduce the disadvantages of the renewable energy sources such as intermittency.

5

Therefore, a novel packed bed thermal storage system is analyzed and carry out a comprehensive study on it. Additionally, by modeling an underground cavern system with regard to heat transfer mechanism heat losses in the underground cavern are calculated.

6. To develop a thermodynamic model of the electrolysis process of hydrogen sulfide and give a detailed information about its basic concepts.

7. To investigate the importance of the hydrogen sulfide splitting process in geothermal power plants and determine the at what rate hydrogen sulfide emissions can be reduced and how much additional energy can be produced through hydrogen fuel by considering the new technologies such as AMIS (AMIS® - acronym for "Abatement of Mercury and Hydrogen Sulfide" in Italian language).

1.3   Hypothesis

This thesis is based on the two different ideas, one of them is to design multigeneration systems in order to obtain more efficient structures than single generation, cogeneration or trigeneration systems. "By designing the renewable based multigeneration systems and integrating the energy storage systems , continuously operate and high efficiency energy system can be obtained." is one of the main assertions of the present study. The results show that overall energy and exergy efficiencies for the studied systems can be reached up to 67.95% and 60.94%, respectively. In addition, the second claim of the thesis is "By decomposing the hydrogen sulfide into the hydrogen and sulfur, hydrogen sulfide emissions can be reduced at a significant rate and also additional energy supply can be obtained by virtue of hydrogen in geothermal power plants". The results suggest that hydrogen sulfide emission can be reduced approximately 738.8 g/s, while the inlet mass flow rate of geothermal steam is 60 kg/s, and also 6.234 MW energy can be produced through hydrogen fuel.

CHAPTER 2

BACKGROUND

2.1   Energy Demand and Scenarios

The growing population and industries are among the main factors of increasing energy demand in the world. Although fossil fuels are expressed as the most hazardous energy resource by virtue of its adverse effects on the environment, still the world is dependent on it and its derivatives in order to produce the required amount of energy. In order to alter this situation, recently in the world energy policies has been touched on the significance of renewable energy sources and new technologies such as carbon capture and storage (CCS).

In 2014, approximately 67% of the world total energy production came from fossil fuels as shown in Figure 2.1 [15]. Hydro, wind and solar energies and other renewables such as biomass and geothermal energy made a 22% contribution to this total amount. Today's distribution is not so different, although many countries pay attention to renewable energy sources.

On the other hand, the 450 Scenario pushes the deployment of renewables significantly beyond the levels implied by today's measures and policy intentions. The power sector will be largely decarbonised by 2040, with the share of renewables in generation, rising to almost 60%. More explicitly, dependence on fossil fuel resources has been decreasing day by day due to developing renewable based technologies and materials. According to this scenario, by 2040, 66% of the total energy production will have come from the renewable energy sources.
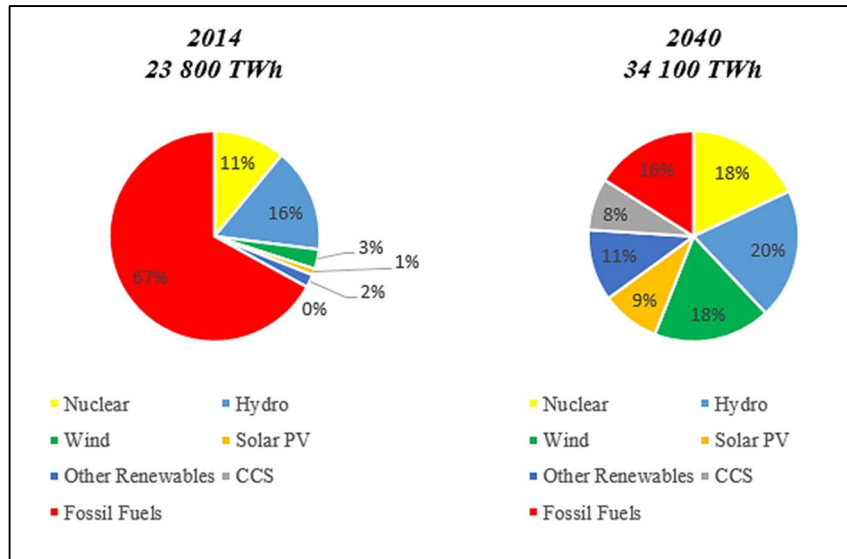
Figure 2.1 Evolution of the power generation in terms of 450 scenario

2.2 Hydrogen as a Clean Energy Source

Hydrogen is a colourless, odourless, tasteless and non-toxic gas. It is the lightest of all molecules (molecular weight = 2.016) and, consequently, has a density of only 0.0899 (kg/m^3). Hydrogen burns cleanly in the air; water is the only product apart from traces of nitrogen oxides at high combustion temperatures. The combination of physical properties exhibited by hydrogen (low density, low boiling point, a wide range of inflammability, low ignition energy, high diffusivity in the air, high flame velocity) is unique among other fuels [16].

An amount of 120.7 MJ lower heating value (LHV) energy can be obtained from 1 kg hydrogen which is equal to 2.1 kg natural gas, 2.8 kg gasoline and 3.1 kg fuel oil as illustrated in Figure 2.2 (Data from Ref [17]).
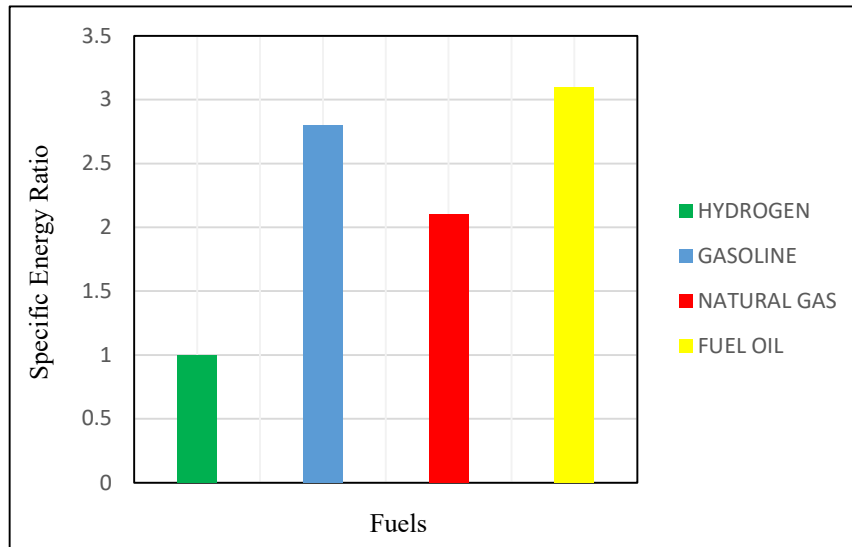
Figure 2.2 Quantities required to obtain energy from fossil fuels that can be obtained from one kilogram of hydrogen

Hydrogen can be produced from various primary energy sources such as fossil fuels (coal, natural gas), renewables (biomass, solar, hydro, wind) or nuclear heat and the major uses of hydrogen are residential, industrial and transportation fields.

Hydrogen has a vast potential to replace fossil fuels since it has no undesirable environmental effects as well as including high energy density. The other advantages of hydrogen are possessing no emission while it is produced from water, higher energy exchange efficiency and capability to be stored in various ways which makes hydrogen highly valuable for the forthcoming population energy requirements.

2.3   Energy Storage Technologies

The worldwide electricity production based on renewable energy sources (RES) such as wind and solar, has shown a dramatic increase over the past decade and it is unavoidable to pursue the same increasing trend for the upcoming near future. Non-hydro RES contribution to the worldwide electricity generation in 2014 was 6% and their contribution is expected to be between 12% and 18% in 2025, depending on the considered policy scenarios [18]. On the other hand, the intermittent nature of solar and wind energy sources, make energy storage technologies a basic requirement so as to improve the flexibility and efficiency of energy systems [19].

Energy storage technologies include pumped hydro energy storage (PHES), compressed air energy storage (CAES), thermal energy storage (TES), superconducting magnetic energy storage (SEMS), flywheel, supercapacitor, battery and hydrogen storage. The distribution of the existing energy storage technologies is shown in Figure 2.3 (Data from Ref [20]). Although the pumped hydro energy storage is the most widely developed large-scale energy storage technology, accounting for 99% of the global installed capacity [21], while the scarcity of water resources and specific geographical conditions confine their widespread application [22]. Compressed air energy storage, on the other hand, is among the promising technologies which has attracted a huge attention in industrial applications and applied science.
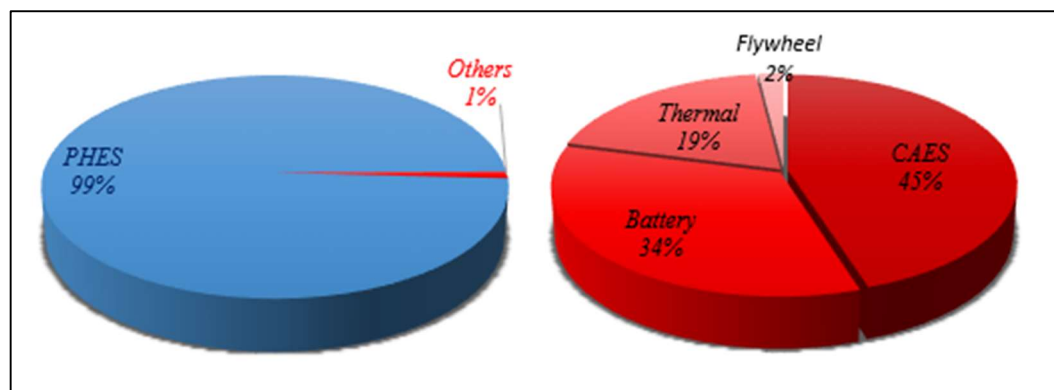
Figure 2.3 Distribution of the existing energy storage technologies by 2013 in the world

2.4   Integrated Systems for Multigeneration

Nowadays, more and more scientists and politicians believe that some concepts play a crucial role in terms of sustainable energy future. The underlying motivation of these concepts are reducing the pollution, obtaining high-efficient energy systems, utilizing from the renewables, and protecting the environment. One significant solution is to design the renewable based energy systems in a more effective way so as to attain higher efficiencies. One way to achieve this goal is to plan the system by using the approaches of cogeneration and especially multigeneration. Therefore, multigenerational systems can provide better efficiency, cost-effectiveness, environment and hence sustainability [23].

Multigeneration energy systems can be operated by utilizing from the renewables (biomass, solar, geothermal, wind etc.), fossil fuels (coal, natural gas etc.) and also nuclear energy. In many studies, more than one energy resources are used together.

Through multigeneration systems, cooling, heating, electricity, desalination and synthetic fuels (H_2, NH_3, C_2H_5OH) can be produced, simultaneously as illustrated in Figure 2.4.
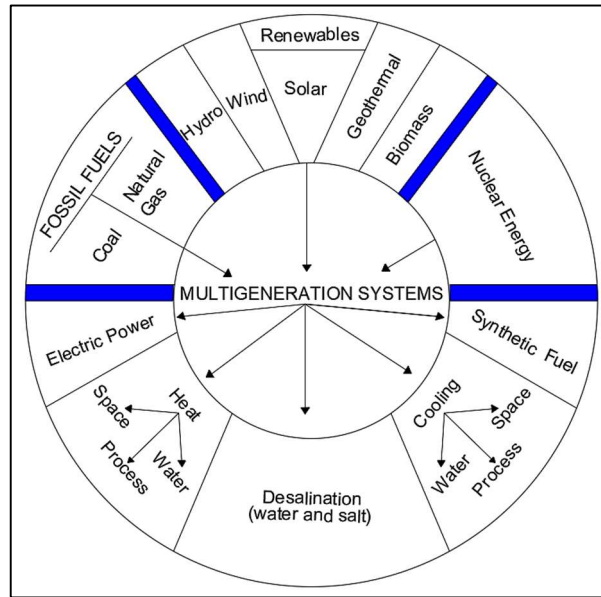
Figure 2.4 Energy sources and useful commodities of multigeneration systems

2.5 Hydrogen Sulfide Emissions

Geothermal energy is a significant renewable energy source such that it is predicted to be an energy carrier for a sustainable energy future in the next decades. However, one of the most significant negativeness related to the geothermal power plants is non-condensable gases (NCG) emissions. Carbon dioxide (CO_2) and methane (CH_4) gases are emitted from the vent stacks in geothermal power plants which cause serious environmental problems. The amount of these emissions are much less in comparison to carbon and fossil fuel plants, which indicates that the contribution of these sources is practically negligible. Geothermal power plants also emit relatively higher amount of hydrogen sulfide (H_2S) due to the employment of hydrogen sulfide as a main constituent of the geothermal fluids. Hydrogen sulfide has many adverse effects on the environment. The presence of hydrogen sulfide in the air, water, soils and vegetation is one of the main environmental concerns [24].

Hydrogen sulfide is normally in the gas phase and can be absorbed in human and animal lungs through inhalation. Health effects include respiratory, ocular, neurological, and metabolic effects and death after single exposures to concentrations higher than 700 mg/m^3 [25]. A summary of these effects is presented in Table 2.1.

11

Table 2.1 The human health effects resulting from exposure to H_2S [25].

Exposure (mg/m³)	Effect/Observation
0.011	Odor threshold
2.8	Bronchial constriction in asthmatic individuals
5.0	Increased eye complaints
7.0–14.0	Increased blood lactate concentration, decreased oxygen uptake
5.0-29.0	Eye irritation
> 140	Oldfactory paralysis
> 560	Respiratory distress
≥ 700	Death

SYSTEM DESCRIPTION

In this thesis, three different types of renewable based multigeneration energy systems are designed and analyzed through the energy and exergy approaches. The main goal of these systems is to produce multiple useful commodities such as power, heating, cooling, domestic hot water and hydrogen without causing harm to the environment. The proposed systems differ from many multigeneration systems in terms of zero fossil resources usage and zero carbon emissions by utilizing renewable based energy sources. Additionally, an electrolyzer unit and AMIS (AMIS® - an acronym for "Abatement of Mercury and Hydrogen Sulfide" in the Italian language) technology are integrated to the studied systems. For the first time, unlike previous studies hydrogen production from hydrogen sulfide is taken into consideration along with electrolysis of water. The underlying motivation of this process is not only to produce hydrogen from hydrogen sulfide but also to reduce the hydrogen sulfide emissions and thereby its adverse effects on the environment in geothermal power plants. High temperature geothermal sources range between 150 and 350 °C for many regions in the world [26]. In these systems, hot geothermal fluid is extracted from the production well above 250 °C. The designed systems include already proven and mature technologies which increase the feasibility of the systems. At the end of this chapter, the electrolysis process of hydrogen sulfide is explained and modeled.

3.1   System 1

Schematic illustration of the system 1 is shown in Figure 3.1. The system comprising absorption cooling system, organic Rankine cycle, a solar driven system and hydrogen production units. The system is designed to generate five outputs namely, power, cooling,

heating, hydrogen and domestic hot water. Detailed descriptions of individual cycles have been summarised below.

3.1.1 Single Effect Absorption Cooling System

In the single effect absorption cooling system (SEACS), a strong ammonia-water solution enters the generator at state (38), and is heated by the geothermal steam. As the strong ammonia-water warms, it starts to evaporate and thus a weak solution of ammonia-water at a higher temperature than state (38) leaves the generator at state (39). The weak solution flows through the heat exchanger 1, where its thermal energy transfers to the incoming strong solution at state (37). The weak solution leaving at state (40) enters the expansion valve 1, where its pressure decreases before it enters the absorber at state (41). The concentrated ammonia-water vapor at state (31) flows into the condenser 1, where the ammonia-water vapor transfers its heat to the domestic water before leaving at state (32). The ammonia-water vapor at state (32) enters the expansion valve 2, where its pressure and temperature decrease. This cooled ammonia-water vapor at state (33) enters the evaporator, where the ammonia-water mixture absorbs heat from the air which is provided from the cold store and leaves at state (34). The weak solution at state (41) and ammonia-water mixture at state (35) flow into the absorber, where they transfer their thermal energy to the domestic water and exit as a strong solution in liquid form at state (36) and passes through the pump 1.

3.1.2 Organic Rankine Cycle

In order to have an efficient ORC, the working fluid in the ORC should have a high critical temperature. One of the typical organic fluid types used to operate the ORC is n-octane, which has a relatively high critical temperature, 296 °C [27]. Therefore it is selected as the working fluid of ORC. Hot geothermal steam at state (2) enters the boiler of the ORC and transfers its heat to the working fluid. Working fluid which is heated and vaporized in boiler goes into the turbine 1 at state (52) to generate power, and leaves at state (53) then enters the condenser 2 to be condensed. During the condensation process, air is extracted from buildings at state (54) and receives the thermal energy of the working fluid and then it is supplied to buildings at state (55) with the aim of space heating. Afterward, working fluid passes through the pump 2.
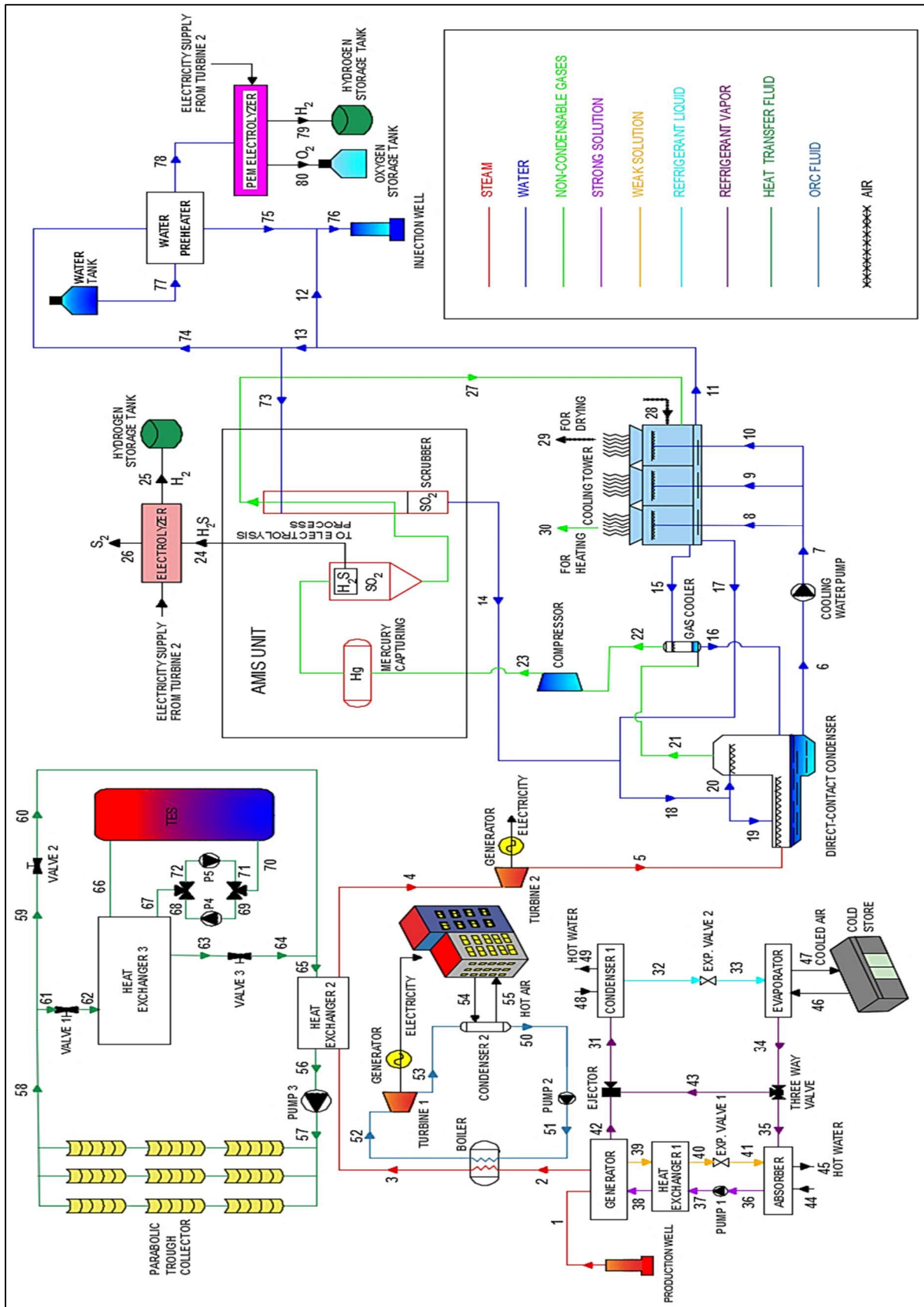
Figure 3.1 Scheme of a solar and geothermal based multigeneration system equipped with AMIS units

3.1.3   The Solar Driven Cycle

A solar driven system with numerous huge parabolic trough collectors are supposed to transfer the solar energy to the heat transfer fluid of the solar driven cycle. Main advantages of using Syltherm 800 are environmentally-friendly characteristics, no troublesome phase change, and higher working temperatures and hence Syltherm 800 is chosen as the heat transfer fluid of the solar driven system. Due to the intermittency of the solar energy, a thermal energy storage (TES) tank is integrated into the solar driven system. The system operates in three different scenarios: a) charging period, b) storing period and c) discharging period.

During the charging period, heat transfer fluid which leaves the parabolic trough collector at state (58) as heated is divided into two streams. Some part of the working fluid flows into the heat exchanger 3 at state (62) and where its heat transfers to the incoming flow at state (67) which circulates inside the TES. Heat transfer fluid which leaves the heat exchanger 3 at state (66) as heated passes through the TES tank and transfers its thermal energy to the phase change material (PCM) which is located inside the tank. Both sensible and latent heat transfer occur in this period. The latent heat storage can be achieved through solid-solid, solid-liquid, solid-gas, and liquid-gas phase changes. Liquid-gas transitions have a higher heat of transformation than solid-liquid transitions. However, liquid-gas phase changes are not practical because of the large volumes or high pressures required to store the materials when they are in their gas phase states. Solid-solid phase change process is typically very slow and has a rather low heat of transformation [28]. Therefore, in the present study, the proposed system is designed for the solid-liquid phase change. Afterward, heat transfer fluid leaves the TES tank as cooled at state (70). The rest part of the fluid at state (59), after circulating inside the pipe line connects with the incoming flow at state (65) and then enters the heat exchanger 2. The main objective of the solar driven system is to increase the temperature of the geothermal steam which flows into the heat exchanger 2 at state (3) and leaves it at higher temperatures so that more electrical power can be obtained from turbine 2.

During the storing period, valve 1 and valve 3 are closed. Therefore, heat transfer fluid is not divided into two streams. The whole part of the heat transfer fluid which leaves the parabolic trough collector at state (58) as heated circulates through the pipe line and enters the heat exchanger 2 for the purpose of heating the incoming geothermal steam.

During the discharging period, only valve 2 is closed. The whole part of the heat transfer fluid which leaves the parabolic trough collector at state (58) as heated flows into the heat exchanger 3 at state (62). Opposite to the charging period, during the discharging period, cold heat transfer fluid enters to the TES tank and by circulating around the PCM receives its heat and leaves the TES tank at state (66) as heated. In addition, at the end of the discharging period, PCM returns to its initial conditions through freezing.

3.1.4   Water Electrolyzer

The Proton Exchange Membrane (PEM) systems include some specific advantages as compared to alkaline systems such as integrattion with renewable energies. In comparison with alkaline systems, PEM electrolyzer presents higher efficiencies and production rates. Moreover, it can operate at lower temperatures and hence PEM is chosen as electrolyzer type for the electrolysis process of water.

A PEM electrolyzer has a simple structure and operating principle such that in which a solid proton conducting membrane separates an anode chamber from a cathode chamber. During the electrolysis process of water, a direct current is provided to the system in order to split the water into hydrogen and oxygen as shown in Figure 3.2.
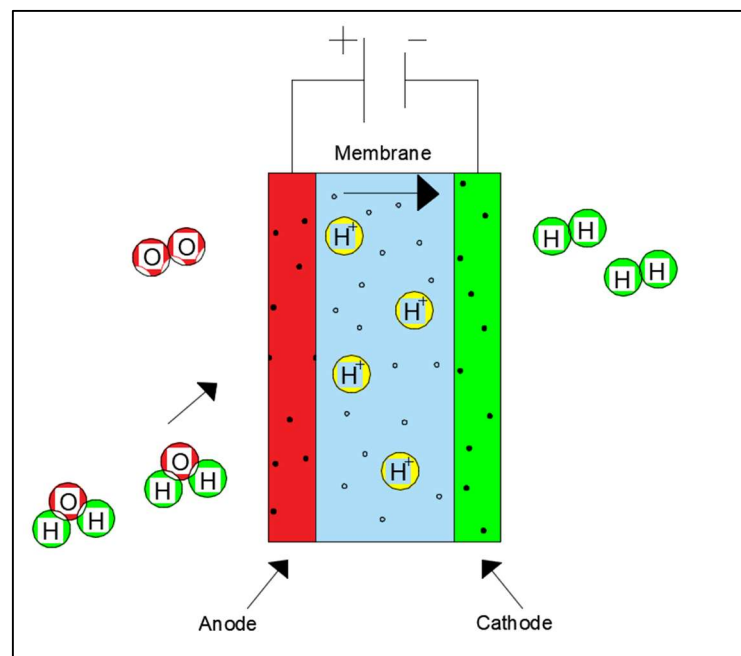
Figure 3.2 Operating principle of the PEM electrolyzer

The reactions for the anode and cathode of the PEM electrolyzer can be expressed respectively as follows:

$$H_2O \ (l) \rightarrow \frac{1}{2}O_2 \ (g) + 2H^+ \ (aq) + 2e^- \qquad (3.1)$$

$$2H^+ \ (aq) + 2e^- \ \rightarrow \ H_2 \ (g) \qquad (3.2)$$

In the proposed system, water is supplied from a water tank and the water primarily enters the water preheater at state (77). On the other side, the water which leaves the cooling tower at higher temperatures flows into the preheater at state (74) and so before it is sent to the injection well, its heat is transferred to the water which will in the subsequent step enter the electrolyzer unit at state (78) at the appropriate temperature level for the electrolysis process.

3.2   System 2

Figure 3.3 illustrates a comprehensive schematic view of the designed multigeneration system, and how the subsystems interact with each other. According to the figure, the system includes, double flash steam cycle, a solar driven system, absorption cooling system, steam Rankine cycle, a wind farm and hydrogen production units. The system is designed to generate five outputs namely, power, heating, cooling, hydrogen and domestic hot water. Detailed descriptions of individual cycles have been summarised below.

3.2.1   Double Flash Steam Cycle

The geothermal fluid is extracted from the production well and enters the expansion valve at state (1). Here, the pressure of the stream is reduced which later enters the separator 1 at state (2). In the separator, steam is extracted at state (3) and the saturated mixture leave from the bottom at state (7). The steam extracted at state (3) enters the high pressure turbine (HPT) and expands to state (4) to produce electricity. On the other side, flow at state (7) enters the second expansion valve and leaves it at a lower pressure level at state (8). Afterward, stream at state (8) passes through the separator 2 and again steam is extracted at state (10) and saturated mixture leaves the separator 2 at state (9) and flows into the injection well. Steam at state (10) mixes with the stream coming from state (4) to enter the low pressure turbine (LPT). In the LPT, steam from state (5) expands to state

(6) to produce power. Temperature-entropy process diagram for double flash steam cycle with a two stage turbine is shown in Figure 3.4.

3.2.2 Single Effect Absorption Cooling System

In the single effect absorption cooling system, a strong ammonia-water solution enters the generator at state (23), and is heated by the geothermal steam. As the strong ammonia-water warms, it starts to vaporize and consequently a weak solution of ammonia-water at a higher temperature than state (23) leaves the generator at state (24). The weak solution flows through the heat exchanger 2, where its thermal energy transfers to the incoming strong solution at state (22). The weak solution leaving at state (25) enters the expansion valve 1, where its pressure decreases before it enters the absorber at state (26). The concentrated ammonia-water vapor at state (16) flows into the condenser 1, where the ammonia-water vapor transfers its heat to the domestic water before leaving at state (17). The ammonia-water vapor at state (17) enters the expansion valve 2, where its pressure and temperature decrease. This cooled ammonia-water vapor at state (18) enters the evaporator, where the ammonia-water mixture absorbs heat from the air which is provided from the cold store and leaves at state (19). The weak solution at state (26) and ammonia-water mixture at state (20) flow into the absorber, where they transfer their thermal energy to the domestic water and exit as a strong solution in liquid form at state (21) and passes through the pump 2.

3.2.3 The Solar Driven Cycle

The solar driven system with numerous huge parabolic trough collectors are supposed to transfer the solar energy to the heat transfer fluid of the solar driven cycle. Similar to system 1, Syltherm 800 is chosen as the heat transfer fluid of the solar driven system. The heat transfer fluid which leaves the parabolic trough collector at state (14) as heated circulates through the pipe line and enters the heat exchanger 1 for the purpose of heating the incoming geothermal fluid at state (6).
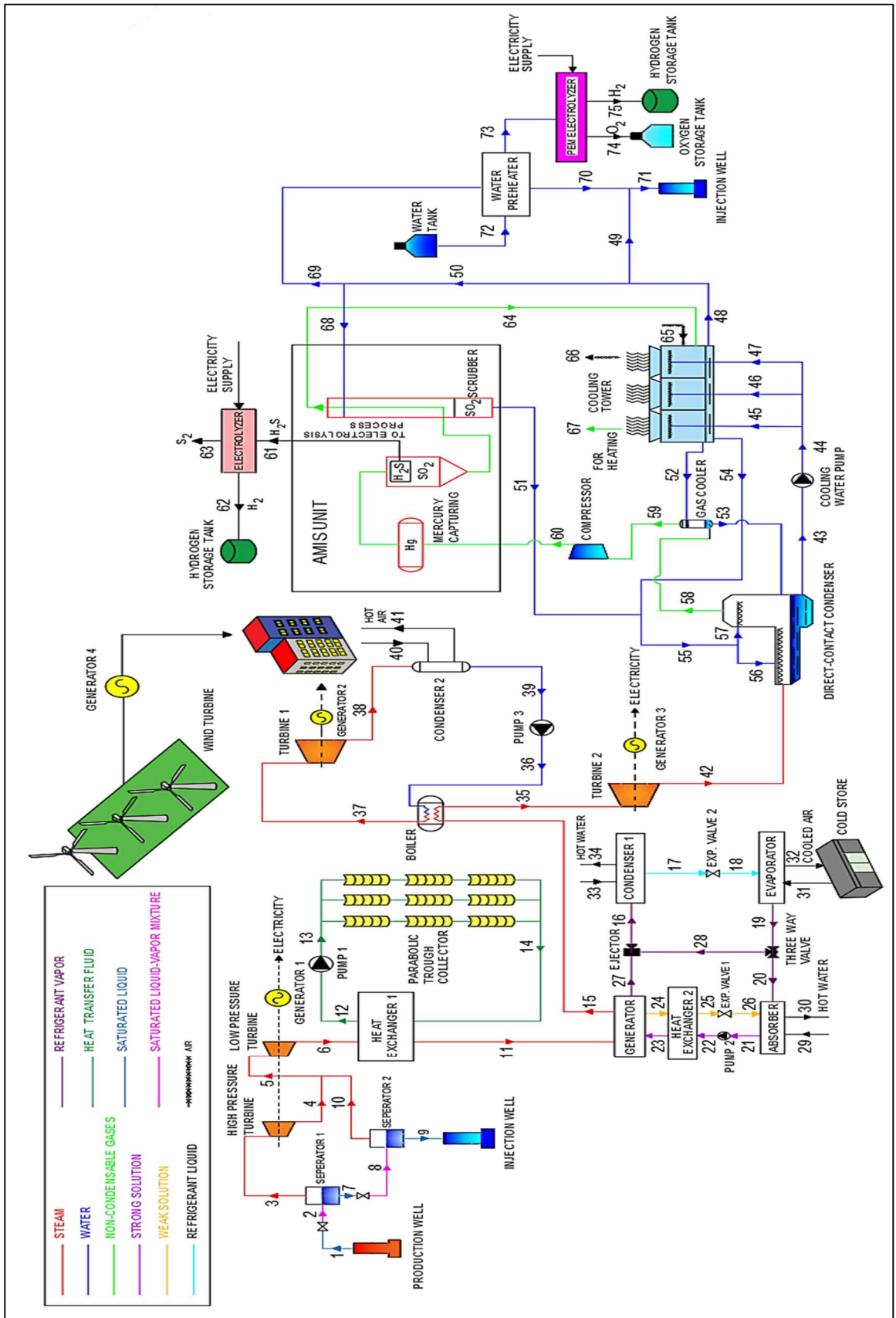
Figure 3.3 Scheme of a solar, wind and geothermal based multigeneration system equipped with AMIS units
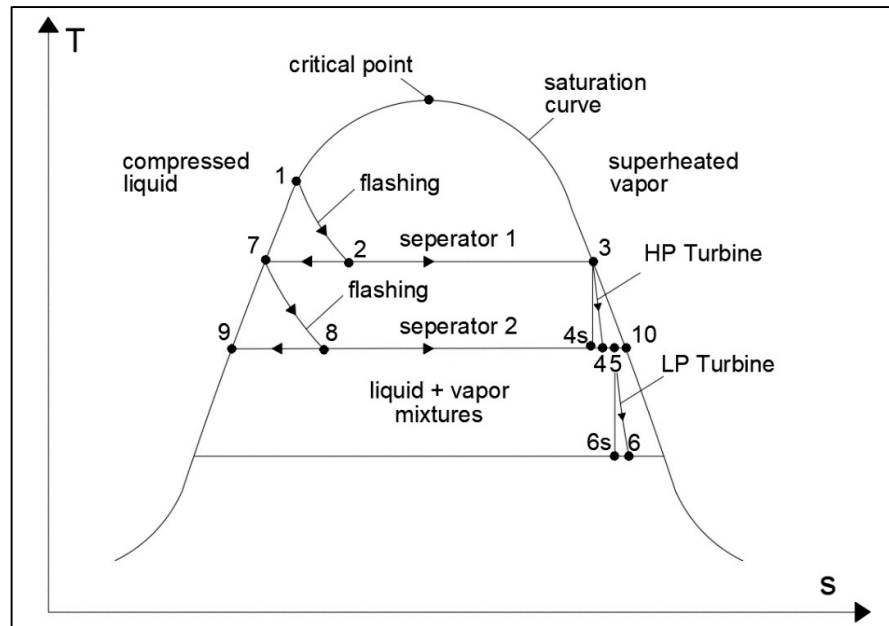
Figure 3.4 Temperature-entropy diagram for double flash steam cycle with a two stage turbine

3.2.4 Steam Rankine Cycle

In system 2, steam Rankine cycle is preferred instead of organic Rankine cycle, as compared to system 1. Hot geothermal steam at state (15) enters the boiler of the Rankine cycle and transfers its heat to the working fluid. Working fluid which is heated and vaporized in boiler goes into the turbine 1 at state (37) to generate power, and leaves at state (38) then enters the condenser 2 to be condensed. During the condensation process, air is extracted from buildings at state (40) and receives the thermal energy of the working fluid and then it is supplied to buildings at state (41) with the aim of space heating. Afterward, working fluid passes through the pump 3.

3.2.5 Wind Farm

Wind turbines has a simple operating principle. The energy in the wind accelerate the blades of wind turbine located around a rotor. The rotor is connected to the main shaft, which turns a generator for the purpose of producing electricity. In addition, wind farms consist of in a multitude of wind turbines which are placed in the same region in order to generate higher amounts of electric power. In system 2, a wind farm is integrated into the designed system in order to provide additional power to buildings.

3.2.6 Water Electrolyzer

Similar to system 1, a proton exchange membrane is operated inside the proposed system in order to produce hydrogen and oxygen by splitting the water. In system 2, water is supplied from a water tank and the water primarily enters the water preheater at state (72). On the other side, the water which leaves the cooling tower at higher temperatures flows into the preheater at state (69) and so before it is sent to the injection well, its heat is transferred to the water which will in the subsequent step enter the electrolyzer unit at state (73) at the appropriate temperature level for the electrolysis process.

3.3 System 3

Schematic of system 3 is shown in Figure 3.5. The main aim in system 3 is to design a new renewable based multigeneration energy system equipped with compressed air and thermal energy storage subsystems. In order to minimise the heat losses in the underground cavern, a novel packed bed storage system is proposed and detailed performance analysis of the system is carried out. Unlike previous studies, biomass is preferred as a fuel instead of fossil fuels so as to reduce the harmful effects of greenhouse gas emissions.

Firstly, the air is compressed by consuming the available electricity in the grid to activate a motor-compressor train. The thermal energy produced during two-stage compression is removed by intercoolers and after-coolers. Subsequently, the high-pressure and high temperature air leaves the after-cooler at state (5). On the other side, heated air exiting the after-cooler (state 15) is sent to the mixing chamber where it mixes with ambient air. In other words, mixing chamber functions as a preheater. The solar-driven system including several huge parabolic trough collectors (PTC) are supposed to transfer the solar energy to the heat transfer fluid. Due to the intermittency of the solar energy, two storage tanks are integrated into the solar-driven system. When hot air leaves the heat exchanger 1 at state (24) is not hot enough due to the insufficient solar radiation, biomass, then, is supplied to the gasifier to produce gases in the gasification process to flow into the combustion chambers. Thereby, it reacts with the heated air in order to reach the required temperatures at the inlet of the turbines. Detailed descriptions of individual cycles have been summarised below.
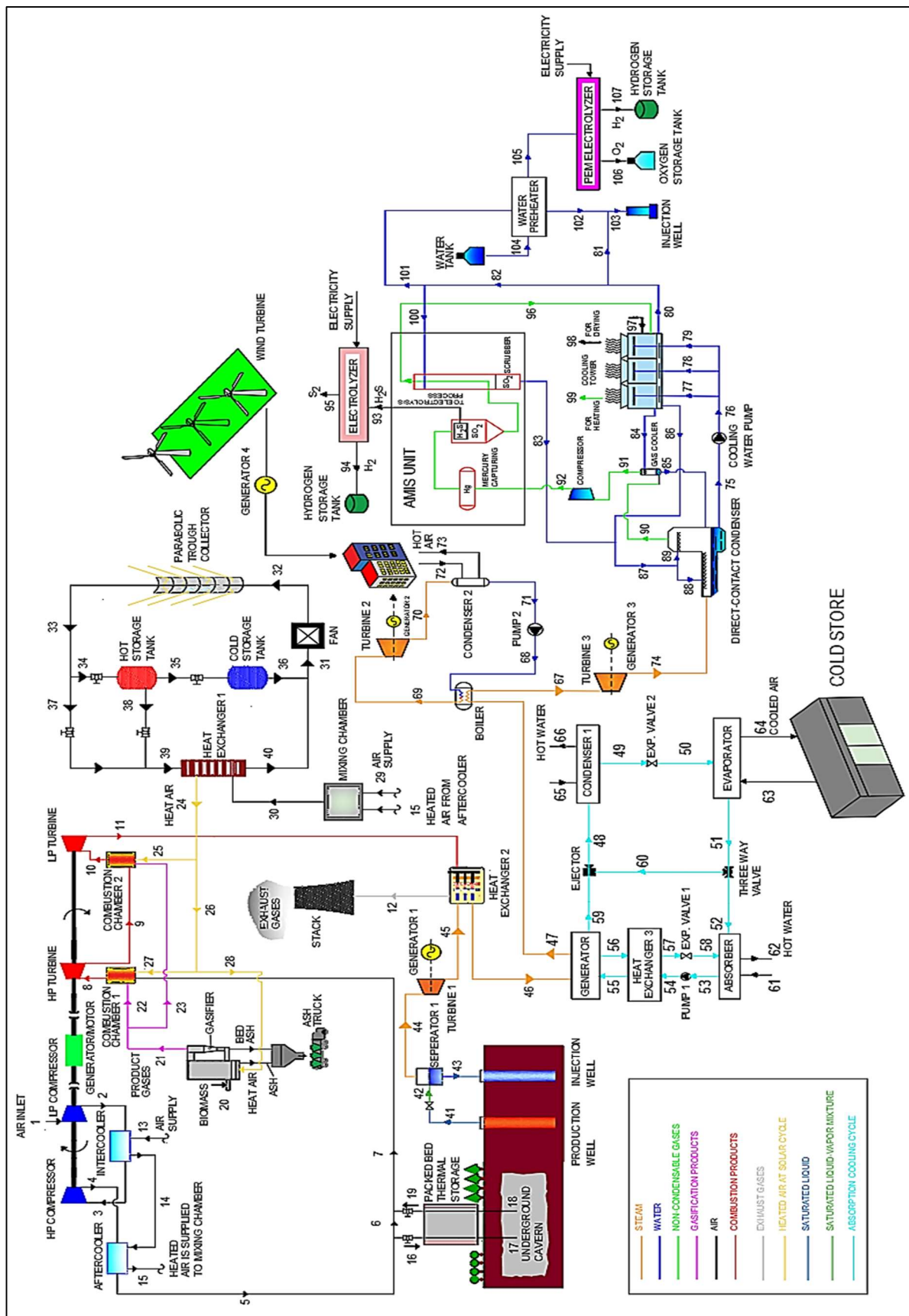
Figure 3.5 Scheme of a renewable based multigeneration system equipped with energy storage and AMIS units

3.3.1 Compressed Air Energy Storage (CAES) Cycle

The power plant works in 3 different scenarios: a) Charging period, b) Storing period and c) Discharging period. During the charging period (generally during off-peak times), high temperature and high-pressure air leaving the after-cooler (state 5) is divided into two streams (states 6 and 16). The specific fraction of the air enters into the expansion train with recuperator and then, reacts with the product gases in the combustion chamber 1. The rest part of the hot and pressurized air, flows through the packed bed thermal energy storage system to transfer its thermal energy to the rock bed as storage energy. This system is added to the integrated system in order to minimize heat losses in the underground cavern. Then, high pressure and low-temperature air passes into the underground cavern.

During the storing period, flow in (16) is shut-downed by the control valve, so the flow at (5) is not divided into two streams as in the charging period and the whole part of the compressed air enters to the expansion train with recuperator. On the other hand, during the discharging period (at peak times), flow in the (18) numbered pipeline is released by a control valve and pressurized air starts to flow into the packed bed thermal energy storage system to receive the heat from the packed rock and leaves the storage system at higher temperatures. Later, heated air is connected to the (6) numbered pipeline and through increasing the air mass flow rate, excess electricity can be obtained from the integrated system.

3.3.2 The Solar Driven System

The solar-driven system including numerous huge parabolic trough collectors are supposed to transfer the solar energy to the heat transfer fluid. Two storage tanks are integrated into the solar-driven system. Similar to the CAES cycle, the solar-driven system operates in 3 different scenarios as illustrated in Figure 3.6. During the charging period, flow at state (34) is released by a control valve and heat transfer fluid enters to the hot storage tank after receiving the solar energy through parabolic trough collectors and its thermal energy transfers to the phase change material which is located in the hot storage tank.
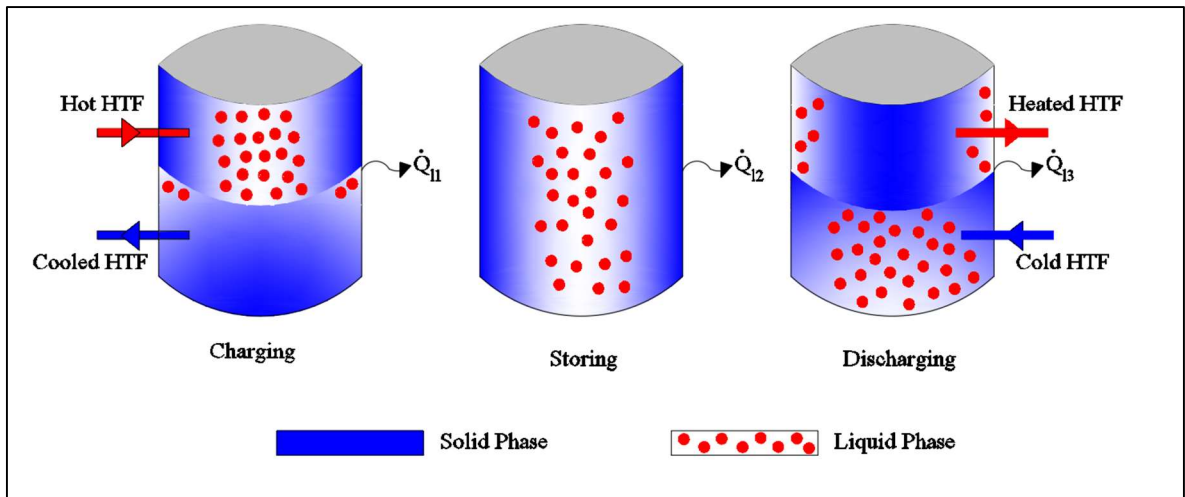
Figure 3.6 Working principle of the hot storage tank during the charging, storing and discharging periods

During the storing period, all valves excluding (37) are closed. Therefore, heat transfer fluid cannot circulate in the storage tanks. Opposite to the charging period, during the discharging period, cold heat transfer fluid circulates in the hot storage tank by receiving the phase change heat and at the end of the discharging period, phase change material returns to its initial conditions through freezing.

3.3.3 Gasifier and Combustion Chambers

Insufficient solar radiation might result in less than required temperature for the air leaving the heat exchanger 1 at the state (24). Thereafter, biomass is supplied to the gasifier and then, the produced gases in the gasification process enter to the combustion chamber where they react with the heated air in order to reach the required temperatures at the turbine inlet. In the gasification process which occurs in a circulating fluidized bed (CFB), air is chosen as the gasifying agent. Circulating fluidized bed is fed by the hot air as well as combustion chambers. It consists of a riser, a cyclone and a solid recycle device as shown in Figure 3.7 (Modified from Ref [29]).
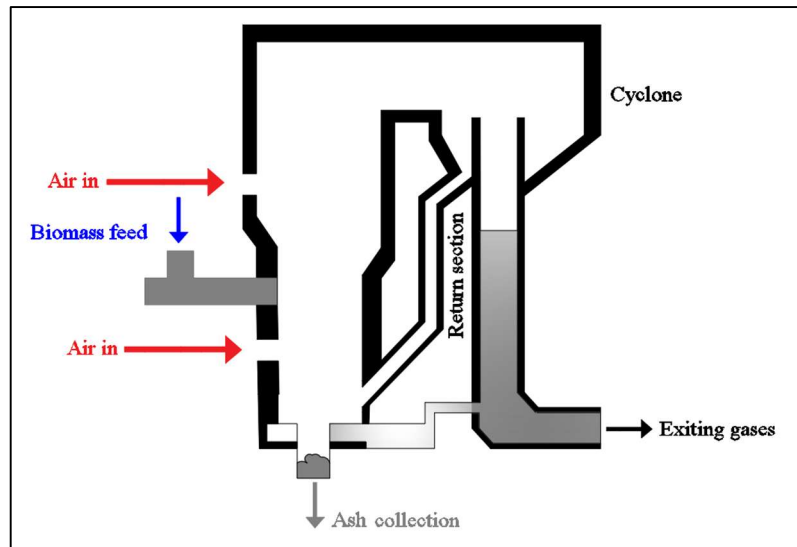
Figure 3.7 Schematic illustration of the circulating fluidized bed gasifier

Product gases in the gasification process, leave the circulating fluidized bed at state (21) and are divided into two streams. The specific fraction of gases enter into the combustion chamber 1 and the rest enters the combustion chamber 2. Consequently, product gases of the combustion chamber 1 and 2 expand in the high-pressure (HP) and low-pressure (LP) turbines blades, respectively.

Working principle of the absorption cooling system, wind farm, steam Rankine cycle and electrolyzer of water are similar to system 2, therefore there is no need to give a detailed information about them once again.

3.4   The AMIS Unit

All designed multigeneration energy systems in this study are equipped with AMIS unit. AMIS technology (Abatement of mercury and hydrogen sulfide), which is mainly used in the power plants of Tuscany region, is designed to reduce the problems related to the gaseous emissions from geothermal power plants and especially the negative effects of hydrogen sulfide such as bad smell. Geothermal fluid mainly consists of steam with some percentage (from less than 1% and up to 15%) of non-condensable gases. In geothermal power plants, which are not equipped with AMIS unit, non-condensable gases release to the atmosphere. However, after integrating the AMIS unit to the energy systems, non-condensable gases are sent to the AMIS system for the purpose of mercury and hydrogen sulfide abatement.

This system includes three fundamental processes;

1. Removal of mercury by chemical absorption,
2. Selective catalytic oxidation of hydrogen sulfide to SO_2,
3. SO_2 scrubbing by geothermal water.

1st Process: Mercury Removal

Elemental mercury is removed from NCG stream by chemical absorption on a fixed bed of sorbent (selenium mass or sulphurized activated carbon).

2nd Process: Catalytic oxidation of hydrogen sulfide

NCG are heated up to the minimum temperature required by the catalyst to promote oxidation according to the reaction:

$$H_2S + \frac{3}{2}O_2 \rightarrow SO_2 + H_2O \tag{3.3}$$

3rd Process: Sulphur dioxide scrubbing by geothermal water

The final step of the process is the absorption of the produced SO_2 by geothermal water. In most cases, geothermal fluids contain basic soluble compounds, especially ammonia, so that these are naturally present in the geothermal water. Basic compounds allow the absorption of acidic components, such as sulphur dioxide (SO_2).

The efficiency of the SO_2 absorption essentially depends on the molar ratio between produced SO_2 and ammonia in the geothermal water. If the geothermal water contains enough ammonia, SO_2 removal is close to 100% without addition of any chemical. Otherwise, it is possible to achieve the same result by adding ammonia water, thereby increasing the natural ammonia content of the geothermal water, or, as an alternative, sodium hydroxide (NaOH). The water leaving the absorption column re-enters the cycle of the geothermal water, controlled by the cooling tower overflow [30].

3.5 Electrolysis Process of Hydrogen Sulfide

In the thesis, we modify the AMIS system for hydrogen production from hydrogen sulfide. Hydrogen sulfide, which is trapped inside the AMIS unit, is sent to an electrolyzer system in order to decompose it into hydrogen and sulfur dimer instead of sending it to the catalytic oxidation process [1]. Understudy system configuration is given in Figure 3.8 (Modified from Ref [24]).

27
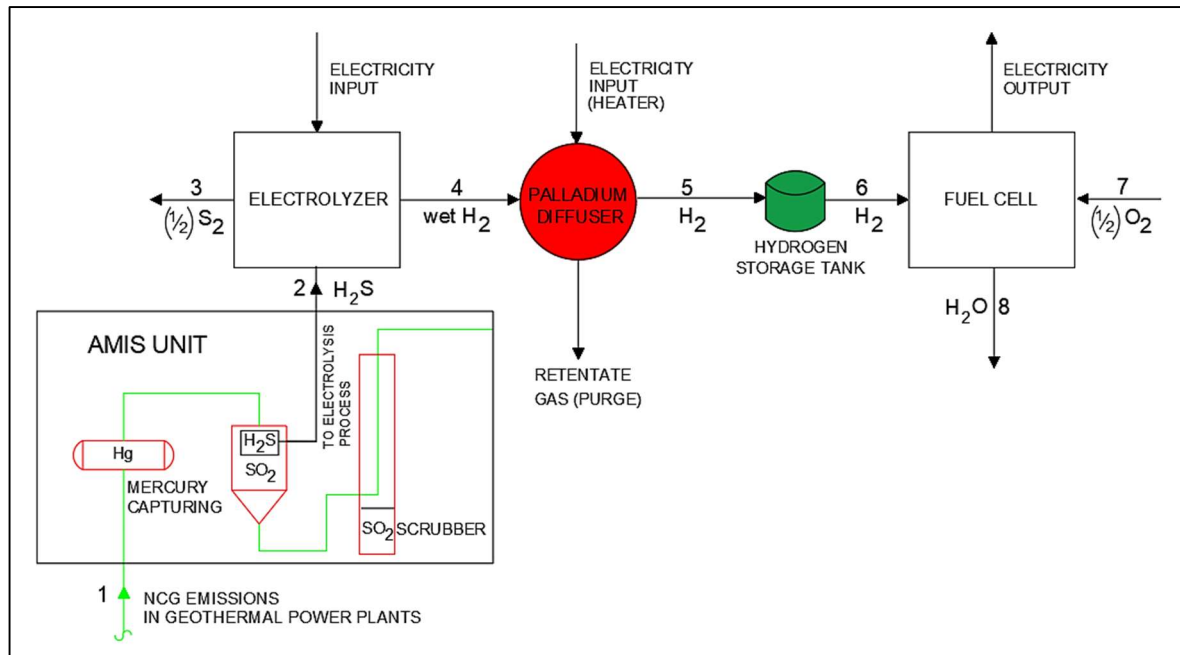
Figure 3.8 Schematic illustration of the modified AMIS system

Non-condensable gases, which are released from the geothermal fluid, flow through the AMIS unit at state (1). Inside the AMIS unit, hydrogen sulfide is separated and trapped. Hydrogen sulfide gas enters the electrolyzer unit at state (2) and splits to hydrogen and gaseous sulfur dimer through electrochemical method. The principle of hydrogen sulfide electrolysis is to pass a direct current between two electrodes in order to decompose hydrogen sulfide into hydrogen and sulfur dimer [1]. Wet hydrogen, which is produced through the electrolysis process, is sent to the palladium diffuser at state (4) for the purpose of purification. Only hydrogen can diffuse through the palladium diffuser. The palladium diffuser can take a number of forms, including an array of tubes, a coiled tube or membrane foil. Next, purified hydrogen is placed into the hydrogen storage tank for later use. Afterward, when electricity production is required, hydrogen is extracted from the storage tank at state (6) and enters the fuel cell system. Fuel cells have a similar working principle with electrolyzer units yet in opposite direction. Along with hydrogen, oxygen gas is supplied to the fuel cell system at state (7) so as to produce electricity from the system. On the other side, the innumerable uses of sulfur make it an important and valuable commodity. It is used for many purposes such as fertilizers, medicals, insecticides, and vulcanization. Therefore produced sulfur is collected and used in a wide range of applications.

28

The chemical reactions taking place in the electrolysis process at the anode and cathode are as follows:

$$H_2S \rightarrow \frac{1}{2}S_2 + 2H^+ + 2e^- \tag{3.4}$$

$$2H^+ + 2e^- \rightarrow H_2 \tag{3.5}$$

The chemical reactions taking place in fuel cell system at the anode and cathode are as follows:

$$H_2 \rightarrow 2H^+ + 2e^- \tag{3.6}$$

$$2H^+ + \frac{1}{2}O_2 + 2e^- \rightarrow H_2O \tag{3.7}$$

CHAPTER 4

SYSTEM ANALYSES

In order to conduct a parametric study and and thermodynamic evaluation of the systems mass, energy, entropy and exergy balance equations are written for each component of the studied systems by employment of Engineering Equation Solver (EES) software. In this way, entropy generations and exergy destructions are determined which provide us to assess the proposed systems in terms of exergy efficiency. In this chapter, detailed analysis of each system is presented, respectively. Before getting the specific system analyses, general balance equations [31] and definitions are given as follows:

The general mass balance equation for the control volume can be expressed as:

$$\sum \dot{m}_{in} = \sum \dot{m}_{out} \tag{4.1}$$

The general energy balance equation for the control volume can be expressed as:

$$\sum \dot{m}_{in} h_{in} + \dot{Q}_{in} + \dot{W}_{in} = \sum \dot{m}_{out} h_{out} + \dot{Q}_{out} + \dot{W}_{out} \tag{4.2}$$

where $\dot{Q}$ and $\dot{W}$ denote the heat transfer and work crossing the component boundaries and $\dot{m}$ and h denote the mass flow rate and the specific enthalpy, respectively.

The steady flow energy balance relation can be expressed for a chemically reacting steady flow system as follows:

$$\dot{Q}_{in} + \dot{W}_{in} + \sum \dot{n}_r \left(\overline{h^0}_f + \overline{h} - \overline{h^0} \right)_r = \dot{Q}_{out} + \dot{W}_{out} + \sum \dot{n}_p \left(\overline{h^0}_f + \overline{h} - \overline{h^0} \right)_p \tag{4.3}$$

where $\overline{h}^o_f$ denotes the enthalpy of formation and $(\overline{h} - \overline{h}^o)$ represents the sensible enthalpy relative to the standard reference state, which is the difference between $\overline{h}$ (sensible

enthalpy at the specified state) and $\bar{h}^o$ (sensible enthalpy at the standard reference state).

The general entropy balance equation for the control volume can be expressed as:

$$\sum \dot{m}_{in} s_{in} + \frac{\dot{Q}_{in}}{T_s} + \dot{S}_{gen} = \sum \dot{m}_{out} s_{out} + \frac{\dot{Q}_{out}}{T_b} \tag{4.4}$$

where $\dot{S}_{gen}$ and s represent the entropy generation rate and the specific entropy, respectively.

The general exergy balance equation for the control volume can be expressed as:

$$\sum \dot{m}_{in} ex_{in} + \dot{Ex}^{Qin} + \dot{W}_{in} = \sum \dot{m}_{out} ex_{out} + \dot{Ex}^{Qout} + \dot{W}_{out} + \dot{Ex}_d \tag{4.5}$$

Here, $\dot{Ex}_d$ and ex represent the exergy destruction rate and the specific exergy, respectively. Also, $\dot{Ex}^Q$ represents the exergy rate due to heat transfer across the system boundaries. The exergy transfer due to heat can be expressed as follows:

$$\dot{Ex}^Q = \dot{Q}\left(1 - \frac{T_0}{T_s}\right) \tag{4.6}$$

The exergy destruction rate is calculated by multiplication of ambient temperature with entropy generation in each component as follows:

$$\dot{Ex}_d = T_0 \times \dot{S}_{gen} \tag{4.7}$$

The exergy term is the sum of physical and chemical exergies as:

$$ex = ex_{ph} + ex_{ch} \tag{4.8}$$

The physical exergy for (i) state can be defined as follows:

$$ex_{ph,i} = h_i - h_0 - T_0\left(s_i - s_0\right) \tag{4.9}$$

4.1   System 1

In order to analyse the system, the following assumptions are made:

- The processes are steady state and steady flow.
- The expansion valves, pumps, compressors and turbines are assumed as adiabatic.
- Ammonia-water is selected as the working fluid of the absorption cooling system.
- Syltherm 800 is chosen as the heat transfer fluid of the solar driven system.
- LiNO$_3$ is chosen as the phase change material.
- n-octane is chosen as the working fluid of the ORC.
- The ambient conditions are 25 °C and 101.3 kPa.
- There is no chemical reaction takes place between the absorbent and refrigerant. Therefore, chemical exergy term is negligible.

Balance equations of the each component of the system 1 are presented in Table 4.1.

Table 4.1 The balance equations of system 1 components

Component	Balance equations
Generator	$\dot{m}_1 = \dot{m}_2$; $\dot{m}_{38} = \dot{m}_{39} + \dot{m}_{42}$
	$\dot{m}_1 h_1 + \dot{m}_{38} h_{38} = \dot{m}_2 h_2 + \dot{m}_{39} h_{39} + \dot{m}_{42} h_{42}$
	$\dot{m}_1 s_1 + \dot{m}_{38} s_{38} + \dot{S}_{gen} = \dot{m}_2 s_2 + \dot{m}_{39} s_{39} + \dot{m}_{42} s_{42}$
	$\dot{m}_1 ex_1 + \dot{m}_{38} ex_{38} = \dot{m}_2 ex_2 + \dot{m}_{39} ex_{39} + \dot{m}_{42} ex_{42} + \dot{Ex}_d$
Condenser 1	$\dot{m}_{31} = \dot{m}_{32}$; $\dot{m}_{48} = \dot{m}_{49}$
	$\dot{m}_{31} h_{31} + \dot{m}_{48} h_{48} = \dot{m}_{32} h_{32} + \dot{m}_{49} h_{49}$
	$\dot{m}_{31} s_{31} + \dot{m}_{48} s_{48} + \dot{S}_{gen} = \dot{m}_{32} s_{32} + \dot{m}_{49} s_{49}$
	$\dot{m}_{31} ex_{31} + \dot{m}_{48} ex_{48} = \dot{m}_{32} ex_{32} + \dot{m}_{49} ex_{49} + \dot{Ex}_d$
Evaporator	$\dot{m}_{33} = \dot{m}_{34}$; $\dot{m}_{46} = \dot{m}_{47}$
	$\dot{m}_{33} h_{33} + \dot{m}_{46} h_{46} = \dot{m}_{34} h_{34} + \dot{m}_{47} h_{47}$
	$\dot{m}_{33} s_{33} + \dot{m}_{46} s_{46} + \dot{S}_{gen} = \dot{m}_{34} s_{34} + \dot{m}_{47} s_{47}$
	$\dot{m}_{33} ex_{33} + \dot{m}_{46} ex_{46} = \dot{m}_{34} ex_{34} + \dot{m}_{47} ex_{47} + \dot{Ex}_d$
Absorber	$\dot{m}_{44} = \dot{m}_{45}$; $\dot{m}_{36} = \dot{m}_{35} + \dot{m}_{41}$
	$\dot{m}_{35} h_{35} + \dot{m}_{41} h_{41} + \dot{m}_{44} h_{44} = \dot{m}_{36} h_{36} + \dot{m}_{45} h_{45}$
	$\dot{m}_{35} s_{35} + \dot{m}_{41} s_{41} + \dot{m}_{44} s_{44} + \dot{S}_{gen} = \dot{m}_{36} s_{36} + \dot{m}_{45} s_{45}$
	$\dot{m}_{35} ex_{35} + \dot{m}_{41} ex_{41} + \dot{m}_{44} ex_{44} = \dot{m}_{36} ex_{36} + \dot{m}_{45} ex_{45} + \dot{Ex}_d$

Table 4.1 The balance equations of system 1 components (continued)

Component	Equations
Heat Exchanger 1	$\dot{m}_{37} = \dot{m}_{38}$; $\dot{m}_{39} = \dot{m}_{40}$
	$\dot{m}_{37}h_{37} + \dot{m}_{39}h_{39} = \dot{m}_{38}h_{38} + \dot{m}_{40}h_{40}$
	$\dot{m}_{37}s_{37} + \dot{m}_{39}s_{39} + \dot{S}_{gen} = \dot{m}_{38}s_{38} + \dot{m}_{40}s_{40}$
	$\dot{m}_{37}ex_{37} + \dot{m}_{39}ex_{39} = \dot{m}_{38}ex_{38} + \dot{m}_{40}ex_{40} + \dot{Ex}_{d}$
Boiler	$\dot{m}_{2} = \dot{m}_{3}$; $\dot{m}_{51} = \dot{m}_{52}$
	$\dot{m}_{2}h_{2} + \dot{m}_{51}h_{51} = \dot{m}_{3}h_{3} + \dot{m}_{52}h_{52}$
	$\dot{m}_{2}s_{2} + \dot{m}_{51}s_{51} + \dot{S}_{gen} = \dot{m}_{3}s_{3} + \dot{m}_{52}s_{52}$
	$\dot{m}_{2}ex_{2} + \dot{m}_{51}ex_{51} = \dot{m}_{3}ex_{3} + \dot{m}_{52}ex_{52} + \dot{Ex}_{d}$
Turbine 1	$\dot{m}_{52} = \dot{m}_{53}$
	$\dot{m}_{52}h_{52} = \dot{m}_{53}h_{53} + \dot{W}_{Turbine}$
	$\dot{m}_{52}s_{52} + \dot{S}_{gen} = \dot{m}_{53}s_{53}$
	$\dot{m}_{52}ex_{52} = \dot{m}_{53}ex_{53} + \dot{W}_{Turbine} + \dot{Ex}_{d}$
Condenser 2	$\dot{m}_{50} = \dot{m}_{53}$; $\dot{m}_{54} = \dot{m}_{55}$
	$\dot{m}_{53}h_{53} + \dot{m}_{54}h_{54} = \dot{m}_{50}h_{50} + \dot{m}_{55}h_{55}$
	$\dot{m}_{53}s_{53} + \dot{m}_{54}s_{54} + \dot{S}_{gen} = \dot{m}_{50}s_{50} + \dot{m}_{55}s_{55}$
	$\dot{m}_{53}ex_{53} + \dot{m}_{54}ex_{54} = \dot{m}_{50}ex_{50} + \dot{m}_{55}ex_{55} + \dot{Ex}_{d}$
Heat Exchanger 2	$\dot{m}_{3} = \dot{m}_{4}$; $\dot{m}_{56} = \dot{m}_{65}$
	$\dot{m}_{3}h_{3} + \dot{m}_{65}h_{65} = \dot{m}_{4}h_{4} + \dot{m}_{56}h_{56}$
	$\dot{m}_{3}s_{3} + \dot{m}_{65}s_{65} + \dot{S}_{gen} = \dot{m}_{4}s_{4} + \dot{m}_{56}s_{56}$
	$\dot{m}_{3}ex_{3} + \dot{m}_{65}ex_{65} = \dot{m}_{4}ex_{4} + \dot{m}_{56}ex_{56} + \dot{Ex}_{d}$
Heat Exchanger 3	$\dot{m}_{62} = \dot{m}_{63}$; $\dot{m}_{66} = \dot{m}_{67}$
	$\dot{m}_{62}h_{62} + \dot{m}_{67}h_{67} = \dot{m}_{63}h_{63} + \dot{m}_{66}h_{66}$
	$\dot{m}_{62}s_{62} + \dot{m}_{67}s_{67} + \dot{S}_{gen} = \dot{m}_{63}s_{63} + \dot{m}_{66}s_{66}$
	$\dot{m}_{62}ex_{62} + \dot{m}_{67}ex_{67} = \dot{m}_{63}ex_{63} + \dot{m}_{66}ex_{66} + \dot{Ex}_{d}$
Parabolic Trough Collector	$\dot{m}_{57} = \dot{m}_{58}$
	$\dot{m}_{57}h_{57} + \dot{Q}_{solar} = \dot{m}_{58}h_{58}$
	$\dot{m}_{57}s_{57} + \dfrac{\dot{Q}_{solar}}{T_{sun}} + \dot{S}_{gen} = \dot{m}_{58}s_{58}$
	$\dot{m}_{57}ex_{57} + \dot{Ex}^{Q_{solar}} = \dot{m}_{58}ex_{58} + \dot{Ex}_{d}$
Direct-Contact Condenser	$\dot{m}_{5} + \dot{m}_{16} + \dot{m}_{19} + \dot{m}_{20} = \dot{m}_{6} + \dot{m}_{21}$
	$\dot{m}_{5}h_{5} + \dot{m}_{16}h_{16} + \dot{m}_{19}h_{19} + \dot{m}_{20}h_{20} = \dot{m}_{6}h_{6} + \dot{m}_{21}h_{21}$
	$\dot{m}_{5}s_{5} + \dot{m}_{16}s_{16} + \dot{m}_{19}s_{19} + \dot{m}_{20}s_{20} + \dot{S}_{gen} = \dot{m}_{6}s_{6} + \dot{m}_{21}s_{21}$

Table 4.1 The balance equations of system 1 components (continued)

	$\dot{m}_5 ex_5 + \dot{m}_{16} ex_{16} + \dot{m}_{19} ex_{19} + \dot{m}_{20} ex_{20} = \dot{m}_6 ex_6 + \dot{m}_{21} ex_{21} + \dot{Ex}_d$
Gas Cooler	$\dot{m}_{15} = \dot{m}_{16}$; $\dot{m}_{21} = \dot{m}_{22}$
	$\dot{m}_{15} h_{15} + \dot{m}_{21} h_{21} = \dot{m}_{16} h_{16} + \dot{m}_{22} h_{22}$
	$\dot{m}_{15} s_{15} + \dot{m}_{21} s_{21} + \dot{S}_{gen} = \dot{m}_{16} s_{16} + \dot{m}_{22} s_{22}$
	$\dot{m}_{15} ex_{15} + \dot{m}_{21} ex_{21} = \dot{m}_{16} ex_{16} + \dot{m}_{22} ex_{22} + \dot{Ex}_d$
Compressor	$\dot{m}_{22} = \dot{m}_{23}$
	$\dot{m}_{22} h_{22} + \dot{W}_{Compressor} = \dot{m}_{23} h_{23}$
	$\dot{m}_{22} s_{22} + \dot{S}_{gen} = \dot{m}_{23} s_{23}$
	$\dot{m}_{22} ex_{22} + \dot{W}_{Compressor} = \dot{m}_{23} ex_{23} + \dot{Ex}_d$
Turbine 2	$\dot{m}_4 = \dot{m}_5$
	$\dot{m}_4 h_4 = \dot{m}_5 h_5 + \dot{W}_{Turbine}$
	$\dot{m}_4 s_4 + \dot{S}_{gen} = \dot{m}_5 s_5$
	$\dot{m}_4 ex_4 = \dot{m}_5 ex_5 + \dot{W}_{Turbine} + \dot{Ex}_d$
Water Preheater	$\dot{m}_{77} = \dot{m}_{78}$; $\dot{m}_{74} = \dot{m}_{75}$
	$\dot{m}_{74} h_{74} + \dot{m}_{77} h_{77} = \dot{m}_{75} h_{75} + \dot{m}_{78} h_{78}$
	$\dot{m}_{74} s_{74} + \dot{m}_{77} s_{77} + \dot{S}_{gen} = \dot{m}_{75} s_{75} + \dot{m}_{78} s_{78}$
	$\dot{m}_{74} ex_{74} + \dot{m}_{77} ex_{77} = \dot{m}_{75} ex_{75} + \dot{m}_{78} ex_{78} + \dot{Ex}_d$
Pump 1	$\dot{m}_{36} = \dot{m}_{37}$
	$\dot{m}_{36} h_{36} + \dot{W}_{Pump} = \dot{m}_{37} h_{37}$
	$\dot{m}_{36} s_{36} + \dot{S}_{gen} = \dot{m}_{37} s_{37}$
	$\dot{m}_{36} ex_{36} + \dot{W}_{Pump} = \dot{m}_{37} ex_{37} + \dot{Ex}_d$
Pump 2	$\dot{m}_{50} = \dot{m}_{51}$
	$\dot{m}_{50} h_{50} + \dot{W}_{Pump} = \dot{m}_{51} h_{51}$
	$\dot{m}_{50} s_{50} + \dot{S}_{gen} = \dot{m}_{51} s_{51}$
	$\dot{m}_{50} ex_{50} + \dot{W}_{Pump} = \dot{m}_{51} ex_{51} + \dot{Ex}_d$
Cooling Water Pump	$\dot{m}_6 = \dot{m}_7$
	$\dot{m}_6 h_6 + \dot{W}_{Pump} = \dot{m}_7 h_7$
	$\dot{m}_6 s_6 + \dot{S}_{gen} = \dot{m}_7 s_7$
	$\dot{m}_6 ex_6 + \dot{W}_{Pump} = \dot{m}_7 ex_7 + \dot{Ex}_d$
Expansion Valve 1	$\dot{m}_{40} = \dot{m}_{41}$
	$\dot{m}_{40} h_{40} = \dot{m}_{41} h_{41}$
	$\dot{m}_{40} s_{40} + \dot{S}_{gen} = \dot{m}_{41} s_{41}$

Table 4.1 The balance equations of system 1 components (continued)

	$\dot{m}_{40}ex_{40} = \dot{m}_{41}ex_{41} + \dot{Ex}_d$
Expansion Valve 2	$\dot{m}_{32} = \dot{m}_{33}$
	$\dot{m}_{32}h_{32} = \dot{m}_{33}h_{33}$
	$\dot{m}_{32}s_{32} + \dot{S}_{gen} = \dot{m}_{33}s_{33}$
	$\dot{m}_{32}ex_{32} = \dot{m}_{33}ex_{33} + \dot{Ex}_d$

4.1.1   Energy Efficiency Definitions for System 1

For the studied systems, the energy efficiency term is defined as the division of useful energy output to the total energy input. The energy efficiency definitions are given for system 1 as follows:

The energy efficiency of the organic Rankine cycle can be defined by,

$$\eta_{ORC} = \frac{\dot{W}_{net} + \dot{Q}_{Cooling}}{(\dot{m}_2 h_2 - \dot{m}_3 h_3)} \tag{4.10}$$

Energetic COP of the absorption cooling system can be given as:

$$COP_{en,ACS} = \frac{\dot{Q}_{evaporator}}{\dot{Q}_{generator} + \dot{W}_{pump,1}} \tag{4.11}$$

By taking into consideration all useful commodities and total energy inputs, the overall energy efficiency of system 1 can be written as follows:

$$\eta_{overall} = \frac{\dot{W}_{net} + \dot{Q}_{Heating} + \dot{Q}_{Drying} + \dot{Q}_{Cooling} + \dot{m}_{H2,PEM} \times LHV_{H_2} + \dot{m}_{H2,electrolyzer} \times h_{H_2}}{\dot{E}^{Geo} + \dot{E}^{Solar}} \tag{4.12}$$

where $\dot{Q}_{Heating}$ is the sum of domestic hot water and space heating outputs of the designed system. Also, $\dot{Q}_{Drying}$ denotes the total drying heat which is provided through the heated air which leaves the cooling tower at state (29).

4.1.2   Exergy Efficiency Definitions for System 1

For the studied systems, the exergy efficiency term is defined as the division of useful exergy output to the total exergy input. The exergy efficiency definitions are given for system 1 as follows:

The exergy efficiency of the organic Rankine cycle can be defined by,

$$\psi_{ORC} = \frac{\dot{W}_{net} + \dot{E}x^{Q_{Cooling}}}{\left(\dot{m}_2 ex_2 - \dot{m}_3 ex_3\right)} \tag{4.13}$$

Exergetic COP of the absorption cooling system can be given as:

$$COP_{ex,ACS} = \frac{\dot{E}x^{Q_{Evaporator}}}{\dot{E}x^{Q_{generator}} + \dot{W}_{pump,1}} \tag{4.14}$$

Overall exergy efficiency of the designed system also can be written as:

$$\psi_{overall} = \frac{\dot{W}_{net} + \dot{E}x^{Q_{Heating}} + \dot{E}x^{Q_{Drying}} + \dot{E}x^{Q_{Cooling}} + \dot{m}_{H_2} \times \left(ex_{ph} + ex_{ch}\right)_{H_2}}{\dot{E}x^{Q_{Geo}} + \dot{E}x^{Q_{Solar}}} \tag{4.15}$$

In addition, the main assumptions of system 1 are given in Table 4.2.

Table 4.2 The data used for system 1

Parameter	Value
Mass flow rate of the geothermal steam; $\dot{m}_1$	60 kg/s
Inlet temperature of geothermal steam; T_1	515 K
Inlet pressure of geothermal steam; P_1	2000 kPa
Ambient temperature, T_0	298 K
Ambient pressure, P_0	101.325 kPa
Temperature of the sun, T_{sun}	6000 K
Average hourly solar radiation during the charging period, $I_{av,c}$	2.16 MJ/m^{2}h
Average hourly solar radiation during the storing period, $I_{av,s}$	1.26 MJ/m^{2}h
Average hourly solar radiation during the discharging period, $I_{av,d}$	0.36 MJ/m^{2}h
Charging period, $t_{charging}$	7 h
Storing period, $t_{storing}$	10 h
Discharging period, $t_{discharging}$	7 h
Width of the collector	4 m
Length of the collector	50 m
Reflection rate	0.8

4.2 System 2

The assumptions made for the analysis of system 2 are listed as follows:

- The processes are steady state and steady flow.
- The expansion valves, pumps, compressors and turbines are assumed as adiabatic.

- Ammonia-water is selected as the working fluid of the absorption cooling system.

- Syltherm 800 is chosen as the heat transfer fluid of the solar driven system.

- The ambient conditions are 25 °C and 101.3 kPa.

- There is no chemical reaction takes place between the absorbent and refrigerant. Therefore, chemical exergy term is negligible.

Balance equations of the each component of the system 2 are presented in Table 4.3.

Table 4.3 The balance equations of system 2 components

Component	Balance equations
HP Turbine	$\dot{m}_3 = \dot{m}_4$
	$\dot{m}_3 h_3 = \dot{m}_4 h_4 + \dot{W}_{Turbine}$
	$\dot{m}_3 s_3 + \dot{S}_{gen} = \dot{m}_4 s_4$
	$\dot{m}_3 ex_3 = \dot{m}_4 ex_4 + \dot{W}_{Turbine} + \dot{Ex}_d$
LP Turbine	$\dot{m}_5 = \dot{m}_6$
	$\dot{m}_5 h_5 = \dot{m}_6 h_6 + \dot{W}_{Turbine}$
	$\dot{m}_5 s_5 + \dot{S}_{gen} = \dot{m}_6 s_6$
	$\dot{m}_5 ex_5 = \dot{m}_6 ex_6 + \dot{W}_{Turbine} + \dot{Ex}_d$
Heat Exchanger 1	$\dot{m}_6 = \dot{m}_{11}$; $\dot{m}_{12} = \dot{m}_{14}$
	$\dot{m}_6 h_6 + \dot{m}_{14} h_{14} = \dot{m}_{11} h_{11} + \dot{m}_{12} h_{12} + \dot{Q}_{losses}$
	$\dot{m}_6 s_6 + \dot{m}_{14} s_{14} + \dot{S}_{gen} = \dot{m}_{11} s_{11} + \dot{m}_{12} s_{12} + \dfrac{\dot{Q}_{losses}}{T_b}$
	$\dot{m}_6 ex_6 + \dot{m}_{14} ex_{14} = \dot{m}_{11} ex_{11} + \dot{m}_{12} ex_{12} + \dot{Ex}^{Q_{losses}} + \dot{Ex}_d$
Pump 1	$\dot{m}_{12} = \dot{m}_{13}$
	$\dot{m}_{12} h_{12} + \dot{W}_{Pump} = \dot{m}_{13} h_{13}$
	$\dot{m}_{12} s_{12} + \dot{S}_{gen} = \dot{m}_{13} s_{13}$
	$\dot{m}_{12} ex_{12} + \dot{W}_{Pump} = \dot{m}_{13} ex_{13} + \dot{Ex}_d$
Parabolic Trough Collector	$\dot{m}_{13} = \dot{m}_{14}$
	$\dot{m}_{13} h_{13} + \dot{Q}_{solar} = \dot{m}_{14} h_{14}$
	$\dot{m}_{13} s_{13} + \dfrac{\dot{Q}_{solar}}{T_{sun}} + \dot{S}_{gen} = \dot{m}_{14} s_{14}$
	$\dot{m}_{13} ex_{13} + \dot{Ex}^{Q_{solar}} = \dot{m}_{14} ex_{14} + \dot{Ex}_d$
Generator	$\dot{m}_{11} = \dot{m}_{15}$; $\dot{m}_{23} = \dot{m}_{24} + \dot{m}_{27}$

Table 4.3 The balance equations of system 2 components (continued)

	$\dot{m}_{11}h_{11} + \dot{m}_{23}h_{23} = \dot{m}_{15}h_{15} + \dot{m}_{24}h_{24} + \dot{m}_{27}h_{27}$
	$\dot{m}_{11}s_{11} + \dot{m}_{23}s_{23} + \dot{S}_{gen} = \dot{m}_{15}s_{15} + \dot{m}_{24}s_{24} + \dot{m}_{27}s_{27}$
	$\dot{m}_{11}ex_{11} + \dot{m}_{23}ex_{23} = \dot{m}_{15}ex_{15} + \dot{m}_{24}ex_{24} + \dot{m}_{27}ex_{27} + \dot{E}x_d$
Condenser 1	$\dot{m}_{16} = \dot{m}_{17}$; $\dot{m}_{33} = \dot{m}_{34}$
	$\dot{m}_{16}h_{16} + \dot{m}_{33}h_{33} = \dot{m}_{17}h_{17} + \dot{m}_{34}h_{34}$
	$\dot{m}_{16}s_{16} + \dot{m}_{33}s_{33} + \dot{S}_{gen} = \dot{m}_{17}s_{17} + \dot{m}_{34}s_{34}$
	$\dot{m}_{16}ex_{16} + \dot{m}_{33}ex_{33} = \dot{m}_{17}ex_{17} + \dot{m}_{34}ex_{34} + \dot{E}x_d$
Evaporator	$\dot{m}_{18} = \dot{m}_{19}$; $\dot{m}_{31} = \dot{m}_{32}$
	$\dot{m}_{18}h_{18} + \dot{m}_{31}h_{31} = \dot{m}_{19}h_{19} + \dot{m}_{32}h_{32}$
	$\dot{m}_{18}s_{18} + \dot{m}_{31}s_{31} + \dot{S}_{gen} = \dot{m}_{19}s_{19} + \dot{m}_{32}s_{32}$
	$\dot{m}_{18}ex_{18} + \dot{m}_{31}ex_{31} = \dot{m}_{19}ex_{19} + \dot{m}_{32}ex_{32} + \dot{E}x_d$
Absorber	$\dot{m}_{29} = \dot{m}_{30}$; $\dot{m}_{21} = \dot{m}_{20} + \dot{m}_{26}$
	$\dot{m}_{20}h_{20} + \dot{m}_{26}h_{26} + \dot{m}_{29}h_{29} = \dot{m}_{21}h_{21} + \dot{m}_{30}h_{30}$
	$\dot{m}_{20}s_{20} + \dot{m}_{26}s_{26} + \dot{m}_{29}s_{29} + \dot{S}_{gen} = \dot{m}_{21}s_{21} + \dot{m}_{30}s_{30}$
	$\dot{m}_{20}ex_{20} + \dot{m}_{26}ex_{26} + \dot{m}_{29}ex_{29} = \dot{m}_{21}ex_{21} + \dot{m}_{30}ex_{30} + \dot{E}x_d$
Heat Exchanger 2	$\dot{m}_{22} = \dot{m}_{23}$; $\dot{m}_{24} = \dot{m}_{25}$
	$\dot{m}_{22}h_{22} + \dot{m}_{24}h_{24} = \dot{m}_{23}h_{23} + \dot{m}_{25}h_{25}$
	$\dot{m}_{22}s_{22} + \dot{m}_{24}s_{24} + \dot{S}_{gen} = \dot{m}_{23}s_{23} + \dot{m}_{25}s_{25}$
	$\dot{m}_{22}ex_{22} + \dot{m}_{24}ex_{24} = \dot{m}_{23}ex_{23} + \dot{m}_{25}ex_{25} + \dot{E}x_d$
Boiler	$\dot{m}_{15} = \dot{m}_{35}$; $\dot{m}_{36} = \dot{m}_{37}$
	$\dot{m}_{15}h_{15} + \dot{m}_{36}h_{36} = \dot{m}_{35}h_{35} + \dot{m}_{37}h_{37}$
	$\dot{m}_{15}s_{15} + \dot{m}_{36}s_{36} + \dot{S}_{gen} = \dot{m}_{35}s_{35} + \dot{m}_{37}s_{37}$
	$\dot{m}_{15}ex_{15} + \dot{m}_{36}ex_{36} = \dot{m}_{35}ex_{35} + \dot{m}_{37}ex_{37} + \dot{E}x_d$
Turbine 1	$\dot{m}_{37} = \dot{m}_{38}$
	$\dot{m}_{37}h_{37} = \dot{m}_{38}h_{38} + \dot{W}_{Turbine}$
	$\dot{m}_{37}s_{37} + \dot{S}_{gen} = \dot{m}_{38}s_{38}$
	$\dot{m}_{37}ex_{37} = \dot{m}_{38}ex_{38} + \dot{W}_{Turbine} + \dot{E}x_d$
Condenser 2	$\dot{m}_{38} = \dot{m}_{39}$; $\dot{m}_{40} = \dot{m}_{41}$
	$\dot{m}_{38}h_{38} + \dot{m}_{40}h_{40} = \dot{m}_{39}h_{39} + \dot{m}_{41}h_{41}$
	$\dot{m}_{38}s_{38} + \dot{m}_{40}s_{40} + \dot{S}_{gen} = \dot{m}_{39}s_{39} + \dot{m}_{41}s_{41}$
	$\dot{m}_{38}ex_{38} + \dot{m}_{40}ex_{40} = \dot{m}_{39}ex_{39} + \dot{m}_{41}ex_{41} + \dot{E}x_d$

Table 4.3 The balance equations of system 2 components (continued)

Direct-Contact Condenser	$\dot{m}_{42} + \dot{m}_{53} + \dot{m}_{56} + \dot{m}_{57} = \dot{m}_{43} + \dot{m}_{58}$
	$\dot{m}_{42}h_{42} + \dot{m}_{53}h_{53} + \dot{m}_{56}h_{56} + \dot{m}_{57}h_{57} = \dot{m}_{43}h_{43} + \dot{m}_{58}h_{58}$
	$\dot{m}_{42}s_{42} + \dot{m}_{53}s_{53} + \dot{m}_{56}s_{56} + \dot{m}_{57}s_{57} + \dot{S}_{gen} = \dot{m}_{43}s_{43} + \dot{m}_{58}s_{58}$
	$\dot{m}_{42}ex_{42} + \dot{m}_{53}ex_{53} + \dot{m}_{56}ex_{56} + \dot{m}_{57}ex_{57} = \dot{m}_{43}ex_{43} + \dot{m}_{58}ex_{58} + \dot{Ex}_d$
Gas Cooler	$\dot{m}_{52} = \dot{m}_{53}\,;\ \dot{m}_{58} = \dot{m}_{59}$
	$\dot{m}_{52}h_{52} + \dot{m}_{58}h_{58} = \dot{m}_{53}h_{53} + \dot{m}_{59}h_{59} + \dot{Q}_{losses}$
	$\dot{m}_{52}s_{52} + \dot{m}_{58}s_{58} + \dot{S}_{gen} = \dot{m}_{53}s_{53} + \dot{m}_{59}s_{59} + \dfrac{\dot{Q}_{losses}}{T_b}$
	$\dot{m}_{52}ex_{52} + \dot{m}_{58}ex_{58} = \dot{m}_{53}ex_{53} + \dot{m}_{59}ex_{59} + \dot{Ex}^{Q_{losses}} + \dot{Ex}_d$
Compressor	$\dot{m}_{59} = \dot{m}_{60}$
	$\dot{m}_{59}h_{59} + \dot{W}_{Compressor} = \dot{m}_{60}h_{60}$
	$\dot{m}_{59}s_{59} + \dot{S}_{gen} = \dot{m}_{60}s_{60}$
	$\dot{m}_{59}ex_{59} + \dot{W}_{Compressor} = \dot{m}_{60}ex_{60} + \dot{Ex}_d$
Turbine 2	$\dot{m}_{35} = \dot{m}_{42}$
	$\dot{m}_{35}h_{35} = \dot{m}_{42}h_{42} + \dot{W}_{Turbine}$
	$\dot{m}_{35}s_{35} + \dot{S}_{gen} = \dot{m}_{42}s_{42}$
	$\dot{m}_{35}ex_{35} = \dot{m}_{42}ex_{42} + \dot{W}_{Turbine} + \dot{Ex}_d$
Water Preheater	$\dot{m}_{69} = \dot{m}_{70}\,;\ \dot{m}_{72} = \dot{m}_{73}$
	$\dot{m}_{69}h_{69} + \dot{m}_{72}h_{72} = \dot{m}_{70}h_{70} + \dot{m}_{73}h_{73} + \dot{Q}_{losses}$
	$\dot{m}_{69}s_{69} + \dot{m}_{72}s_{72} + \dot{S}_{gen} = \dot{m}_{70}s_{70} + \dot{m}_{73}s_{73} + \dfrac{\dot{Q}_{losses}}{T_b}$
	$\dot{m}_{69}ex_{69} + \dot{m}_{72}ex_{72} = \dot{m}_{70}ex_{70} + \dot{m}_{73}ex_{73} + \dot{Ex}^{Q_{losses}} + \dot{Ex}_d$
Pump 1	$\dot{m}_{12} = \dot{m}_{13}$
	$\dot{m}_{12}h_{12} + \dot{W}_{Pump} = \dot{m}_{13}h_{13}$
	$\dot{m}_{12}s_{12} + \dot{S}_{gen} = \dot{m}_{13}s_{13}$
	$\dot{m}_{12}ex_{12} + \dot{W}_{Pump} = \dot{m}_{13}ex_{13} + \dot{Ex}_d$
Pump 2	$\dot{m}_{21} = \dot{m}_{22}$
	$\dot{m}_{21}h_{21} + \dot{W}_{Pump} = \dot{m}_{22}h_{22}$
	$\dot{m}_{21}s_{21} + \dot{S}_{gen} = \dot{m}_{22}s_{22}$
	$\dot{m}_{21}ex_{21} + \dot{W}_{Pump} = \dot{m}_{22}ex_{22} + \dot{Ex}_d$

Table 4.3 The balance equations of system 2 components (continued)

Cooling Water Pump	$\dot{m}_{43} = \dot{m}_{44}$
	$\dot{m}_{43}h_{43} + \dot{W}_{Pump} = \dot{m}_{44}h_{44}$
	$\dot{m}_{43}s_{43} + \dot{S}_{gen} = \dot{m}_{44}s_{44}$
	$\dot{m}_{43}ex_{43} + \dot{W}_{Pump} = \dot{m}_{44}ex_{44} + \dot{Ex}_d$
Expansion Valve 1	$\dot{m}_{25} = \dot{m}_{26}$
	$\dot{m}_{25}h_{25} = \dot{m}_{26}h_{26}$
	$\dot{m}_{25}s_{25} + \dot{S}_{gen} = \dot{m}_{26}s_{26}$
	$\dot{m}_{25}ex_{25} = \dot{m}_{26}ex_{26} + \dot{Ex}_d$
Expansion Valve 2	$\dot{m}_{17} = \dot{m}_{18}$
	$\dot{m}_{17}h_{17} = \dot{m}_{18}h_{18}$
	$\dot{m}_{17}s_{17} + \dot{S}_{gen} = \dot{m}_{18}s_{18}$
	$\dot{m}_{17}ex_{17} = \dot{m}_{18}ex_{18} + \dot{Ex}_d$

4.2.1 Energy Efficiency Definitions for System 2

Energetic COP of the absorption cooling system can be given as:

$$COP_{en,ACS} = \frac{\dot{Q}_{evaporator}}{\dot{Q}_{generator} + \dot{W}_{pump,2}} \tag{4.16}$$

By taking into consideration all useful commodities and total energy inputs, the overall energy efficiency of system 2 can be written as follows:

$$\eta_{overall} = \frac{\dot{W}_{net} + \dot{Q}_{Heating} + \dot{Q}_{Cooling} + \dot{m}_{H_2,PEM} \times LHV_{H_2} + \dot{m}_{H_2,electrolyzer} \times h_{H_2}}{\dot{E}^{Geo} + \dot{E}^{Solar} + \dot{E}^{Wind}} \tag{4.17}$$

where $\dot{Q}_{Heating}$ is the sum of domestic hot water and space heating outputs of the designed system.

4.2.2 Exergy Efficiency Definitions for System 2

Exergetic COP of the absorption cooling system can be given as:

$$COP_{ex,ACS} = \frac{\dot{Ex}^{Q_{Evaporator}}}{\dot{Ex}^{Q_{generator}} + \dot{W}_{pump,2}} \tag{4.18}$$

Overall exergy efficiency of the designed system also can be written as:

$$\psi_{overall} = \frac{\dot{W}_{net} + \dot{Ex}^{Q_{Heating}} + \dot{Ex}^{Q_{Cooling}} + \dot{m}_{H_2} \times \left(ex_{ph} + ex_{ch}\right)_{H_2}}{\dot{Ex}^{Q_{Geo}} + \dot{Ex}^{Q_{Solar}} + \dot{Ex}^{Wind}} \qquad (4.19)$$

In addition, the main assumptions of system 2 are given in Table 4.4.

Table 4.4 The data used for system 2

Parameter	Value
Mass flow rate of the geothermal steam; $\dot{m}_1$	60 kg/s
Inlet temperature of geothermal steam; T_1	515.7 K
Inlet pressure of geothermal steam; P_1	3500 kPa
Ambient temperature, T_0	298 K
Ambient pressure, P_0	101.325 kPa
Temperature of the sun, T_{sun}	6000 K
Average hourly solar radiation, I_{av}	2.16 MJ/m^{2}h
Width of the collector	4 m
Length of the collector	50 m
Reflection rate	0.8
Blade length of wind turbine	8 m
Inlet velocity of the wind to the wind turbine	7.5 m/s
Outlet velocity of the wind from the wind turbine	2.5 m/s
The number of wind turbines	50
Wind Turbine conversion efficiency	80%

4.3 System 3

In this section, before analyzing the whole system through energy and exergy approaches, detailed information is given about packed bed thermal storage system, underground cavern system, solar-driven system, and gasifier and combustion chambers, respectively.

4.3.1 Packed Bed Thermal Storage System

In the compressed air energy storage system calculations, it is important to take into consideration heat losses during all three periods. In the existing system, prior to entering the compressed air to the underground cavern, it flows through the packed bed storage system so as to transfer its own energy to the packed rock. Before getting into packed bed thermal storage system analyses, design parameters of the system are determined as shown in Table 4.5. The following assumptions are made for analysis and assessment:

- The processes take place in the packed bed thermal storage system are assumed to be steady-state and steady-flow.
- Packed bed system is well-insulated and the heat transfer to/from ambient is neglected.
- At the end of the storage period, there will be uniform temperatures through the rock bed.
- The convection heat transfer coefficient is constant.
- Pressure drops in the pipes are neglected.
- Fluid and packed rock properties are constant.
- Flow regime in both charging and discharging pipes is turbulent (Re > 10000).
- The inner surfaces of the pipes are smooth.

Table 4.5 The design parameters of the packed bed thermal storage system

Parameter	Value
Radius of the charging and discharging pipes, r	0.25 m
Length of the packed bed system, H	100 m
Radius of the packed rock, R	1 m
Distance between the charging and discharging pipes, b	0.5 m
Initial temperature of the rock, T_{ir}	298 K

The heat transfer problem in the packed bed thermal storage system is the sum of the internal forced convection which occurs inside the pipe and heat conduction which takes place through the pipe thickness and the packed rock. Heat transfer equations related to the turbulent internal forced convection can be defined as follows [32]:

$$Re = \frac{V_m \times D}{\nu_{air}} \qquad (4.20)$$

where V_m is the mean fluid velocity, D is the inner diameter of the pipe and ν_{air} is the kinematic viscosity of the air.

$$Nu = \frac{\left(\dfrac{f}{8}\right) \times (Re - 1000) \times Pr}{1 + 12.7 \times \left(\dfrac{f}{8}\right)^{0.5} \times (Pr^{\frac{2}{3}} - 1)} \qquad (0.5 \leq Pr \leq 2000); \ (3 \times 10^3 < Re < 5 \times 10^6) \qquad (4.21)$$

Here, Pr is the Prandtl number, and f is the friction factor in turbulent flow which can be determined from the *Petukhov equation* given as:

Smooth tubes: $f = (0.790 \ln Re - 1.64)^{-2}$ $\qquad (10^4 < Re < 10^6)$ $\qquad\qquad$ (4.22)

In a circular tube Nusselt number can be also defined as:

$$Nu = \frac{h_c \times D}{k_{air}} \qquad\qquad\qquad (4.23)$$

Here, h_c represents the convection heat transfer coefficient of the charging period and k_{air} denotes the thermal conductivity of the air.

The exit temperature of the air from the packed bed system (T_{ec}) can be written as:

$$T_{ec} = T_s - (T_s - T_{ic}) \exp\left(\frac{-h_c A_s}{\dot{m} C_p}\right) \qquad\qquad (4.24)$$

where T_{ic} is the inlet temperature of the air to packed bed system, A_s is the heat transfer surface area, C_p is the specific heat of the air and T_s is the surface temperature of the charging pipe.

The rate of heat transfer from the air to the packed rock can be defined as follows:

$$\dot{Q}_1 = h_c \times A_s \times \Delta T_{ln} \qquad\qquad (4.25)$$

where ΔT_{ln} is the logarithmic mean temperature difference and can be determined accordingly.

$$\Delta T_{ln} = \frac{(T_{ic} - T_{ec})}{\ln\left(\dfrac{T_s - T_{ec}}{T_s - T_{ic}}\right)} \qquad\qquad (4.26)$$

The total amount of heat which transfers to the packed rock during the charging period can be calculated as:

$$Q_1 = t_{charging} \times \dot{Q}_1 \qquad\qquad (4.27)$$

where $t_{charging}$ denotes the charging period.

Final temperature of the rock at the end of the storing period (T_{fr}) can be determined as:

$$Q_1 = \rho_{rock} \times V_{rock} \times c_{rock} \times (T_{fr} - T_{ir}) \qquad\qquad (4.28)$$

Here, ρ_{rock}, V_{rock}, c_{rock} represent the density, volume and specific heat of the rock, respectively. Also, T_{ir} is the temperature value of the rock at the beginning of the charging period. Volume of the rock can be determined from (Figure 4.1):

$$V_{rock} = (\pi R^2 - 2\pi r^2) \times H \tag{4.29}$$

$$R = \frac{b}{2} + 2r + a \tag{4.30}$$
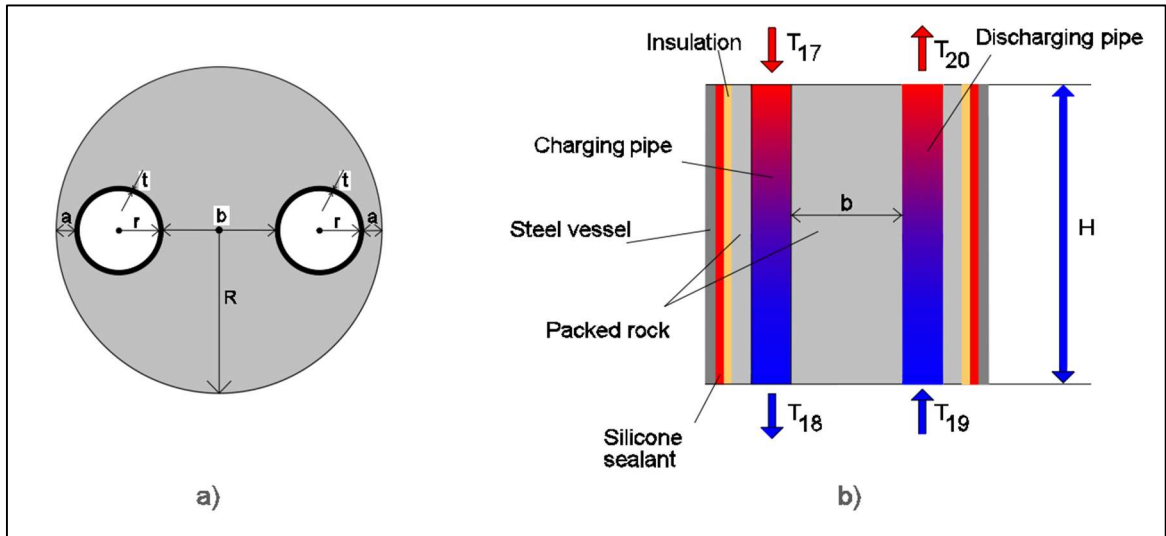
Figure 4.1 (a) Top view of the packed bed storage system (b) Front view of the packed bed storage system with dimensions

The outlet temperature of the air from the packed bed system during the discharging period (T_{op}) can be found from:

$$T_{op} = T_{fr} - (T_{fr} - T_{ip})\exp\left(\frac{-h_d A_s}{\dot{m} C_p}\right) \tag{4.31}$$

where h_d represents the convection heat transfer coefficient of the discharging period. Also, T_{ip} is the inlet temperature of the air into the packed bed during the discharging period.

In the present study, although packed rock material is chosen as limestone, three different rock properties are given in Table 4.6 in order to conduct a comparative study.

Table 4.6 The rock properties of the packed bed thermal storage system [33].

Rock type	Density (kg/m³)	Specific heat (kJ/kgK)	Thermal Conductivity (W/mK)
Limestone	2700	0.91	3
Sandstone	2550	0.844	2.5
Siltstone	2550	0.795	1.58

4.3.2 Underground Cavern System

In order to evaluate the compressed air storage system performance, heat losses of the underground cavern should be determined. In the underground cavern, time-depended heat conduction will take place. In the considered system, the stored air in the underground cavern is surrounded with the soil. Due to the temperature difference, heat will flow from the air causing its temperature to change over time. At the end of this time dependent process a new steady-state temperature distribution will develop. Before getting into the underground cavern system analyses, the following assumptions are made for the specific analysis.

- The thermal properties of the soil are constant.
- Heat transfer mechanism inside the underground cavern is modelled according to the natural convection principle and the upper surface of the underground cavern is assumed as a horizontal plane.
- Both charging and discharging pipes are well-insulated and heat losses from the pipes are neglected.
- The thermal properties of the air and the heat transfer coefficient are constant.
- Underground cavern is modelled as a cylinder (Figure 4.2).
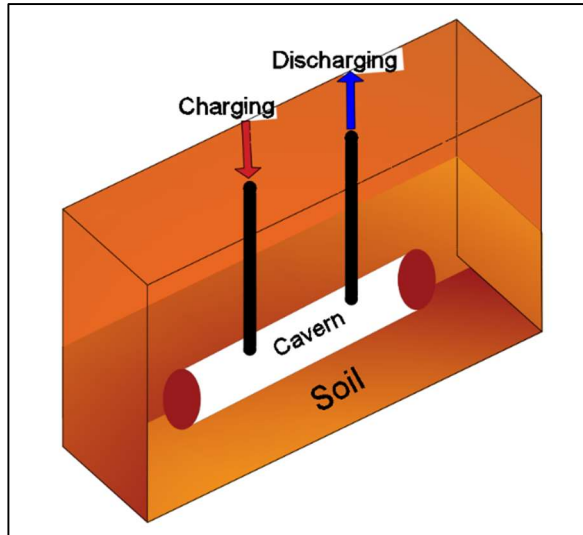
Figure 4.2 3D modelling of the underground cavern

The soil temperature change depending on the ambient temperature can be written as follows [32]:

$$\frac{T(x,t) - T_{is}}{T_a - T_{is}} = \text{erfc}\left(\frac{x}{2\sqrt{at}}\right) \tag{4.32}$$

where $T(x,t)$ is the one-dimensional time-dependent temperature of the soil, T_{is} is the initial temperature of the soil at depth x, T_a is the ambient temperature, x is the depth of the soil from the earth surface which surrounds the underground cavern which is illustrated in Figure 4.3.
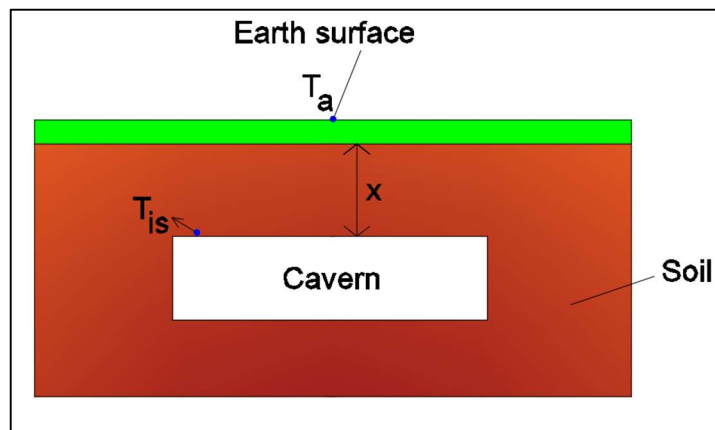
Figure 4.3 Schematic illustration of the underground cavern

$$\varepsilon = \frac{x}{2\sqrt{at}} \tag{4.33}$$

The heat transfer mechanism inside the underground cavern is modelled according to natural convection principle and upper surface of the underground cavern is assumed as a horizontal plane. After this behavior modelling, convection heat transfer coefficient of the air inside the underground cavern can be found as:

$$Ra_L = \frac{g\beta(T_{soil} - T_{air})L_c^3\,Pr}{\nu_{air}^2} \tag{4.34}$$

Here, g denotes the gravitational acceleration, β is the coefficient of volume expansion, L_c is the characteristic length of the underground cavern.

$$Nu_L = 0.15 \times Ra_L^{1/3} \quad (10^7 \leq Ra_L \leq 10^{11}) \tag{4.35}$$

In the present study, underground cavern is modelled as a cylinder and transient heat transfer problem equations related to the underground cavern can be given as follows:

$$Bi = \frac{h_{na} \times r_c}{k} \tag{4.36}$$

where h_{na} is the natural convection heat transfer coefficient in the underground cavern which can be found via (4.35) numbered equation. In addition, r_c and k represent radius of the underground cavern and thermal conductivity of the air, respectively. Dimensionless time (Fourier number) can be defined for a cylinder:

$$\tau = \frac{at}{r_c^2} \tag{4.37}$$

$$\theta_{0,\,cyl} = \frac{(T_0 - T_{soil})}{(T_i - T_{soil})} = A_1\,e^{-\lambda_1^2\tau} \tag{4.38}$$

where T_{soil} is the soil temperature which surrounds the underground cavern and is assumed as constant. Also, T_i is the initial temperature of the air which is the inlet temperature of the air to the underground cavern during the charging period. On the other side, T_0 denotes the center temperature of the air in the underground cavern. A_1 and λ_1 can be determined from the related table [32] depending on the Bi number for a cylinder.

$$\left(\frac{Q_{ca}}{Q_{max}}\right)_{cyl} = 1 - 2Q_{0,\,cyl}\frac{J_1(\lambda_1)}{\lambda_1} \tag{4.39}$$

where J represents the Bessel function and can be determined for a cylinder from the related table [32]. Also, Q_{max} is the maximum amount of heat that the underground cavern loses and can be found,

$$Q_{max} = m \times C_p \times (T_i - T_{soil})$$ (4.40)

Here, m and C_p denote the total mass and specific heat of the air, respectively. All in all, heat losses in the underground cavern (Q_{ca}) can be determined from the (4.39) numbered equation.

4.3.3 The Solar Driven System

The solar-driven system comprises parabolic trough collectors and two storage tanks. The solar-driven system including several huge parabolic trough collectors can transfer the solar energy to the heat transfer fluid. A parabolic collector can operate with solar beam and also diffusing of radiation because of its large acceptance angle. Power received by PTC can be calculated as follows:

$$\dot{Q}_{ptc} = I_{av} \times A_a \times \gamma_c$$ (4.41)

Here, I_{av}, A_a, γ_c are the average hourly solar radiation, collector aperture area and reflection rate of the collector, respectively. Average hourly solar radiation value varies with the time and location. Aperture area of the collector can be calculated from the following equation.

$$A_a = w_c \times l_c$$ (4.42)

where w_c and l_c are the aperture width and length of the collector, respectively. Schematic illustration of the parabolic trough collector system is shown in Figure 4.4. The respective design parameters of the parabolic trough collector system are listed in Table 4.7.
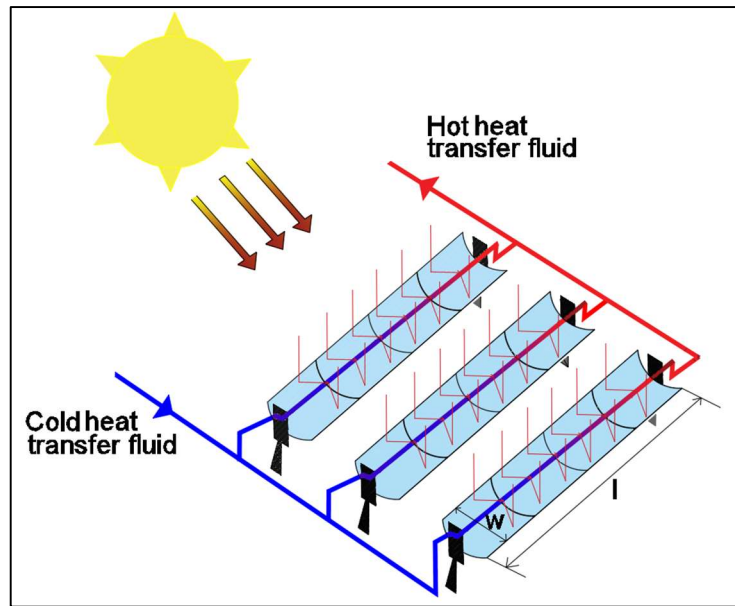
Figure 4.4 Schematic illustration of the parabolic trough collector system

Table 4.7 The design parameters of the parabolic trough collector system

Parameter	Value
Width of the collector, w_c	4 m
Length of the collector, l_c	80 m
Reflection rate, γ_c	0.8
Average hourly solar radiation during the charging period, $I_{av,c}$	0.6 MJ/m²h
Average hourly solar radiation during the storing period, $I_{av,s}$	1.08 MJ/m²h
Average hourly solar radiation during the discharging period, $I_{av,d}$	0.36 MJ/m²h

Due to the intermittency of the solar energy, two storage tanks are integrated to the solar-driven system. Inside the hot storage tank filled with phase change material and heat transfer fluid flows through the hot storage tank via pipe coils. Both latent and sensible heat storage take place into the storage tank. In order to determine and compare the effect of phase change material properties on the storage performance, different types of phase change materials are chosen as listed in Table 4.8.

Table 4.8 The thermal properties of the phase change materials [34].

Phase change material	Mol (%)	Freezing/Melting point (K)	$C_{ps,av}$ (kJ/kgK)	$C_{pl,av}$ (kJ/kgK)	(ΔH_m) (kJ/kg)
$LiNO_3$	100	528	1.20	1.84	372
$NaNO_3$	100	580	1.12	1.51	180
$LiNO_3$-$NaNO_3$-KNO_3	38-15-47	400	1.50	1.63	136

The total heat stored by a solid to liquid phase changing material between initial and final temperatures would be estimated by [28]:

$$q_{stored} = mC_{ps,av}(T_m - T_i) + m\Delta H_m + mC_{pl,av}(T_f - T_m) \qquad (T_f > T_m > T_i) \qquad (4.43)$$

where m is the mass of the phase changing material, $C_{ps,av}$ and $C_{pl,av}$ are the average heat capacities for solid and liquid phases, respectively, T_m is the melting temperature, T_i and T_f are the initial and final temperatures, respectively and ΔH_m is the heat of fusion. Also, in the proposed system air is chosen as the heat transfer fluid.

4.3.4 Gasifier and Combustion Chambers

In the present study, wet wood ($CH_{1.46}O_{0.64}N_{0.002}$) is chosen as the fuel. Ultimate and proximate analysis of the wet wood are given in Table 4.9.

Table 4.9 The ultimate and proximate analysis of the wet wood [35].

Ultimate analysis		Proximate analysis	
Chemical Element	Mass Percent	Component	Mass Percent
C	50.41	Combustible substance	84.5
H	6.15	Moisture	15
O	43.31	Ash	0.5
N	0.12	LHV (MJ/kg wet wood)	15.32
S	0	Chemical exergy ash (MJ/kg ash)	1.7

The chemical equation of the gasification process by neglecting the small amount of nitrogen contained in biomass can be written as follows:

$$\dot{n}CH_{1.46}O_{0.64} + \dot{n}xO_2 + \dot{n}yN_2 \rightarrow \dot{n}CO + \dot{n}aH_2O + \dot{n}bH_2 + \dot{n}yN_2 \tag{4.44}$$
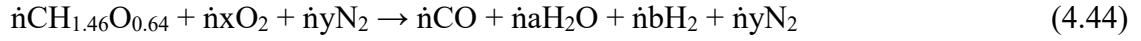
Here, $\dot{n}$ denotes the molar flow rate of the biomass and x, y, a, and b are the coefficients of the oxygen, nitrogen, steam and hydrogen, respectively. These coefficients vary depending on the equivalence ratio.

$$x = 1.045ER \tag{4.45}$$

$$y = 3.95ER \tag{4.46}$$

$$a = 2x - 0.36 \tag{4.47}$$

$$b = 1.09 - 2x \tag{4.48}$$

Also, equivalence ratio is defined as:

$$ER = \frac{Air\ added}{Air\ stoichiome\ tric} \tag{4.49}$$

The produced gases of the gasification process include carbon monoxide (CO), steam (H_2O), hydrogen (H_2) and nitrogen (N_2). Product gases are divide into two stream at state (21) where a defined fraction of the gases enters to the combustion chamber 1 and the rest part flows to the combustion chamber 2. In order to determine how much product gases flow into the first combustion chamber, a factor is defined which is represented by (k) letter ($0 \leq k \leq 1$). Correspondingly, the amount of the product gases which flows through the second combustion chamber at state (23) can be defined with (1-k). Chemical equation of the combustion processes can be written as below which occur in combustion chambers 1 and 2, respectively.

$$k\dot{n}CO + k\dot{n}aH_2O + k\dot{n}bH_2 + k\dot{n}yN_2 + k\dot{n}\frac{b}{2}O_2 + k\dot{n}1.89bN_2 \rightarrow k\dot{n}CO + k\dot{n}(a+b)H_2O + k\dot{n}(y+1.89b)N_2 \tag{4.50}$$

$$\dot{n}CO + \dot{n}(kb + a)H_2O + \dot{n}(1.89bk + y)N_2 + (1-k)\dot{n}bH_2 + 0.5\dot{n}(1+b-kb)O_2 + 1.89\dot{n}(1+b-kb)N_2 \rightarrow \dot{n}CO_2 + \dot{n}(a+b)H_2O + \dot{n}(y+1.89b+1.89)N_2 \tag{4.51}$$
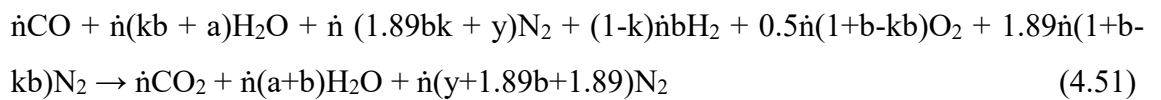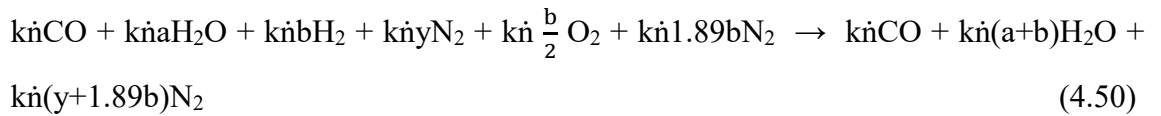
4.3.5 Energy and Exergy Analyses for System 3

The mass, energy, entropy and exergy balance equations for each component of system 3 are listed in Table 4.10.

Table 4.10 The balance equations of system 3 components

Component	Balance equations
LP Compressor	$\dot{m}_1 = \dot{m}_2$
	$\dot{m}_1 h_1 + \dot{W}_{LP,Compressor} = \dot{m}_2 h_2$
	$\dot{m}_1 s_1 + \dot{S}_{gen} = \dot{m}_2 s_2$
	$\dot{m}_1 ex_1 + \dot{W}_{LP,Compressor} = \dot{m}_2 ex_2 + \dot{Ex}_d$
Intercooler	$\dot{m}_2 = \dot{m}_3 \ ; \ \dot{m}_{13} = \dot{m}_{14}$
	$\dot{m}_2 h_2 + \dot{m}_{13} h_{13} = \dot{m}_3 h_3 + \dot{m}_{14} h_{14}$
	$\dot{m}_2 s_2 + \dot{m}_{13} s_{13} + \dot{S}_{gen} = \dot{m}_3 s_3 + \dot{m}_{14} s_{14}$
	$\dot{m}_2 ex_2 + \dot{m}_{13} ex_{13} = \dot{m}_3 ex_3 + \dot{m}_{14} ex_{14} + \dot{Ex}_d$
HP Compressor	$\dot{m}_3 = \dot{m}_4$
	$\dot{m}_3 h_3 + \dot{W}_{HP,Compressor} = \dot{m}_4 h_4$
	$\dot{m}_3 s_3 + \dot{S}_{gen} = \dot{m}_4 s_4$
	$\dot{m}_3 ex_3 + \dot{W}_{HP,Compressor} = \dot{m}_4 ex_4 + \dot{Ex}_d$
Aftercooler	$\dot{m}_4 = \dot{m}_5 \ ; \ \dot{m}_{14} = \dot{m}_{15}$
	$\dot{m}_4 h_4 + \dot{m}_{14} h_{14} = \dot{m}_5 h_5 + \dot{m}_{15} h_{15} + \dot{Q}_{out}$
	$\dot{m}_4 s_4 + \dot{m}_{14} s_{14} + \dot{S}_{gen} = \dot{m}_5 s_5 + \dot{m}_{15} s_{15} + \dfrac{\dot{Q}_{out}}{T_b}$
	$\dot{m}_4 ex_4 + \dot{m}_{14} ex_{14} = \dot{m}_5 ex_5 + \dot{m}_{15} ex_{15} + \dot{Ex}^{Q_{out}} + \dot{Ex}_d$
Heat Exchanger 2	$\dot{m}_{11} = \dot{m}_{12} \ ; \ \dot{m}_{45} = \dot{m}_{46}$
	$\dot{m}_{11} h_{11} + \dot{m}_{45} h_{45} = \dot{m}_{12} h_{12} + \dot{m}_{46} h_{46} + \dot{Q}_{out}$
	$\dot{m}_{11} s_{11} + \dot{m}_{45} s_{45} + \dot{S}_{gen} = \dot{m}_{12} s_{12} + \dot{m}_{46} s_{46} + \dfrac{\dot{Q}_{out}}{T_b}$
	$\dot{m}_{11} ex_{11} + \dot{m}_{45} ex_{45} = \dot{m}_{12} ex_{12} + \dot{m}_{46} ex_{46} + \dot{Ex}^{Q_{out}} + \dot{Ex}_d$
HP Turbine	$\dot{m}_8 = \dot{m}_9$
	$\dot{m}_8 h_8 = \dot{m}_9 h_9 + \dot{W}_{HP,Turbine}$
	$\dot{m}_8 s_8 + \dot{S}_{gen} = \dot{m}_9 s_9$
	$\dot{m}_8 ex_8 = \dot{m}_9 ex_9 + \dot{W}_{HP,Turbine} + \dot{Ex}_d$

Table 4.10 The balance equations of system 3 components (continued)

LP Turbine	$\dot{m}_{10} = \dot{m}_{11}$
	$\dot{m}_{10}h_{10} = \dot{m}_{11}h_{11} + \dot{W}_{LP,Turbine}$
	$\dot{m}_{10}s_{10} + \dot{S}_{gen} = \dot{m}_{11}s_{11}$
	$\dot{m}_{10}ex_{10} = \dot{m}_{11}ex_{11} + \dot{W}_{LP,Turbine} + \dot{Ex}_d$
Mixing Chamber	$\dot{m}_{15} + \dot{m}_{29} = \dot{m}_{30}$
	$\dot{m}_{15}h_{15} + \dot{m}_{29}h_{29} = \dot{m}_{30}h_{30}$
	$\dot{m}_{15}s_{15} + \dot{m}_{29}s_{29} + \dot{S}_{gen} = \dot{m}_{30}s_{30}$
	$\dot{m}_{15}ex_{15} + \dot{m}_{29}ex_{29} = \dot{m}_{30}ex_{30} + \dot{Ex}_d$
Heat Exchanger 1	$\dot{m}_{39} = \dot{m}_{40}$; $\dot{m}_{24} = \dot{m}_{30}$
	$\dot{m}_{30}h_{30} + \dot{m}_{39}h_{39} = \dot{m}_{24}h_{24} + \dot{m}_{40}h_{40} + \dot{Q}_{out}$
	$\dot{m}_{30}s_{30} + \dot{m}_{39}s_{39} + \dot{S}_{gen} = \dot{m}_{24}s_{24} + \dot{m}_{40}s_{40} + \dfrac{\dot{Q}_{out}}{T_b}$
	$\dot{m}_{30}ex_{30} + \dot{m}_{39}ex_{39} = \dot{m}_{24}ex_{24} + \dot{m}_{40}ex_{40} + \dot{Ex}^{Q_{out}} + \dot{Ex}_d$
Parabolic Trough Collector	$\dot{m}_{32} = \dot{m}_{33}$
	$\dot{m}_{32}h_{32} + \dot{Q}_{solar} = \dot{m}_{33}h_{33}$
	$\dot{m}_{32}s_{32} + \dfrac{\dot{Q}_{solar}}{T_{sun}} + \dot{S}_{gen} = \dot{m}_{33}s_{33}$
	$\dot{m}_{32}ex_{32} + \dot{Ex}^{Q_{solar}} = \dot{m}_{33}ex_{33} + \dot{Ex}_d$
Generator	$\dot{m}_{46} = \dot{m}_{47}$; $\dot{m}_{55} = \dot{m}_{56} + \dot{m}_{59}$
	$\dot{m}_{46}h_{46} + \dot{m}_{55}h_{55} = \dot{m}_{47}h_{47} + \dot{m}_{56}h_{56} + \dot{m}_{59}h_{59}$
	$\dot{m}_{46}s_{46} + \dot{m}_{55}s_{55} + \dot{S}_{gen} = \dot{m}_{47}s_{47} + \dot{m}_{56}s_{56} + \dot{m}_{59}s_{59}$
	$\dot{m}_{46}ex_{46} + \dot{m}_{55}ex_{55} = \dot{m}_{47}ex_{47} + \dot{m}_{24}ex_{24} + \dot{m}_{56}ex_{56} + \dot{Ex}_d$
Condenser 1	$\dot{m}_{48} = \dot{m}_{49}$; $\dot{m}_{65} = \dot{m}_{66}$
	$\dot{m}_{48}h_{48} + \dot{m}_{65}h_{65} = \dot{m}_{49}h_{49} + \dot{m}_{66}h_{66}$
	$\dot{m}_{48}s_{48} + \dot{m}_{65}s_{65} + \dot{S}_{gen} = \dot{m}_{49}s_{49} + \dot{m}_{66}s_{66}$
	$\dot{m}_{48}ex_{48} + \dot{m}_{65}ex_{65} = \dot{m}_{49}ex_{49} + \dot{m}_{66}ex_{66} + \dot{Ex}_d$

Table 4.10 The balance equations of system 3 components (continued)

Evaporator	$\dot{m}_{50} = \dot{m}_{51}$; $\dot{m}_{63} = \dot{m}_{64}$
	$\dot{m}_{50}h_{50} + \dot{m}_{63}h_{63} = \dot{m}_{51}h_{51} + \dot{m}_{64}h_{64}$
	$\dot{m}_{50}s_{50} + \dot{m}_{63}s_{63} + \dot{S}_{gen} = \dot{m}_{51}s_{51} + \dot{m}_{64}s_{64}$
	$\dot{m}_{50}ex_{50} + \dot{m}_{63}ex_{63} = \dot{m}_{51}ex_{51} + \dot{m}_{64}ex_{64} + \dot{Ex}_d$
Absorber	$\dot{m}_{61} = \dot{m}_{62}$; $\dot{m}_{53} = \dot{m}_{52} + \dot{m}_{58}$
	$\dot{m}_{52}h_{52} + \dot{m}_{58}h_{58} + \dot{m}_{61}h_{61} = \dot{m}_{53}h_{53} + \dot{m}_{62}h_{62}$
	$\dot{m}_{52}s_{52} + \dot{m}_{58}s_{58} + \dot{m}_{61}s_{61} + \dot{S}_{gen} = \dot{m}_{53}s_{53} + \dot{m}_{62}s_{62}$
	$\dot{m}_{52}ex_{52} + \dot{m}_{58}ex_{58} + \dot{m}_{61}ex_{61} = \dot{m}_{53}ex_{53} + \dot{m}_{62}ex_{62} + \dot{Ex}_d$
Heat Exchanger 3	$\dot{m}_{54} = \dot{m}_{55}$; $\dot{m}_{56} = \dot{m}_{57}$
	$\dot{m}_{54}h_{54} + \dot{m}_{56}h_{56} = \dot{m}_{55}h_{55} + \dot{m}_{57}h_{57}$
	$\dot{m}_{54}s_{54} + \dot{m}_{56}s_{56} + \dot{S}_{gen} = \dot{m}_{55}s_{55} + \dot{m}_{57}s_{57}$
	$\dot{m}_{54}ex_{54} + \dot{m}_{56}ex_{56} = \dot{m}_{55}ex_{55} + \dot{m}_{57}ex_{57} + \dot{Ex}_d$
Boiler	$\dot{m}_{47} = \dot{m}_{67}$; $\dot{m}_{68} = \dot{m}_{69}$
	$\dot{m}_{47}h_{47} + \dot{m}_{68}h_{68} = \dot{m}_{67}h_{67} + \dot{m}_{69}h_{69}$
	$\dot{m}_{47}s_{47} + \dot{m}_{68}s_{68} + \dot{S}_{gen} = \dot{m}_{67}s_{67} + \dot{m}_{69}s_{69}$
	$\dot{m}_{47}ex_{47} + \dot{m}_{68}ex_{68} = \dot{m}_{67}ex_{67} + \dot{m}_{69}ex_{69} + \dot{Ex}_d$
Turbine 2	$\dot{m}_{69} = \dot{m}_{70}$
	$\dot{m}_{69}h_{69} = \dot{m}_{70}h_{70} + \dot{W}_{Turbine}$
	$\dot{m}_{69}s_{69} + \dot{S}_{gen} = \dot{m}_{70}s_{70}$
	$\dot{m}_{69}ex_{69} = \dot{m}_{70}ex_{70} + \dot{W}_{Turbine} + \dot{Ex}_d$
Condenser 2	$\dot{m}_{70} = \dot{m}_{71}$; $\dot{m}_{72} = \dot{m}_{73}$
	$\dot{m}_{70}h_{70} + \dot{m}_{72}h_{72} = \dot{m}_{71}h_{71} + \dot{m}_{73}h_{73}$
	$\dot{m}_{70}s_{70} + \dot{m}_{72}s_{72} + \dot{S}_{gen} = \dot{m}_{71}s_{71} + \dot{m}_{73}s_{73}$
	$\dot{m}_{70}ex_{70} + \dot{m}_{72}ex_{72} = \dot{m}_{71}ex_{71} + \dot{m}_{73}ex_{73} + \dot{Ex}_d$
Direct-Contact Condenser	$\dot{m}_{74} + \dot{m}_{85} + \dot{m}_{88} + \dot{m}_{89} = \dot{m}_{75} + \dot{m}_{90}$
	$\dot{m}_{74}h_{74} + \dot{m}_{85}h_{85} + \dot{m}_{88}h_{88} + \dot{m}_{89}h_{89} = \dot{m}_{75}h_{75} + \dot{m}_{90}h_{90}$
	$\dot{m}_{74}s_{74} + \dot{m}_{85}s_{85} + \dot{m}_{88}s_{88} + \dot{m}_{89}s_{89} + \dot{S}_{gen} = \dot{m}_{75}s_{75} + \dot{m}_{90}s_{90}$
	$\dot{m}_{74}ex_{74} + \dot{m}_{85}ex_{85} + \dot{m}_{88}ex_{88} + \dot{m}_{89}ex_{89} = \dot{m}_{75}ex_{75} + \dot{m}_{90}ex_{90} + \dot{Ex}_d$

Table 4.10 The balance equations of system 3 components (continued)

Gas Cooler	$\dot{m}_{84} = \dot{m}_{85}$; $\dot{m}_{90} = \dot{m}_{91}$
	$\dot{m}_{84}h_{84} + \dot{m}_{90}h_{90} = \dot{m}_{85}h_{85} + \dot{m}_{91}h_{91} + \dot{Q}_{losses}$
	$\dot{m}_{84}s_{84} + \dot{m}_{90}s_{90} + \dot{S}_{gen} = \dot{m}_{85}s_{85} + \dot{m}_{91}s_{91} + \dfrac{\dot{Q}_{losses}}{T_b}$
	$\dot{m}_{84}ex_{84} + \dot{m}_{90}ex_{90} = \dot{m}_{85}ex_{85} + \dot{m}_{91}ex_{91} + \dot{Ex}^{Q_{losses}} + \dot{Ex}_d$
Compressor	$\dot{m}_{91} = \dot{m}_{92}$
	$\dot{m}_{91}h_{91} + \dot{W}_{Compressor} = \dot{m}_{92}h_{92}$
	$\dot{m}_{91}s_{91} + \dot{S}_{gen} = \dot{m}_{92}s_{92}$
	$\dot{m}_{91}ex_{91} + \dot{W}_{Compressor} = \dot{m}_{92}ex_{92} + \dot{Ex}_d$
Turbine 3	$\dot{m}_{67} = \dot{m}_{74}$
	$\dot{m}_{67}h_{67} = \dot{m}_{74}h_{74} + \dot{W}_{Turbine}$
	$\dot{m}_{67}s_{67} + \dot{S}_{gen} = \dot{m}_{74}s_{74}$
	$\dot{m}_{67}ex_{67} = \dot{m}_{74}ex_{74} + \dot{W}_{Turbine} + \dot{Ex}_d$
Water Preheater	$\dot{m}_{101} = \dot{m}_{102}$; $\dot{m}_{104} = \dot{m}_{105}$
	$\dot{m}_{101}h_{101} + \dot{m}_{104}h_{104} = \dot{m}_{102}h_{102} + \dot{m}_{105}h_{105} + \dot{Q}_{losses}$
	$\dot{m}_{101}s_{101} + \dot{m}_{104}s_{104} + \dot{S}_{gen} = \dot{m}_{102}s_{102} + \dot{m}_{105}s_{105} + \dfrac{\dot{Q}_{losses}}{T_b}$
	$\dot{m}_{101}ex_{101} + \dot{m}_{104}ex_{104} = \dot{m}_{102}ex_{102} + \dot{m}_{105}ex_{105} + \dot{Ex}^{Q_{losses}} + \dot{Ex}_d$
Pump 1	$\dot{m}_{53} = \dot{m}_{54}$
	$\dot{m}_{53}h_{53} + \dot{W}_{Pump} = \dot{m}_{54}h_{54}$
	$\dot{m}_{53}s_{53} + \dot{S}_{gen} = \dot{m}_{54}s_{54}$
	$\dot{m}_{53}ex_{53} + \dot{W}_{Pump} = \dot{m}_{54}ex_{54} + \dot{Ex}_d$
Pump 2	$\dot{m}_{71} = \dot{m}_{68}$
	$\dot{m}_{71}h_{71} + \dot{W}_{Pump} = \dot{m}_{68}h_{68}$
	$\dot{m}_{71}s_{71} + \dot{S}_{gen} = \dot{m}_{68}s_{68}$
	$\dot{m}_{71}ex_{71} + \dot{W}_{Pump} = \dot{m}_{68}ex_{68} + \dot{Ex}_d$

Table 4.10 The balance equations of system 3 components (continued)

Cooling Water Pump	$\dot{m}_{75} = \dot{m}_{76}$
	$\dot{m}_{75}h_{75} + \dot{W}_{Pump} = \dot{m}_{76}h_{76}$
	$\dot{m}_{75}s_{75} + \dot{S}_{gen} = \dot{m}_{76}s_{76}$
	$\dot{m}_{75}ex_{75} + \dot{W}_{Pump} = \dot{m}_{76}ex_{76} + \dot{Ex}_d$
Expansion Valve 1	$\dot{m}_{57} = \dot{m}_{58}$
	$\dot{m}_{57}h_{57} = \dot{m}_{58}h_{58}$
	$\dot{m}_{57}s_{57} + \dot{S}_{gen} = \dot{m}_{58}s_{58}$
	$\dot{m}_{57}ex_{57} = \dot{m}_{58}ex_{58} + \dot{Ex}_d$
Expansion Valve 2	$\dot{m}_{49} = \dot{m}_{50}$
	$\dot{m}_{49}h_{49} = \dot{m}_{50}h_{50}$
	$\dot{m}_{49}s_{49} + \dot{S}_{gen} = \dot{m}_{50}s_{50}$
	$\dot{m}_{49}ex_{49} = \dot{m}_{50}ex_{50} + \dot{Ex}_d$

In addition, the balance equations and energy and exergy efficiencies of the packed bed thermal storage and underground cavern systems are given in Table 4.11.

Table 4.11 The balance equations of the packed bed and underground cavern

Component	Balance equations	Energy and exergy efficiencies
Packed Bed Thermal Storage	$\dot{m}_{16} = \dot{m}_{17}$; $\dot{m}_{18} = \dot{m}_{19}$	$\eta = \dfrac{\dot{m}_{19}h_{19}}{\dot{m}_{16}h_{16}}$
	$\dot{m}_{16}h_{16} + \dot{m}_{18}h_{18} = \dot{m}_{17}h_{17} + \dot{m}_{19}h_{19} + \dot{Q}_{stored}$	
	$\dot{m}_{16}s_{16} + \dot{m}_{18}s_{18} + \dot{S}_{gen} = \dot{m}_{17}s_{17} + \dot{m}_{19}s_{19} + \dfrac{\dot{Q}_{stored}}{T_b}$	$\psi = \dfrac{\dot{m}_{19}ex_{19}}{\dot{m}_{16}ex_{16}}$
	$\dot{m}_{16}ex_{16} + \dot{m}_{18}ex_{18} = \dot{m}_{17}ex_{17} + \dot{m}_{19}ex_{19} + \dot{Ex}^{Q_{stored}} + \dot{Ex}_d$	
Underground Cavern	$\dot{m}_{17} = \dot{m}_{18}$	$\eta = \dfrac{\dot{m}_{18}h_{18}}{\dot{m}_{17}h_{17}}$
	$\dot{m}_{17}h_{17} = \dot{m}_{18}h_{18} + \dot{Q}_{losses}$	
	$\dot{m}_{17}s_{17} + \dot{S}_{gen} = \dot{m}_{18}s_{18} + \dfrac{\dot{Q}_{losses}}{T_b}$	$\psi = \dfrac{\dot{m}_{18}ex_{18}}{\dot{m}_{17}ex_{17}}$
	$\dot{m}_{17}ex_{17} = \dot{m}_{18}ex_{18} + \dot{Ex}^{Q_{losses}} + \dot{Ex}_d$	

4.3.5.1 Energy and Exergy Analyses of Gasifier and Combustion Chambers

The lower heating value of the combustible substance (LHV_{cs}) in the fuel is expressed per unit mass of the wet fuel, according to the following relationship [35]:

$$LHV_{cs} = LHV_{wf} + z_{H_2O} \Delta H_{H_2O} \qquad \text{(MJ/kg wet fuel)} \qquad (4.52)$$

Here, LHV_{wf} is the lower heating value of the wet fuel. Also, z_{H_2O} and ΔH_{H_2O} are the mass fraction of water and the enthalpy of water vaporization, respectively. The ratio χ for wood ($z_O / z_C \leq 1$) can be defined as follows [35]:

$$\chi = \frac{1.0142 + 0.2160\left(\dfrac{z_H}{z_C}\right) - 0.2499\left(\dfrac{z_O}{z_C}\right)\left[1 + 0.7784\left(\dfrac{z_H}{z_C}\right)\right] + 0.0450\left(\dfrac{z_N}{z_C}\right)}{1 - 0.3035\left(\dfrac{z_O}{z_C}\right)} \qquad (4.53)$$

The chemical exergy of a wet fuel ($ex_{ch,wf}$) depends on the exergy contributions of the combustible substance (organic matter), water, ash, and sulfur in a technical fuel according to the following equation (*Szargut et al.,* Ref.[35]):

$$ex_{ch,wf} = \beta LHV_{cs} + z_{H_2O} ex_{ch,H_2O} + z_{ash} ex_{ch,ash} + z_s \left(ex_{ch,s} - LHV_s\right) \qquad (4.54)$$

where ex_{ch,H_2O}, $ex_{ch,ash}$, $ex_{ch,s}$ denote the chemical exergy of liquid water, ash and sulfur, respectively, z_{ash} and z_s denote the mass fractions of ash and sulfur in the wet fuel, respectively, and LHV_s is the lower heating value of sulfur. Additionally, the enthalpy of the wet biomass can be calculated depending on its specific heat as follows [36]:

$$c_{p,db} = 0.266 + 0.00116T \qquad (4.55)$$

where $c_{p,db}$ represents the specific heat of the dry biomass. Also, the specific heat of the wet biomass can be calculated as:

$$c_{p,wb} = z_{H_2O} C_{H_2O} + (1 - z_{H_2O}) c_{p,db} \qquad (4.56)$$

Thus,

$$h_{wb} = c_{p,wb} T \qquad (4.57)$$

where T is absolute temperature of the biomass.

The enthalpy of formation of dry biomass can be calculated from [36]:

$$h^\circ_{f,db} = 349.1C + 1178.2H - 103.4O - 15.1N + 100.5S \qquad (4.58)$$

where C, H, O, N and S are the weight fractions of the ultimate compositions in the biomass. Through the following correlation, the enthalpy of formation of moist biomass is defined as:

$$h^\circ_{f,wb} = h^\circ_{f,db}(1 - z_{H_2O}) - 2.44z_{H_2O}(1 - z_{H_2O}) - 21.83H(1 - z_{H_2O}) \qquad (4.59)$$

The product gases of the gasification process are divided into two streams at state (21) and mass flow rates of the gasification products are determined depending on the division factor (d_f) as follows (4.60 numbered Equation):

$$\dot{m}_{108} + \dot{m}_{109} + \dot{m}_{110} + \dot{m}_{111} = \dot{m}_{108I} + \dot{m}_{109I} + \dot{m}_{110I} + \dot{m}_{111I} + \dot{m}_{108II} + \dot{m}_{109II} + \dot{m}_{110II} + \dot{m}_{111II}$$

(I) and (II) subcripts are related to combustion chamber 1 and combustion chamber 2, respectively.

$$\dot{m}_{108I} + \dot{m}_{109I} + \dot{m}_{110I} + \dot{m}_{111I} = d_f \times (\dot{m}_{108} + \dot{m}_{109} + \dot{m}_{110} + \dot{m}_{111}) \qquad (4.61)$$

$$\dot{m}_{108II} + \dot{m}_{109II} + \dot{m}_{110II} + \dot{m}_{111II} = (1 - d_f) \times (\dot{m}_{108} + \dot{m}_{109} + \dot{m}_{110} + \dot{m}_{111}) \qquad (4.62)$$

The enthalpy of formations of the system compounds are given in Table 4.12.

Table 4.12 The enthalpy of formations of the system compounds [37].

Compound	Enthalpy of formation ($\bar{h}^\circ_f$) (kJ/kmol)
CO	-110500
$H_2O(g)$	-241800
H_2	0
N_2	0
CO_2	-393520

Also, standard chemical exergies of the each compound are given in Table 4.13.

Table 4.13 The standard chemical exergies of the system compounds [38].

Compound	Standard chemical exergy (ex^o_{ch}) (kJ/kmol)
CO	274710
$H_2O(g)$	9490
H_2	236100
N_2	720
CO_2	19480

4.3.5.2 Energy and Exergy Efficiency Definitions for System 3

By taking into consideration all useful commodities and total energy inputs, the overall energy efficiency of system 3 can be written as follows:

$$\eta_{overall} = \frac{\dot{W}_{net} + \dot{Q}_{Heating} + \dot{Q}_{Drying} + \dot{Q}_{Cooling} + \dot{m}_{H_2,PEM} \times LHV_{H_2} + \dot{m}_{H_2,electrolyzer} \times h_{H_2}}{\dot{E}^{Geo} + \dot{E}^{Solar} + \dot{E}^{Wind} + \dot{E}^{Biomass}} \quad (4.63)$$

where $\dot{Q}_{Heating}$ is the sum of domestic hot water and space heating outputs of the designed system. Also, $\dot{Q}_{Drying}$ denotes the total drying heat which is provided through the heated air which leaves the cooling tower at state (98).

Overall exergy efficiency of the designed system also can be written as:

$$\psi_{overall} = \frac{\dot{W}_{net} + \dot{Ex}^{Q_{Heating}} + \dot{Ex}^{Q_{Drying}} + \dot{Ex}^{Q_{Cooling}} + \dot{m}_{H_2} \times \left(ex_{ph} + ex_{ch}\right)_{H_2}}{\dot{Ex}^{Q_{Geo}} + \dot{Ex}^{Q_{Solar}} + \dot{Ex}^{Wind} + \dot{m}_{biomass}\left(ex_{ph,biomass} + ex_{ch,biomass}\right)} \quad (4.64)$$

The main assumptions of system 3 are presented in Table 4.14.

Table 4.14 The main assumptions of system 3

Parameter	Value
Mass flow rate of the compressed air during the charging period	10 kg/s
Mass flow rate of the compressed air during the storing period	13 kg/s
Mass flow rate of the compressed air during the discharging period	15 kg/s
Ambient temperature, T_0	298 K
Ambient pressure, P_0	101.325 kPa
Temperature of the sun, T_{sun}	6000 K
Equivalence ratio, ER	29%

Table 4.14 The main assumptions of system 3 (continued)

Moisture content of the biomass	15%
Mass flow rate of biomass during the charging period	7.6 kg/s
Mass flow rate of biomass during the storing period	11.5 kg/s
Mass flow rate of biomass during the discharging period	12.5 kg/s
Charging period, $t_{charging}$	4 h
Storing period, $t_{storing}$	16 h
Discharging period, $t_{discharging}$	4 h
Initial soil temperature, T_{is}	283 K
Phase change material	$LiNO_3$
Mass flow rate of the geothermal steam	60 kg/s
Inlet temperature of geothermal steam	515.7 K
Inlet pressure of geothermal steam	3500 kPa
Blade length of wind turbine	8 m
Inlet velocity of the wind to the wind turbine	7.5 m/s
Outlet velocity of the wind from the wind turbine	2.5 m/s
Number of wind turbines	50
Wind Turbine conversion efficiency	80%

4.4   System 4

In this section the designed system (Figure 3.8) will be analysed through energy and exergy approaches along with emission rates in order to give a detailed information about the electrolysis process of hydrogen sulfide and the amount of energy which is provided through the fuel cell system. Table 4.15 gives the average chemical compositions of non-condensable gases in mole percent and the following calculations are based on these data.

Table 4.15 The average chemical compositions of non-condensable gases [39].

Compound	Composition (% mole)
Nitrogen	26.76
Oxygen	18.55
Methane	15.77
Carbon Dioxide	31.14
Hydrogen Sulfide	7.78

In addition, for the analysis the following assumptions are made accordingly:

- The heat transfer between the designed system and the environment is negligible.

- The auxiliary components are well insulated and capable of conducting electricity without losses.

- The changes in both potential and kinetic energies and exergies are negligible.
- The processes occur in steady-state and steady-flow.
- Mass flow rate of hydrogen sulfide is 0.3 kg/s.
- The temperature and pressure of the hydrogen sulfide are 423 K and 200 kPa, respectively.
- The temperature and pressure of the products of electrolysis process are 500 K and 200 kPa, respectively.
- The ambient temperature (T_0) and pressure (P_o) are 298 K and 101.325 kPa, respectively.

The related equations and efficiency definitions will be given for the studied system. In the electrolysis process, hydrogen sulfide is decomposed to pure hydrogen and sulfur dimer by electrical power. Therefore, electrolysis is a chemically reacting process. The required electrical work of the electrolysis process by neglecting the heat transfer from/to ambient can be defined as follows [31]:

$$\dot{W}_{electrolysis} = \Sigma \dot{n}_p \left(\overline{h^0}_f + \overline{h} - \overline{h^0} \right)_p - \Sigma \dot{n}_r \left(\overline{h^0}_f + \overline{h} - \overline{h^0} \right)_r \tag{4.65}$$

here p and r subcripts represent the products and reactants of the electrolysis process. Products of the process are hydrogen and sulfur dimer and hydrogen sulfide is the only reactant for the electrochemical process. Moreover, reversible work of the electrolysis process can be expressed as follows:

$$\dot{W}_{rev} = \Sigma \dot{n}_r \left(\overline{h^0}_f + \overline{h} - \overline{h^0} - T_0 s \right)_r - \Sigma \dot{n}_p \left(\overline{h^0}_f + \overline{h} - \overline{h^0} - T_0 s \right)_p \tag{4.66}$$

For the electrolysis process the steady-state and steady-flow entropy balance equation can be written as follows:

$$\dot{m}_{H_2S} \times s_{H_2S} + \dot{S}_{gen} = \dot{m}_{H_2} \times s_{H_2} + \dot{m}_{S_2} \times s_{S_2} \tag{4.67}$$

For the electrochemical process which occurs in the fuel cell the produced electricity can be expressed as follows:

$$\dot{W}_{produced} = \Sigma \dot{n}_r \left(\overline{h^0}_f + \overline{h} - \overline{h^0} \right)_r - \Sigma \dot{n}_p \left(\overline{h^0}_f + \overline{h} - \overline{h^0} \right)_p \tag{4.68}$$

Products of the fuel cell conversion process is water and reactants are hydrogen and

oxygen.

For the fuel cell conversion process the steady-state and steady-flow entropy balance equation can be written as follows:

$$\dot{m}_{H_2} \times s_{H_2} + \dot{m}_{O_2} \times s_{O_2} + \dot{S}_{gen} = \dot{m}_{H_2O} \times s_{H_2O} \qquad (4.69)$$

The overall energy efficiency of the designed system which consists of an electrolyzer and a fuel cell can be defined as follows:

$$\eta_{overall} = \frac{\dot{W}_{produced} + \dot{m}_{H_2O} \times h_{H_2O}}{\dot{W}_{electrolysis} + \dot{m}_{H_2S} \times h_{H_2S} + \dot{m}_{O_2} \times h_{O_2} + \dot{m}_{H_2} \times LHV_{H_2}} \qquad (4.70)$$

And also, the overall exergy efficiency of the designed system can be written as:

$$\psi_{overall} = \frac{\dot{W}_{produced} + \dot{m}_{H_2O} \times ex_{H_2O}}{\dot{W}_{electrolysis} + \dot{m}_{H_2S} \times ex_{H_2S} + \dot{m}_{O_2} \times ex_{O_2} + \dot{m}_{H_2} \times \left(ex_{ph} + ex_{ch}\right)_{H_2}} \qquad (4.71)$$

In addition to the identified overall efficiencies, overall energy and exergy efficiencies can also be stated as follows:

$$\eta_{overall,2} = \frac{\dot{W}_{produced} + \dot{m}_{H_2O} \times h_{H_2O}}{\dot{W}_{electrolysis}} \qquad (4.72)$$

$$\psi_{overall,2} = \frac{\dot{W}_{produced} + \dot{m}_{H_2O} \times ex_{H_2O}}{\dot{W}_{electrolysis}} \qquad (4.73)$$

CHAPTER 5

RESULTS AND DISCUSSION

In the previous chapters, three different types of renewable based multigeneration systems are described and analysed as well as electrolysis process of hydrogen sulfide. In this chapter, the results are given for each system. Additionally, both energy and exergy assessments are carried out depending on the changing desing parameters and operating conditions such as ambient temperature, inlet mass flow rate of geothermal fluid, average hourly solar radiation. Furthermore, entropy generations and exergy destructions are determined for each component of the systems.

5.1   System 1 Results

The proposed multigeneration system operates in three different scenarios. In the first scenario, average hourly solar radiation has the highest value and both TES tank and heat exchanger 2 are fed by the heat transfer fluid. In other words, valves 1,2 and 3 open during this period. Thermodynamic properties of the all streams of the first working principle are listed in Table 5.1.

Table 5.1 Thermodynamic properties of the charging period

State	$\dot{m}_i$ (kg/s)	P_i (kPa)	T_i (K)	h_i (kJ/kg)	s_i (kJ/kgK)	x (kg/kg)	ex_{ph} (kJ/kg)
1	60	2000	515	2882	6.507		947.6
2	60	2000	510	2869	6.481		942
3	60	2000	490	2812	6.368		919.2
4	60	2000	598	3081	6.866		1040
5	60	250	403	2722	7.066		620.8
6	3871	200	392	498.9	1.515		51.83

Table 5.1 Thermodynamic properties of the charging period (continued)

7	3871	250	392	499	1.515		51.89
8	1290	250	392	499	1.515		51.89
9	1290	250	392	499	1.515		51.89
10	1290	250	392	499	1.515		51.89
11	70	200	388	481.9	1.472		47.83
12	48	200	388	481.9	1.472		47.83
13	22	200	388	481.9	1.472		47.83
14	19	200	385	469.2	1.439		44.92
15	30	200	384	465	1.428		43.96
16	30	200	384.8	468.4	1.437		44.73
17	3771	200	385	469.2	1.439		44.92
18	3790	200	385	469.2	1.439		44.92
19	2527	200	385	469.2	1.439		44.92
20	1263	200	385	469.2	1.439		44.92
21	9	150	398	177	1.789		44.77
22	9	150	387	164.9	1.758		41.87
23	9	200	423	204.5	1.782		74.33
24	0.7388	200	423	126.6	0.187		70.46
25	0.0433	200	500	6850	58.04		1528
26	0.6933	200	500	107.1	3.839		25.464
27	8.2612	200	350	131.5	1.717		56.51
28	1738	130	320	320.4	6.86		22.09
29	1738	130	385	386	7.047		32.09
30	8.2612	200	385	169.3	1.82		63.65
31	7.667	332.5	318.7	1396	5.184	0.99	170.5
32	7.667	332.5	282.1	1258	4.727	0.99	169.3
33	7.667	130	249	1160	4.777	0.99	55.78
34	7.667	130	302	1370	5.549	0.99	35.82
35	5.75	130	302	1370	5.549	0.99	35.82
36	50	156.5	278	42.86	0.8166	0.6	35.52
37	50	400	299.6	61.74	0.8166	0.6	54.4
38	50	400	305	180	1.206	0.6	56.67
39	44.25	400	325	34.04	0.7233	0.4	11.54
40	44.25	400	302	-99.57	0.3009	0.4	3.785
41	44.25	160	298	-91.75	0.3282	0.4	3.477
42	5.75	400	340	1442	5.236	0.99	201
43	1.917	130	255	1204	4.952	0.99	47.78
44	16.66	101.3	276	12.08	0.04363		3.581
45	16.66	101.3	300	112.6	0.3928		0.02795
46	30.23	101.3	308	308.4	6.893		0.1652
47	30.23	101.3	255	255	6.703		3.458

Table 5.1 Thermodynamic properties of the charging period (continued)

48	7.186	101.3	278	20.49	0.07399		2.944
49	7.186	101.3	313	167	0.5702		1.528
50	6.02	100	385	208.3	0.6114		26.17
51	6.02	400	390	221.5	0.6441		29.58
52	6.02	400	505	786	1.899		220.2
53	6.02	100	483.5	742	1.905		174.2
54	187.7	101.3	288	288.2	6.825		0.1727
55	187.7	101.3	305	305.3	6.883		0.08149
56	60	600	510	483.2	1.341		95.38
57	60	1000	520	503.7	1.38		104.4
58	60	600	660	799.6	1.883		250.4
59	42	600	660	799.6	1.883		250.4
60	42	600	660	799.6	1.883		250.4
61	18	600	660	799.6	1.883		250.4
62	18	600	660	799.6	1.883		250.4
63	18	600	590	647	1.639		170.4
64	18	600	590	647	1.639		170.4
65	60	600	639	752.9	1.812		224.9
66	18.17	300	650	776.9	1.849		237.7
67	18.17	300	580	625.7	1.603		159.9
68	18.17	300	580	625.7	1.603		159.9
69	18.17	200	570	604.7	1.567		149.7
70	18.17	200	570	604.7	1.567		149.7
71	No flow during the charging period						
72	No flow during the charging period						
73	19	200	388	481.9	1.472		47.83
74	3	200	388	481.9	1.472		47.83
75	3	200	355	342.8	1.097		20.37
76	51	200	386.1	473.7	1.45		46.21
77	0.2	200	288	62.48	0.222		0.8169
78	0.2	200	350	321.8	1.038		17.13
79	0.022	200	370	4967	53.68		944.7
80	0.1778	200	370	66.03	0.02187		59.56

In the second scenario, the average hourly solar radiation is sufficient only to feed the heat exchanger 2. During this period, valves 1 and 3 are shut-downed. Thermodynamic properties of the all stream points of this mechanism are given in Table 5.2.

Table 5.2 Thermodynamic properties of the storing period

State	$\dot{m}_i$ (kg/s)	P_i (kPa)	T_i (K)	h_i (kJ/kg)	s_i (kJ/kgK)	x (kg/kg)	ex_{ph} (kJ/kg)
1	60	2000	515	2882	6.507		947.6
2	60	2000	510	2869	6.481		942
3	60	2000	490	2812	6.368		919.2
4	60	2000	598	3081	6.866		1040
5	60	250	403	2722	7.066		620.8
6	3871	200	392	498.9	1.515		51.83
7	3871	250	392	499	1.515		51.89
8	1290	250	392	499	1.515		51.89
9	1290	250	392	499	1.515		51.89
10	1290	250	392	499	1.515		51.89
11	70	200	388	481.9	1.472		47.83
12	48	200	388	481.9	1.472		47.83
13	22	200	388	481.9	1.472		47.83
14	19	200	385	469.2	1.439		44.92
15	30	200	384	465	1.428		43.96
16	30	200	384.8	468.4	1.437		44.73
17	3771	200	385	469.2	1.439		44.92
18	3790	200	385	469.2	1.439		44.92
19	2527	200	385	469.2	1.439		44.92
20	1263	200	385	469.2	1.439		44.92
21	9	150	398	177	1.789		44.77
22	9	150	387	164.9	1.758		41.87
23	9	200	423	204.5	1.782		74.33
24	0.7388	200	423	126.6	0.187		70.46
25	0.0433	200	500	6850	58.04		1528
26	0.6933	200	500	107.1	3.839		25.464
27	8.2612	200	350	131.5	1.717		56.51
28	1738	130	320	320.4	6.86		22.09
29	1738	130	385	386	7.047		32.09
30	8.2612	200	385	169.3	1.82		63.65
31	7.667	332.5	318.7	1396	5.184	0.99	170.5
32	7.667	332.5	282.1	1258	4.727	0.99	169.3
33	7.667	130	249	1160	4.777	0.99	55.78
34	7.667	130	302	1370	5.549	0.99	35.82
35	5.75	130	302	1370	5.549	0.99	35.82
36	50	156.5	278	42.86	0.8166	0.6	35.52
37	50	400	299.6	61.74	0.8166	0.6	54.4
38	50	400	305	180	1.206	0.6	56.67
39	44.25	400	325	34.04	0.7233	0.4	11.54

Table 5.2 Thermodynamic properties of the storing period (continued)

40	44.25	400	302	-99.57	0.3009	0.4	3.785
41	44.25	160	298	-91.75	0.3282	0.4	3.477
42	5.75	400	340	1442	5.236	0.99	201
43	1.917	130	255	1204	4.952	0.99	47.78
44	16.66	101.3	276	12.08	0.04363		3.581
45	16.66	101.3	300	112.6	0.3928		0.02795
46	30.23	101.3	308	308.4	6.893		0.1652
47	30.23	101.3	255	255	6.703		3.458
48	7.186	101.3	278	20.49	0.07399		2.944
49	7.186	101.3	313	167	0.5702		1.528
50	6.02	100	385	208.3	0.6114		26.17
51	6.02	400	390	221.5	0.6441		29.58
52	6.02	400	505	786	1.899		220.2
53	6.02	100	483.5	742	1.905		174.2
54	187.7	101.3	288	288.2	6.825		0.1727
55	187.7	101.3	305	305.3	6.883		0.08149
56	60	600	510	483.2	1.341		95.38
57	60	1000	520	503.7	1.38		104.4
58	60	600	604	677	1.689		185.6
59	60	600	604	677	1.689		185.6
60	60	600	604	677	1.689		185.6
61	No flow during the storing period						
62	No flow during the storing period						
63	No flow during the storing period						
64	No flow during the storing period						
65	60	600	604	677	1.689		185.6
66	No flow during the storing period						
67	No flow during the storing period						
68	No flow during the storing period						
69	No flow during the storing period						
70	No flow during the storing period						
71	No flow during the storing period						
72	No flow during the storing period						
73	19	200	388	481.9	1.472		47.83
74	3	200	388	481.9	1.472		47.83
75	3	200	355	342.8	1.097		20.37
76	51	200	386.1	473.7	1.45		46.21
77	0.2	200	288	62.48	0.222		0.8169
78	0.2	200	350	321.8	1.038		17.13
79	0.022	200	370	4967	53.68		944.7
80	0.1778	200	370	66.03	0.02187		59.56

In the last scenario, the average hourly solar radiation is very low. Heat transfer fluid which is circulated in the solar driven system, enters the TES tank and receives the heat of the PCM and leaves the TES tank as heated at state (66). In this period, valve 2 is shut-downed and heat transfer fluid is not divided into two streams at state (58). Thermodynamic properties of the all stream points of this period are given in Table 5.3.

Table 5.3 Thermodynamic properties of the discharging period

State	$\dot{m}_i$ (kg/s)	P_i (kPa)	T_i (K)	h_i (kJ/kg)	s_i (kJ/kgK)	x (kg/kg)	ex_{ph} (kJ/kg)
1	60	2000	515	2882	6.507		947.6
2	60	2000	510	2869	6.481		942
3	60	2000	490	2812	6.368		919.2
4	60	2000	544	2955	6.645		979.5
5	60	250	403	2722	7.066		620.8
6	3871	200	392	498.9	1.515		51.83
7	3871	250	392	499	1.515		51.89
8	1290	250	392	499	1.515		51.89
9	1290	250	392	499	1.515		51.89
10	1290	250	392	499	1.515		51.89
11	70	200	388	481.9	1.472		47.83
12	48	200	388	481.9	1.472		47.83
13	22	200	388	481.9	1.472		47.83
14	19	200	385	469.2	1.439		44.92
15	30	200	384	465	1.428		43.96
16	30	200	384.8	468.4	1.437		44.73
17	3771	200	385	469.2	1.439		44.92
18	3790	200	385	469.2	1.439		44.92
19	2527	200	385	469.2	1.439		44.92
20	1263	200	385	469.2	1.439		44.92
21	9	150	398	177	1.789		44.77
22	9	150	387	164.9	1.758		41.87
23	9	200	423	204.5	1.782		74.33
24	0.7388	200	423	126.6	0.187		70.46
25	0.0433	200	500	6850	58.04		1528
26	0.6933	200	500	107.1	3.839		25.464
27	8.2612	200	350	131.5	1.717		56.51
28	1738	130	320	320.4	6.86		22.09
29	1738	130	385	386	7.047		32.09
30	8.2612	200	385	169.3	1.82		63.65
31	7.667	332.5	318.7	1396	5.184	0.99	170.5

Table 5.3 Thermodynamic properties of the discharging period (continued)

32	7.667	332.5	282.1	1258	4.727	0.99	169.3
33	7.667	130	249	1160	4.777	0.99	55.78
34	7.667	130	302	1370	5.549	0.99	35.82
35	5.75	130	302	1370	5.549	0.99	35.82
36	50	156.5	278	42.86	0.8166	0.6	35.52
37	50	400	299.6	61.74	0.8166	0.6	54.4
38	50	400	305	180	1.206	0.6	56.67
39	44.25	400	325	34.04	0.7233	0.4	11.54
40	44.25	400	302	-99.57	0.3009	0.4	3.785
41	44.25	160	298	-91.75	0.3282	0.4	3.477
42	5.75	400	340	1442	5.236	0.99	201
43	1.917	130	255	1204	4.952	0.99	47.78
44	16.66	101.3	276	12.08	0.04363		3.581
45	16.66	101.3	300	112.6	0.3928		0.02795
46	30.23	101.3	308	308.4	6.893		0.1652
47	30.23	101.3	255	255	6.703		3.458
48	7.186	101.3	278	20.49	0.07399		2.944
49	7.186	101.3	313	167	0.5702		1.528
50	6.02	100	385	208.3	0.6114		26.17
51	6.02	400	390	221.5	0.6441		29.58
52	6.02	400	505	786	1.899		220.2
53	6.02	100	483.5	742	1.905		174.2
54	187.7	101.3	288	288.2	6.825		0.1727
55	187.7	101.3	305	305.3	6.883		0.08149
56	60	600	495	453.9	1.282		83.84
57	60	1000	520	503.7	1.38		104.4
58	60	600	544.7	553	1.474		125.8
59	No flow during the discharging period						
60	No flow during the discharging period						
61	60	600	544.7	553	1.474		125.8
62	60	600	544.7	553	1.474		125.8
63	60	600	567	599	1.556		147.2
64	60	600	567	599	1.556		147.2
65	60	600	567	599	1.556		147.2
66	18.17	200	622	715.2	1.753		204.9
67	18.17	200	548	559.1	1.486		128.1
68	No flow during the discharging period						
69	No flow during the discharging period						
70	18.17	300	560	583.9	1.531		139.7
71	18.17	300	560	583.9	1.531		139.7
72	18.17	200	548	559.1	1.486		128.1

Table 5.3 Thermodynamic properties of the discharging period (continued)

73	19	200	388	481.9	1.472		47.83
74	3	200	388	481.9	1.472		47.83
75	3	200	355	342.8	1.097		20.37
76	51	200	386.1	473.7	1.45		46.21
77	0.2	200	288	62.48	0.222		0.8169
78	0.2	200	350	321.8	1.038		17.13
79	0.022	200	370	4967	53.68		944.7
80	0.1778	200	370	66.03	0.02187		59.56

As mentioned above, the exergy is destructed due to the entropy generation. Figure 5.1 and 5.2 show the entropy generation rates of the main components in system 1. The highest entropy generation rate is observed in the cooling tower with 31.48 kW/K. On the other hand, all devices which are illustrated in Figure 5.1, have entropy generation rates below 1.21 kW/K.
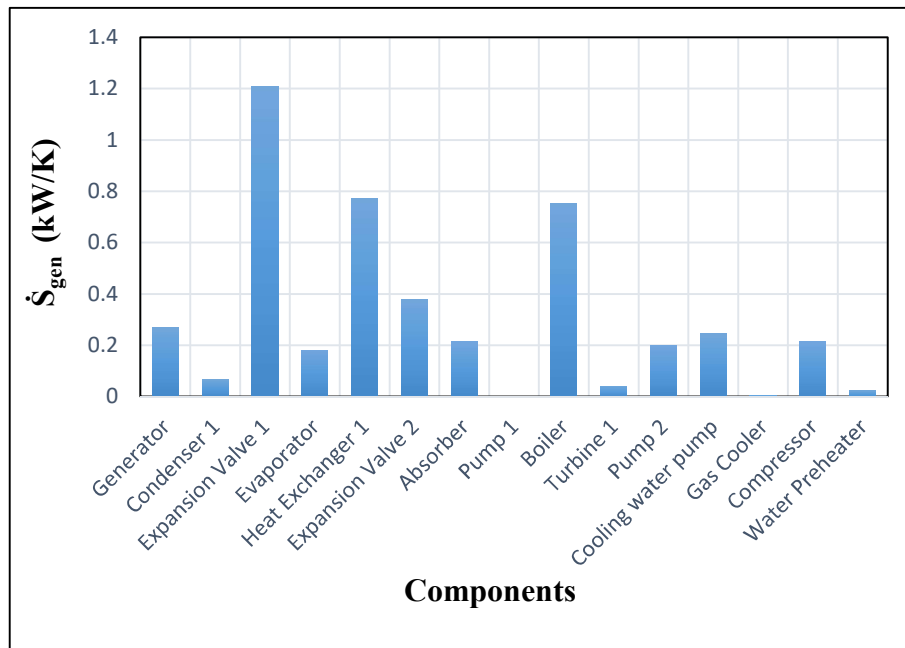
Figure 5.1 Entropy generation rates of the main components of system 1
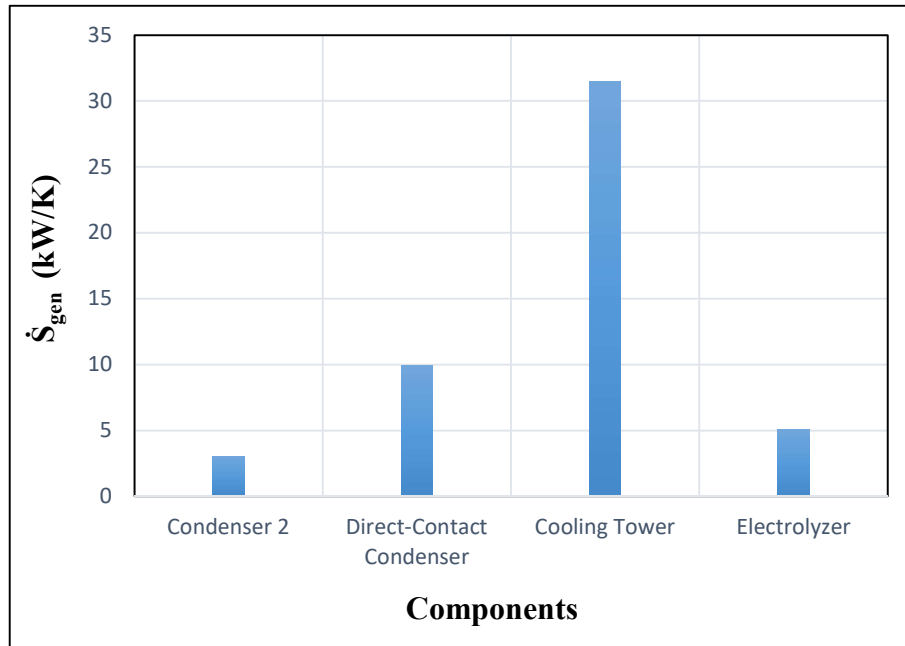
Figure 5.2 The highest entropy generation rates of the main components of system 1

Due to the different operation scenarios, some components of the multigeneration system have different entropy generation rates in the charging, storing and discharging periods. These data are illustrated in Figure 5.3. Entropy generation rate of the parabolic trough collector system in the charging period is 27.24 kW/K. Additionally, its entropy generation rates in the storing and discharging periods are 16.82 kW/K and 5.138 kW/K, respectively.
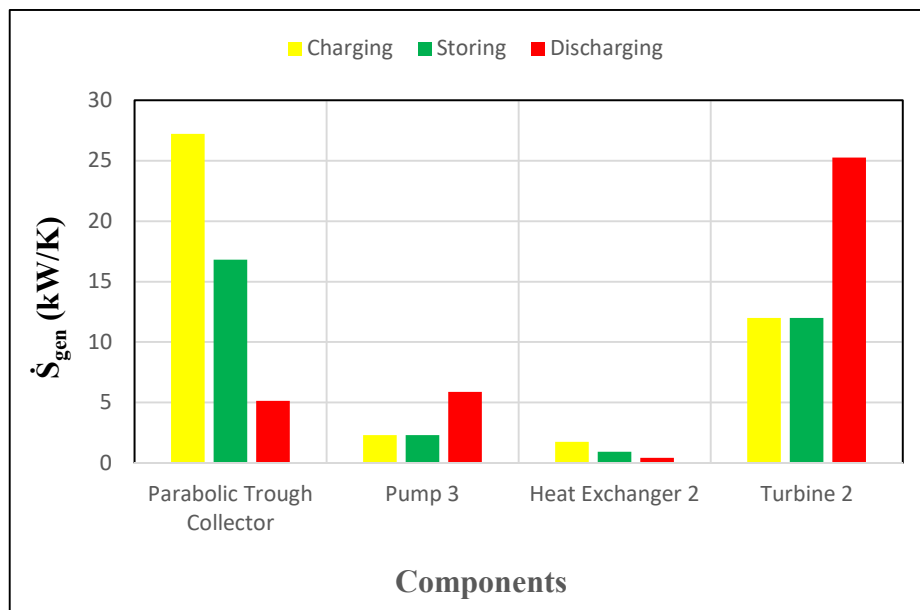
Figure 5.3 Entropy generation rates of some components for 3 different periods

The inlet mass flow rate of the geothermal steam is a significant design criterion for the proposed system. Figure 5.4 demonstrates for each 3 operation periods how overall energy of the designed system changes, depending on the inlet mass flow rate of the geothermal steam. It is clear that, for the all 3 periods overall energy efficiency of the system increases, while inlet mass flow rate rises. The highest overall energy efficiency takes place in the storing period with 71.4% while the mass flow rate of the geothermal steam is about 200 kg/s.
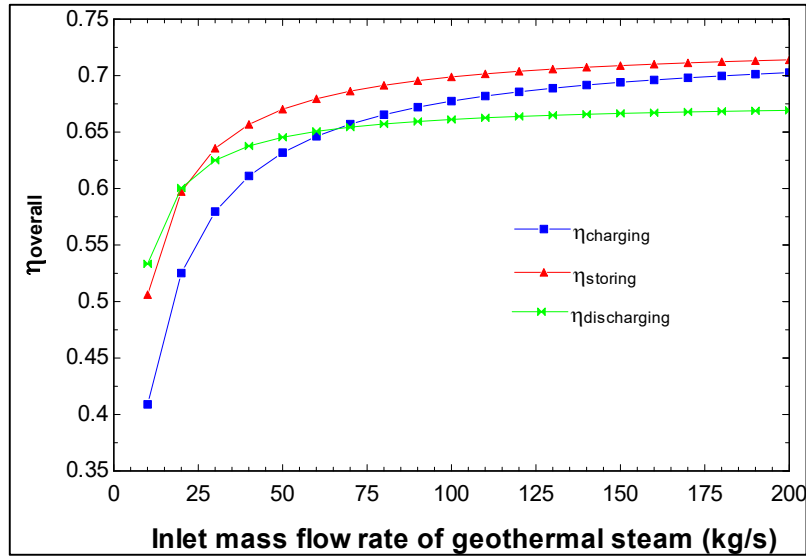
Figure 5.4 Effect of the inlet mass flow rate of geothermal steam on the overall energy efficiency of system 1

Figure 5.5 demonstrates that how overall exergy efficiency of the integrated system changes, depending on the inlet mass flow rate of the geothermal steam. Similarly, overall exergy efficiency of the system rises, while inlet mass flow rate increases. The highest overall exergy efficiency of the system is calculated in the storing period as 71.94%, while the inlet mass flow rate of the geothermal steam is around 200 kg/s.
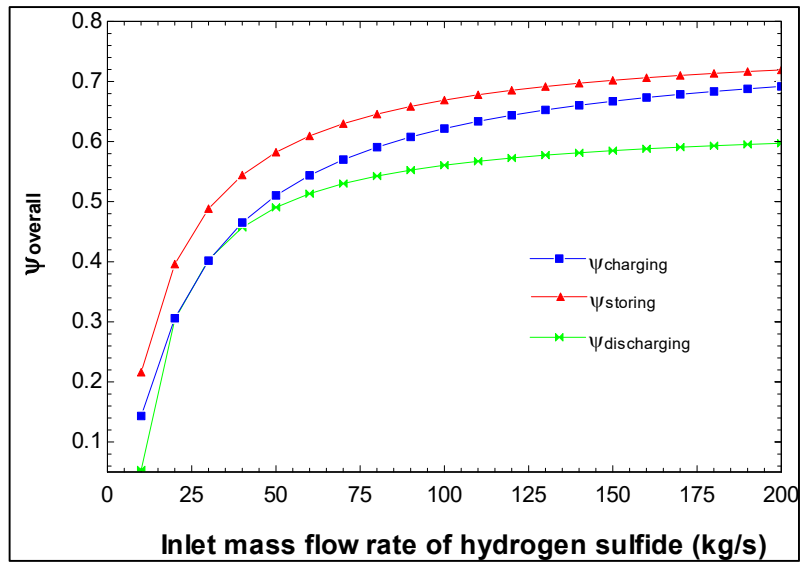
Figure 5.5 Effect of the inlet mass flow rate of geothermal steam on the overall exergy efficiency of system 1

Figure 5.6 shows the effect of ambient temperature on the overall exergy efficiency of the integrated system for each 3 periods. It can be clearly inferenced that the overall exergy efficiency of the system decreases, while ambient temperature rises. In the charging period, the overall exergy efficiency changes between 60.36% and 50.2% when the ambient temperature rises from 273 to 313 K.
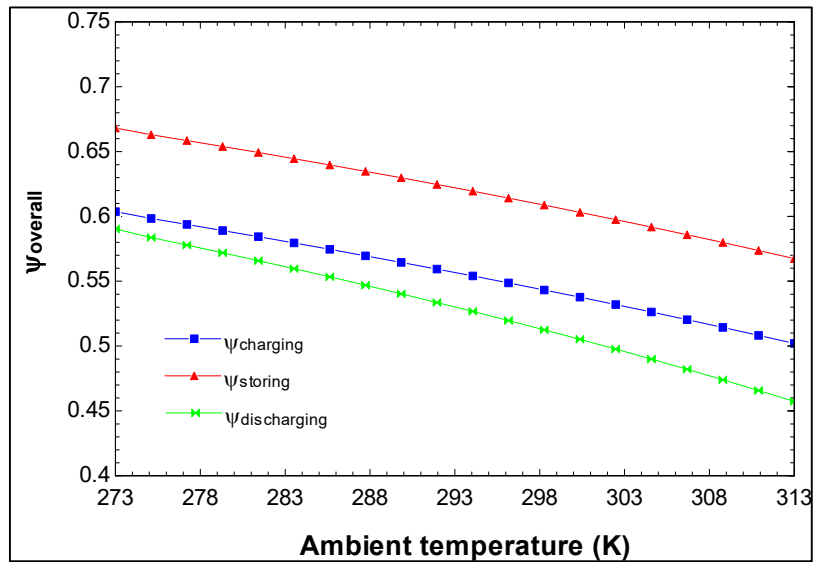
Figure 5.6 Effect of ambient temperature on the overall exergy efficiency of system 1

Figure 5.7 demonstrates how energy and exergy efficiency of the PEM electrolyzer changes depending on the inlet temperature of water. There is a linear relation between the efficiencies and water inlet temperature, such that both energy and exergy efficiency of the PEM electrolyzer increases when the inlet temperature of water rises. The energy and exergy efficiencies are approximately 82.9% and 83.4%, when inlet temperature of the water is around 290 K. Furthermore, as the temperature of the electrolysis process products rise, both energy and exergy efficiency get lower values at the same operating conditions.
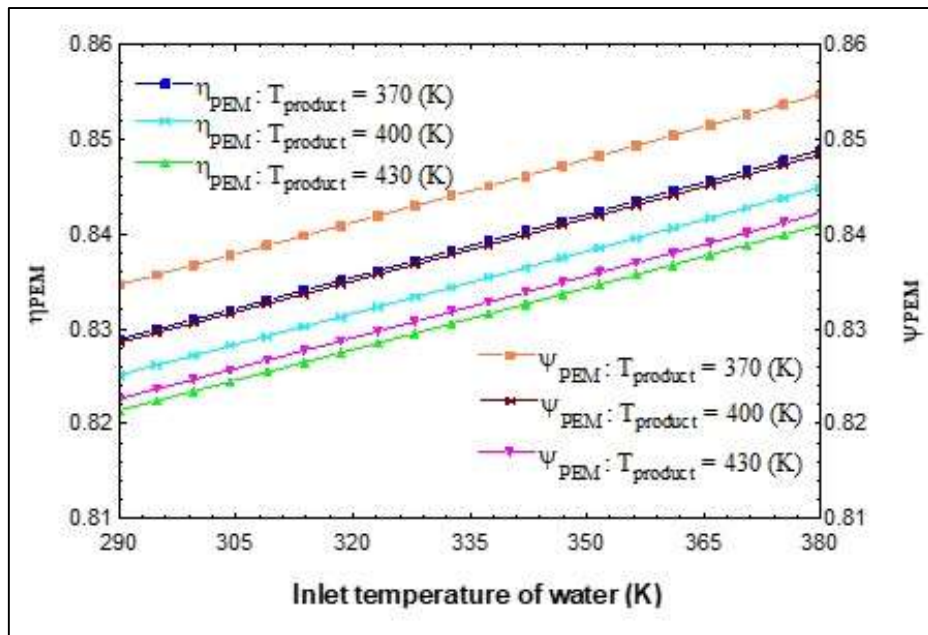
Figure 5.7 Effect of inlet temperature of water on the energy and exergy efficiency of the PEM electrolyzer

The calculated parameters of the designed system are given in Table 5.4 for each period, considering the assumptions. While in the charging and storing periods approximately 21.82 MW electricity is produced from the designed system, in the discharging period this figure decreases to at around 14.26 MW. The highest overall energy and exergy efficiencies are determined in the storing period with 67.95% and 65.06%, respectively.

Table 5.4 The calculated parameters used to evaluate the designed system

Parameters	Charging Period	Storing Period	Discharging Period
Turbine 1 power output	264.9 kW	264.9 kW	264.9 kW
Turbine 2 power output	21554 kW	21554 kW	13994 kW
Solar heat input, $\dot{Q}_{solar}$	17756 kW	10399 kW	2959 kW
The number of collectors	185	185	185
Mass of the phase change material, m_{PCM}	70.571 tons	70.571 tons	70.571 tons
Overall energy efficiency	64.64%	67.95%	65.06%
Overall exergy efficiency	54.39%	60.94%	51.34%

5.2   System 2 Results

Contrary to system 1, system 2 is not designed to operate in three different scenarios, although it includes parabolic trough collectors. However, the effect of changing average hourly solar radiation on the overall energy efficiency is investigated. In addition, in system 1, geothermal fluid is assumed as dry steam. Thus, system 1 does not include the flashing processes. Yet, in system 2, geothermal fluid is assumed to be a liquid-vapor mixture. Therefore, the second system contains a double flash cycle. Moreover, a wind farm is integrated into the main system so as to conduct a comparative study. Thermodynamic properties of all streams of system 2 are listed in Table 5.5.

Table 5.5 Thermodynamic properties of system 2

State	$\dot{m}_i$ (kg/s)	P_i (kPa)	T_i (K)	h_i (kJ/kg)	s_i (kJ/kgK)	x (kg/kg)	ex_{ph} (kJ/kg)
1	60	3500	515.7	1050	2.725	0	242.2
2	60	3000	507	1726	4.061	0.4	520.6
3	24	3000	507	2803	6.185	1	964.5
4	24	2500	497.1	2784	6.219	0.99	935
5	45.6	2500	497.1	2792	6.236	0.9947	938.5
6	45.6	1700	477.5	2718	6.237	0.96	863.6
7	36	3000	507	1008	2.645	0	224.6
8	36	2500	497.1	2066	4.775	0.6	647.7
9	14.4	2500	497.1	962	2.554	0	205.4
10	21.6	2500	497.1	2802	6.256	1	942.4
11	45.6	1700	641.6	3184	7.105		1072
12	67	600	510	483.2	1.341		95.39
13	67	1000	520	503.7	1.38		104.4

Table 5.5 Thermodynamic properties of system 2 (continued)

14	67	600	661.6	803.2	1.889		252.3
15	45.6	1700	636.6	3173	7.088		1066
16	7.385	332.5	318.7	1396	5.184	0.99	172.4
17	7.385	332.5	282.1	1258	4.727	0.99	171.2
18	7.385	130	249	1160	4.777	0.99	57.68
19	7.385	130	302	1370	5.549	0.99	37.71
20	5.539	130	302	1370	5.549	0.99	37.71
21	50	156.7	278	42.47	0.8151	0.6	36.35
22	50	400	299.8	65.09	0.8277	0.6	55.22
23	50	400	305	180	1.206	0.6	57.45
24	44.46	400	325	34.04	0.7233	0.4	11.74
25	44.46	400	303	-95.17	0.3155	0.4	4.045
26	44.46	160	298	-91.75	0.3282	0.4	3.672
27	5.539	400	340	1442	5.236	0.99	202.9
28	1.846	130	255	1204	4.952	0.99	49.67
29	13.78	100	276	12.08	0.04363		3.581
30	13.78	100	300	112.6	0.3928		0.02795
31	29.12	100	308	308.4	6.897		0.1652
32	29.12	100	255	255	6.707		3.458
33	6.922	100	278	20.49	0.07399		2.944
34	6.922	100	313	167	0.5702		1.528
35	45.6	1700	566.6	3018	6.829		987.4
36	2.652	400	390	490.5	1.493		50.01
37	2.652	400	621.6	3167	7.735		866.4
38	2.652	100	483.5	2896	7.878		552.7
39	2.652	100	371	410	1.283		32.31
40	385.3	100	288	288.2	6.829		0.1727
41	385.3	100	305	305.3	6.887		0.08149
42	45.6	250	403	2722	7.066		620.8
43	2941	200	392	498.9	1.515		51.83
44	2941	250	392	499	1.515		51.89
45	980.3	250	392	499	1.515		51.89
46	980.3	250	392	499	1.515		51.89
47	980.3	250	392	499	1.515		51.89
48	70	600	385	469.5	1.439		45.31
49	35.76	600	385	469.5	1.439		45.31
50	34.24	600	385	469.5	1.439		45.31
51	31.24	200	390	490.4	1.494		49.81
52	30	200	384	465	1.428		43.97
53	30	200	384.6	467.5	1.435		44.54
54	2841	200	385	469.2	1.439		44.92

Table 5.5 Thermodynamic properties of system 2 (continued)

55	2872	200	385	469.2	1.439		44.92
56	1915	200	385	469.2	1.439		44.92
57	957.4	200	385	469.2	1.439		44.92
58	6.84	150	398	177	1.789		45.77
59	6.84	150	387	164.9	1.758		42.88
60	6.84	200	423	204.5	1.782		75.34
61	0.5615	200	423	126.6	0.187		71.41
62	0.03293	200	500	6850	58.04		1545
63	0.5269	200	500	107.1	3.839		25.464
64	6.279	200	350	131.5	1.717		57.52
65	1373	130	322	322.4	6.866		23.36
66	1373	130	385	386	7.047		33.22
67	6.279	200	385	169.3	1.82		64.66
68	31.24	600	385	469.5	1.439		45.31
69	3	600	385	469.5	1.439		45.31
70	3	600	355	343.1	1.097		20.77
71	38.76	600	382.7	459.7	1.412		43.41
72	0.2	200	288	62.48	0.222		0.8182
73	0.2	200	350	321.8	1.038		17.13
74	0.1778	200	370	66.03	0.02187		60.58
75	0.02222	200	370	4967	53.68		960.9

Figure 5.8 and 5.9 show the entropy generation rates of the main components in the integrated cycle. The highest entropy generation rate is observed in the cooling tower with 81.13 kW/K. On the other hand, all devices which are illustrated in Figure 5.8, have entropy generation rates below 0.8 kW/K.
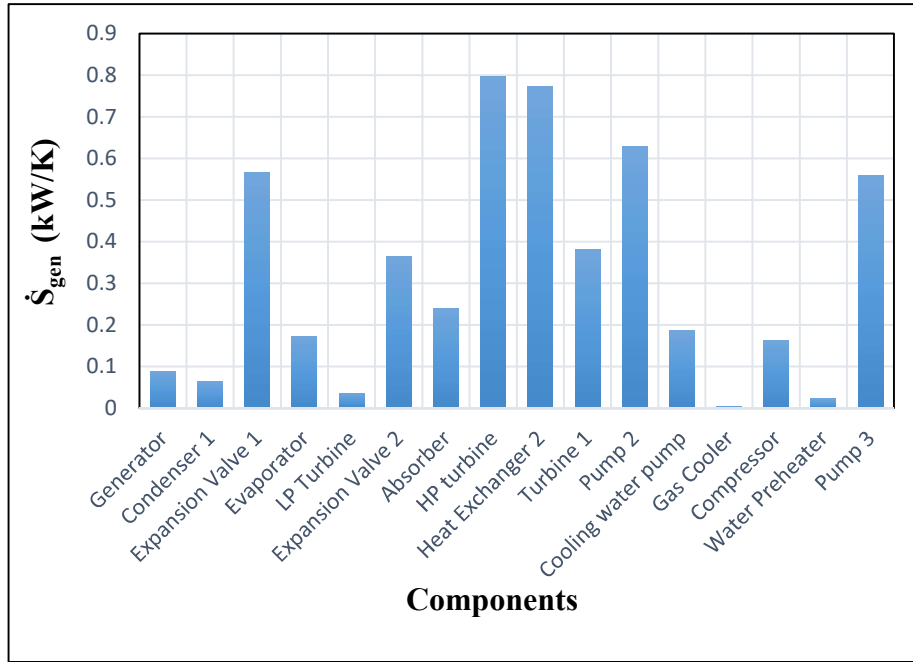
Figure 5.8 Entropy generation rates of main components of system 2
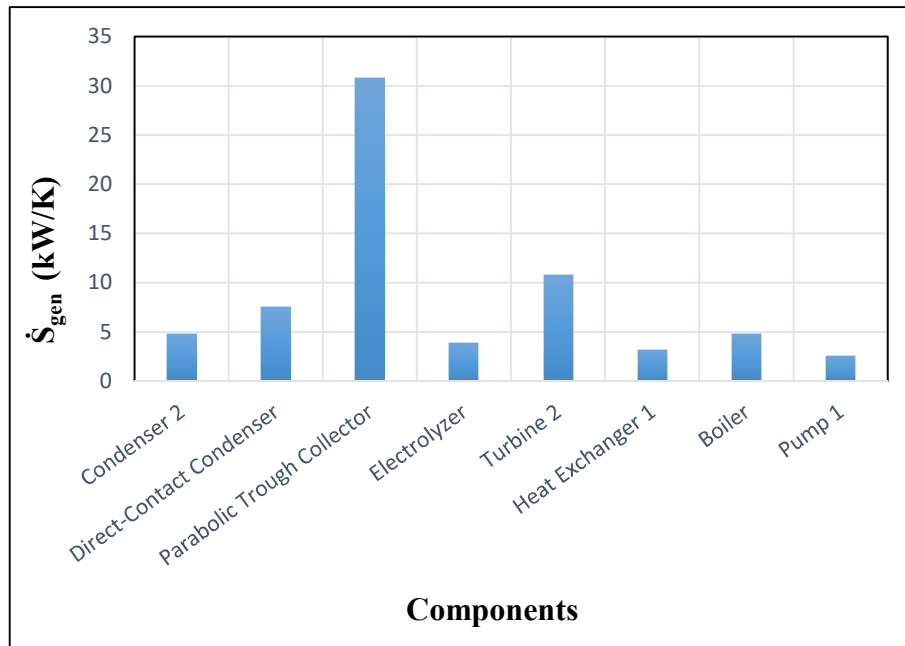
Figure 5.9 The highest entropy generation rates of main components of system 2

Inlet velocity of the wind is a significant criterion for the wind turbine designs. The effects of the inlet velocity of the wind on the produced electricity and exergy destruction rate are presented in Figure 5.10. When inlet velocity of the wind gets higher values, the amount of produced electricity rises correspondingly. While inlet velocity of the air to the

wind turbine is approximately 7.5 m/s, at around 71.2 kW power output can be obtained, considering the design parameters.
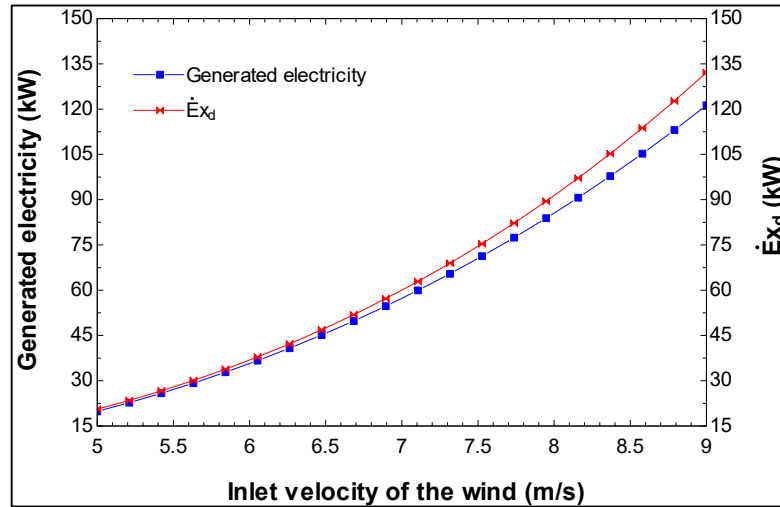
Figure 5.10 Effect of the inlet velocity of the wind on the produced electricity and exergy destruction rate

Figure 5.11 shows how the energy efficiency of the wind turbine changes depending on the inlet velocity of the wind. With the increase in inlet velocity, the energy efficiency of the wind turbine first rises and then decreases after reaching the optimum velocity. It can be inferred from the figure that maximum energy efficiency is obtained from the wind turbine, when the outlet velocity of the wind is equal to one-third of the inlet velocity.
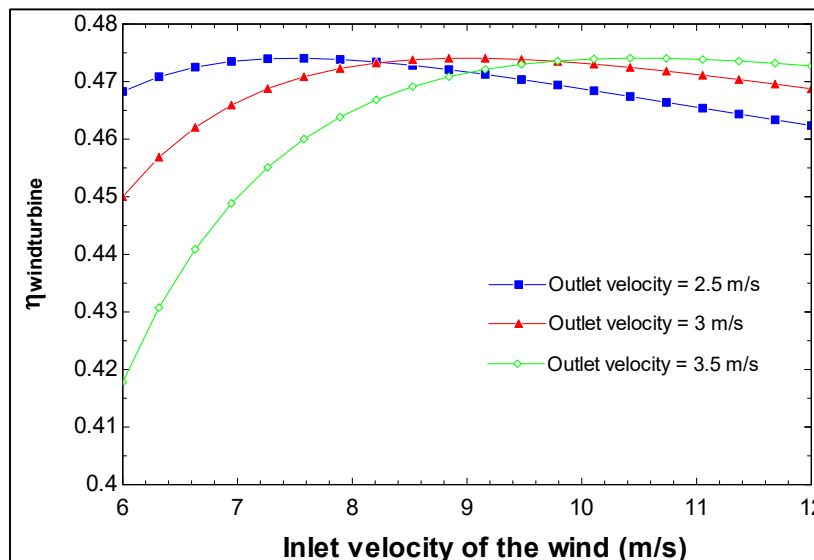
Figure 5.11 Effect of the inlet velocity of the wind on the energy efficiency of the wind turbine at different outlet velocities

Average hourly solar radiation is also a noteworthy design criterion for the solar assisted multigeneration systems. In system 2, the temperature of the geothermal steam is increased by the solar system. As expected, while average hourly solar radiation gets higher values, the geothermal steam temperature increases accordingly which provides us to produce more power from the system. Figure 5.12 illustrates the effect of the average hourly solar radiation on the amount of produced power. While average hourly solar radiation is 2 MJ/m^2h, approximately 12.7 MW power is produced by turbine 2.
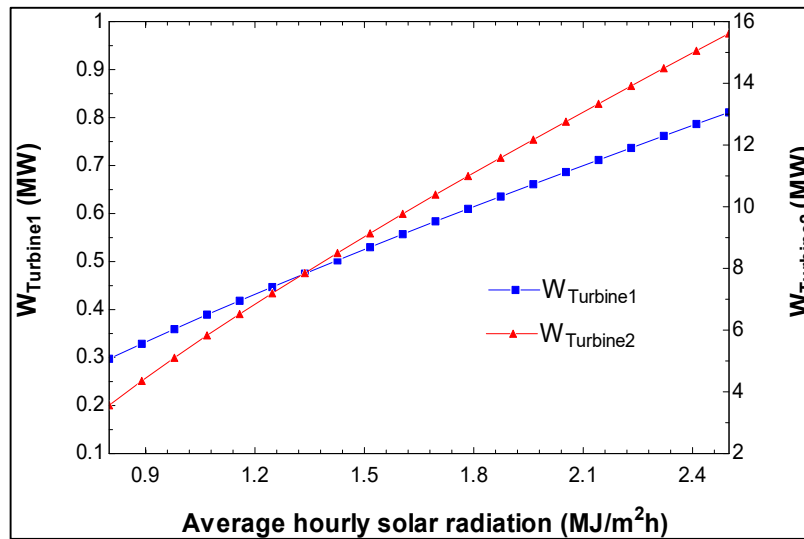
Figure 5.12 Effect of the average hourly solar radiation on the amount of produced power

The effects of the ambient temperature variation on the energetic and exergetic COPs of the absorption cooling system are illustrated in Figure 5.13. As the ambient temperature changes from 273 K to 313 K, the energetic COP stays constant while exergetic COP rises from 0.0034 to 0.1682. This is due to the fact that as the ambient temperature increases the exergetic output of the evaporator increases resulting in the increase in exergetic COP. There is no change in the energetic COP of the single effect absorption cooling system since it is not a function of ambient temperature. The results show that exergy analysis provides a better insight than energy analysis.
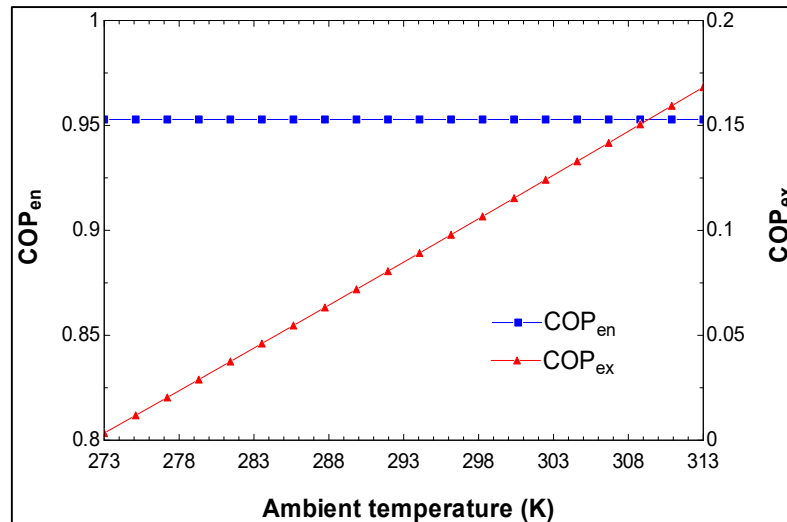
Figure 5.13 Effect of ambient temperature on energetic and exergetic COPs of the single effect absorption cooling system

Figure 5.14 demonstrates how overall energy efficiency of system 2 changes, depending on the inlet mass flow rate of the geothermal fluid. It is clear that, the overall energy efficiency of the system increases, while inlet mass flow rate rises. The highest overall energy efficiency takes place at around 73% while the mass flow rate of the geothermal fluid is about 200 kg/s. In addition, while average hourly solar radiation is equal to 0.80 MJ/m^2h, approximately 55% overall energy efficiency can be obtained at the same inlet mass flow rate value.
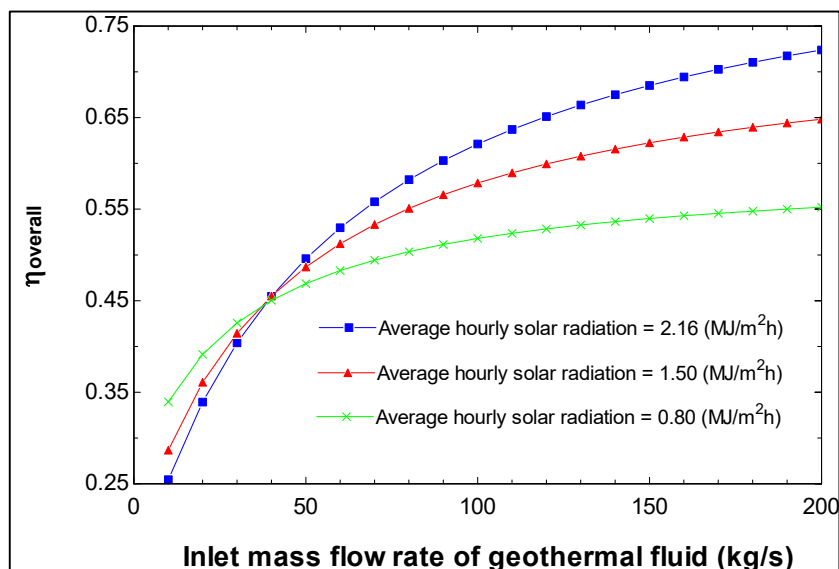
Figure 5.14 Effect of inlet mass flow rate of geothermal fluid on the overall energy efficiency of system 2 at different radiation intakes

The energy and exergy efficiencies of the wind turbine system are determined as approximately 47% and 46% at the specified conditions, respectively. Both of them are lower than the overall energy and exergy efficiencies of system 2. Therefore, the increasing number of wind turbines results with the lower overall efficiencies as shown in Figure 5.15. Here, E_w represents the combined efficiency of the several wind turbine system equipments which involve the turbine blades, the shaft bearings and gear train, the generator and power electronics. From Figure 5.15, it can be clearly seen that while E_w gets lower values, overall energy and exergy efficiency of system 2 slightly decrease.
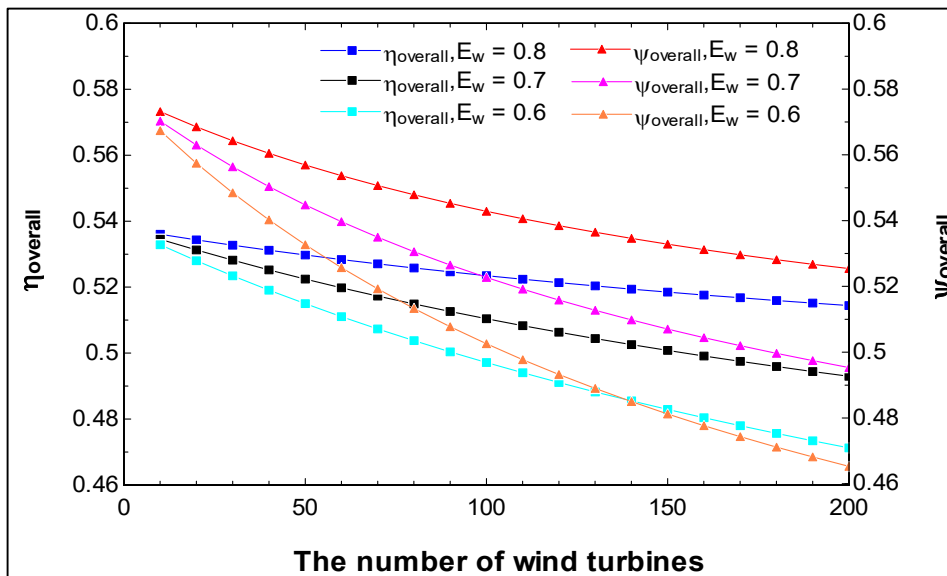
Figure 5.15 Effect of the number wind turbines on the overall energy and exergy efficiency of system 2

The calculated parameters of the integrated system are given in Table 5.6, considering the assumptions. The overall energy and exergy efficiencies are 52.97% and 55.69%, respectively.

Table 5.6 The calculated parameters used to evaluate the system 2

Parameter	Value
HP turbine power output	0.47 MW
LP turbine power output	3.40 MW
Turbine 1 power output	0.72 MW
Turbine 2 power output	13.46 MW
Wind turbine system power output	3.53 MW
Required electrical power for electrolysis of the water	3.17 MW

Table 5.6 The calculated parameters used to evaluate the system 2 (continued)

Solar heat input	20 MW
Wind power input	7.44 MW
The number of collectors	209
Energetic COP of absorption cooling system	0.95
Exergetic COP of absorption cooling system	0.11
Overall energy efficiency	52.97%
Overall exergy efficiency	55.69%

5.3 System 3 Results

In this section, all results related to system 3 will be presented. The surface temperature of the charging pipe inside the packed bed thermal storage system varies, depending on the convection heat transfer coefficient and pipe length as shown in Figure 5.16. There is an exponential relation between the convection heat transfer coefficient and the surface temperature of the charging pipe. While convection heat transfer coefficient has higher values, the surface temperature of the charging pipe increases. In addition, by increasing the charging pipe length, the surface temperature of the charging pipe reaches to 350 K at lower convection transfer coefficients.
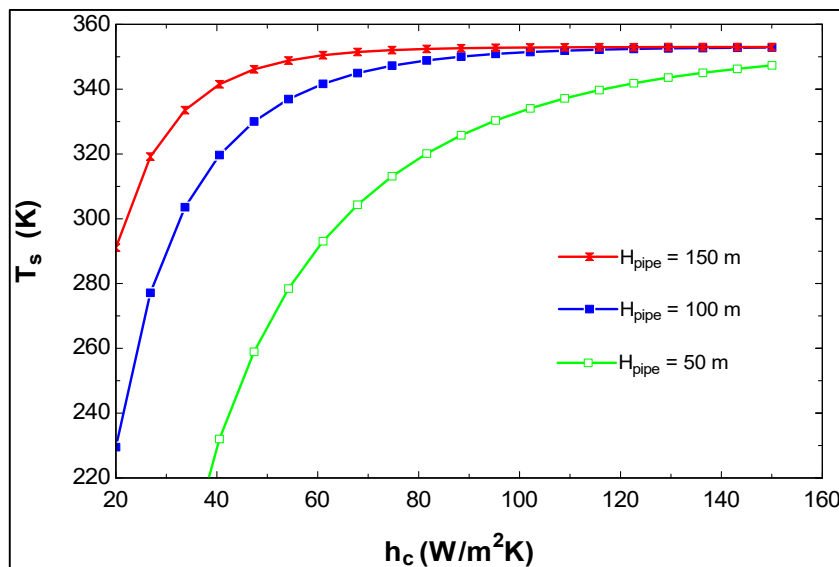
Figure 5.16 Effect of convection heat transfer coefficient on surface temperature of the charging pipe

The final temperature of the rock at the end of the storing period changes and depends on several parameters such as density, specific heat and thermal conductivity of the rock and also design parameters of the packed bed rock system. When the radius of the packed bed

system increases, the final temperature of the rock gets closer to its initial conditions as given in Figure 5.17.
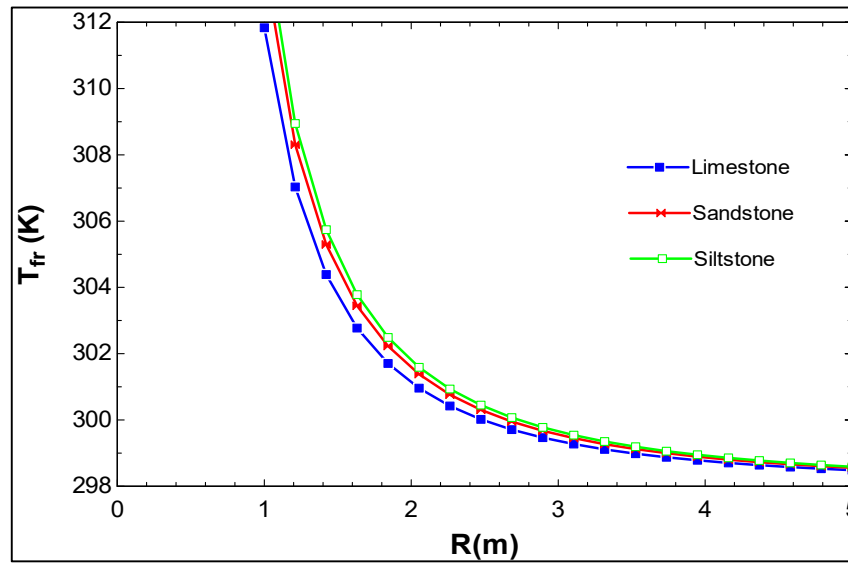
Figure 5.17 Effect of radius of the packed rock system on the final temperature value of the rock

Therefore, it is important to minimize the packed bed radius as much as possible in order to reach higher rock temperatures. Additionally, three different kinds of rocks are compared with each other. Results show that siltstone is the best option in terms of thermal properties. However, in such systems, the endurance of material and cycle life are some significant properties and have to take into consideration during the design stage.

In the underground cavern system, compressed air is stored during the entire storing period. In order to evaluate the underground cavern system performance, it is important to investigate the compressed air heat losses in general and the soil temperature at depth (x) which surrounds the cavern, in particular. From Figure 5.18, one can infer that for the soil depth of 5 meters, the temperature remains constant as its initial temperature. Additionally, storing period is a crucial parameter, such that while storing period increases, soil temperature by 6 meters has lower temperatures.
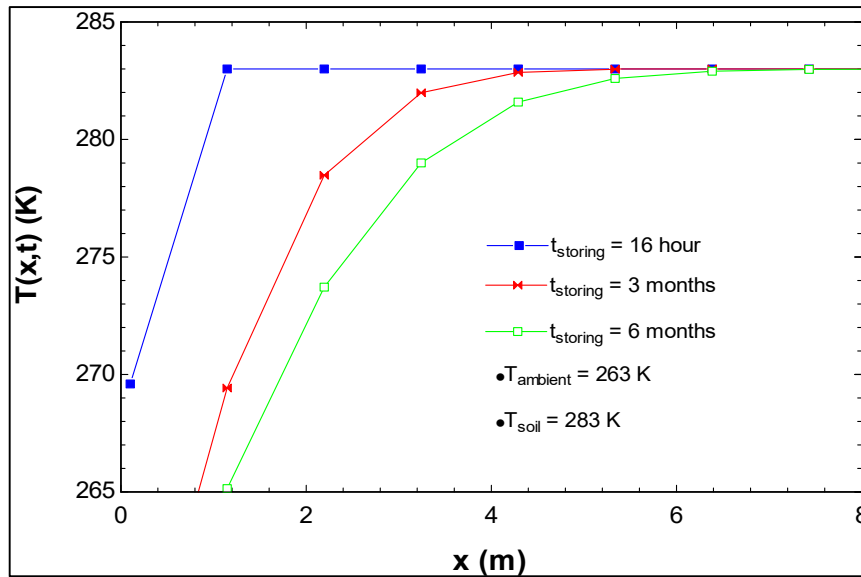
Figure 5.18 Relation between the soil depth and time-dependent soil temperature

Compressed air flows into the underground cavern after passing through the packed bed storage system at a high-pressure (P_{17} = 14.42 MPa). During the storing period, due to the mass and heat transfers from the underground cavern to the surrounded vicinity, the pressure of the compressed air decreases and therefore, the pressure of the air releasing from the underground cavern in the discharging period (P_{18}) would have lower values compared to the initial conditions. The effect of the outlet pressure of the compressed air on the energy and exergy efficiencies of the underground cavern is illustrated in Figure 5.19. The energy efficiency of the underground cavern decreases from 70.32% to 67.40%, while outlet pressure of the compressed air changes between 10 MPa and 14.42 MPa. In contrast, the exergy efficiency of the underground cavern rises from 92.10% to 99.43% at the same changing pressure range.
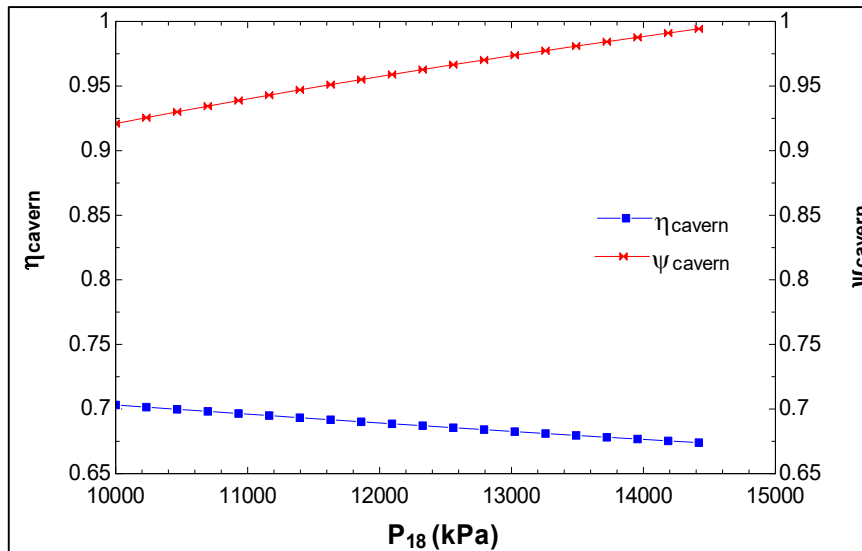
Figure 5.19 Effect of the compressed air outlet pressure on the energy and exergy efficiency of the underground cavern system

Energy and exergy efficiencies of the hot storage tank system vary, depending on the phase change material and heat transfer fluid properties. Melting temperature, specific heat of solid and liquid phases and heat of fusion of the PCM are among the main parameters to determine the most suitable PCM for the system. In the present study, three different types of PCM are examined and their effects on the energy and exergy efficiency of the hot storage tank are shown in Figure 5.20. $LiNO_3$ exhibits the best performance and energy and exergy efficiency of the hot storage tank reaches to at around 82% and 84% while the temperature of the PCM is 800 K at the end of the charging period.

Figure 5.21 illustrates that how energy and exergy efficiencies of the gasifier change, depending on the equivalence ratio during the charging, storing and discharging periods. It can be clearly observed that, the energy efficiency of the gasifier is almost the same for all three periods. On the other hand, exergy efficiency has the highest and lowest values in the storing and charging periods, respectively. While the equivalence ratio is near to 0.30, energy and exergy efficiencies of the gasification process at the discharging period are approximately 26% and 28%, respectively.
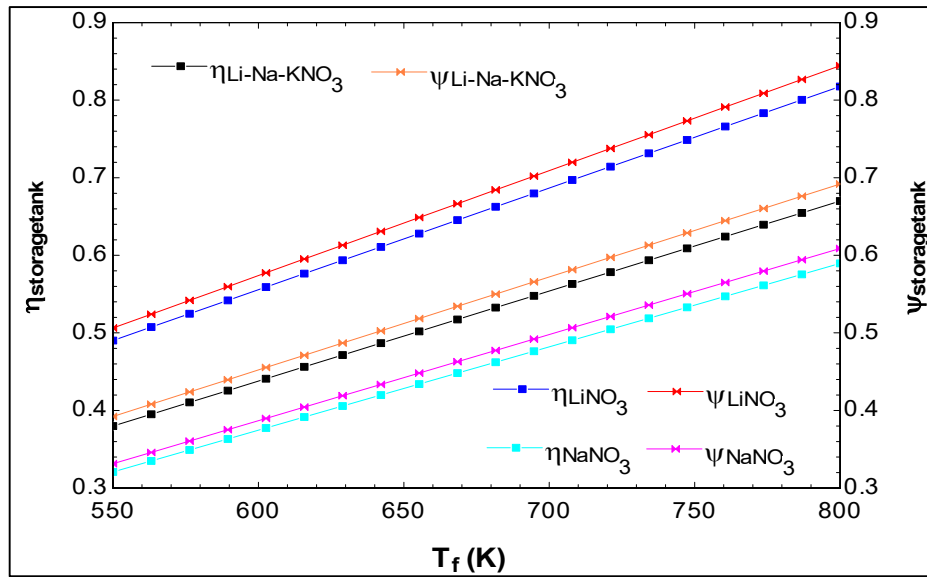
Figure 5.20 Effect of the final temperature of phase change material on the energy and exergy efficiency of the hot storage tank
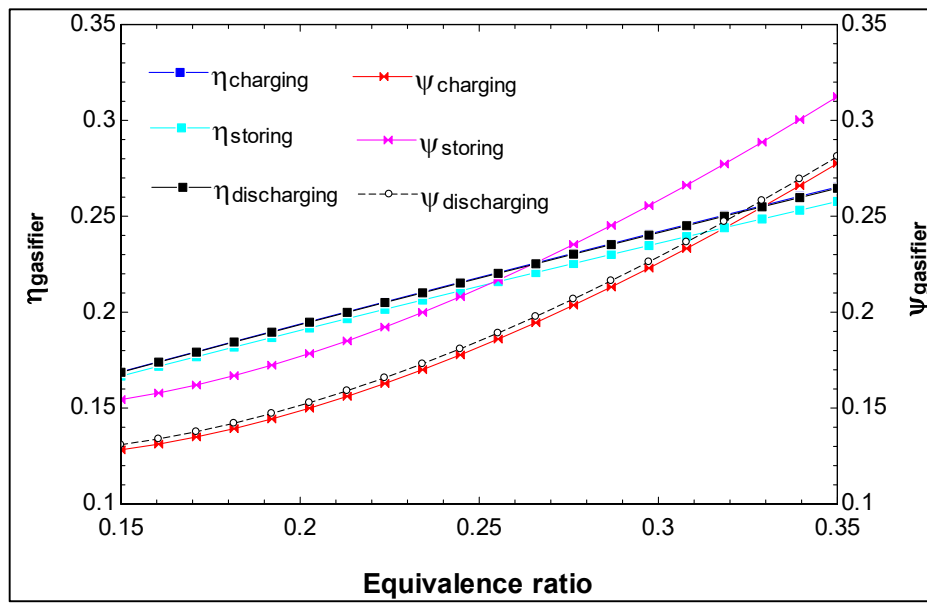
Figure 5.21 Effect of the equivalence ratio on the efficiencies of the gasifier

Proposed multigeneration energy system operates in three different scenarios. In the first scenario, average hourly solar radiation is insufficient to heat the air to the desired temperature levels. In this case, by adding biomass to the gasifier, the expected temperature levels at the inlet of the gas turbines can be obtained. Thermodynamic properties of the all stream points of this mechanism are given in Table 5.7.

Table 5.7 Thermodynamic properties of system 3 during the charging period

State	$\dot{m}_i$ (kg/s)	P_i (kPa)	T_i (K)	h_i (kJ/kg)	s_i (kJ/kgK)	x (kg/kg)	ex_{ph} (kJ/kg)
1	10	101.3	298	298.3	6.86		0
2	10	1250	631.6	640.8	6.906		328.7
3	10	1250	398.1	398	6.427		228.8
4	10	14420	819.4	850	6.479		665.1
5	10	14420	550	553.1	6.04		499
6	7	14420	550	553.1	6.04		499
7	7	14420	550	553.1	6.04		499
8	22.19	8000	1200	Combustion chamber 1 products: State 112-113-114			
9	22.19	4000	750	Expanded combustion chamber 1 products at HP turbine: State 118-119-120			
10	53.81	6000	1000	Combustion chamber 2 products: State 115-116-117			
11	53.81	2000	790	Expanded combustion chamber 2 products at LP turbine: State 121-122-123			
12	53.81	2000	520	Combustion chamber 2 products after leaving the heat exchanger 2: State 124-125-126			
13	29.34	101.3	298	298.3	6.86		0
14	29.34	101.3	380	381	7.105		9.656
15	29.34	101.3	470	472.6	7.321		36.8
16	3	14420	550	553.1	6.04		499
17	3	14420	353	335.6	5.55		427.7
18	0	101.3	298	298.3	6.86		0
19	0	101.3	298	298.3	6.86		0
20	7.6	101.3	298	395.1	6.12		96.78
21	21	5000	1000	Gasifier products : State 108-109-110-111			
22	14.7	5000	1000	Gasifier products flows into the combustion chamber 1: State 108-109-110-111			
23	6.301	5000	1000	Gasifier products flows into the combustion chamber 2: State 108-109-110-111			
24	39.34	101.3	580	586.5	7.539		85.83
25	25.39	101.3	580	586.5	7.539		85.83
26	13.95	101.3	580	586.5	7.539		85.83
27	0.546	101.3	580	586.5	7.539		85.83
28	13.4	101.3	580	586.5	7.539		85.83
29	10	101.3	298	298.3	6.86		0
30	39.34	101.3	426.3	428	7.222		21.87
31	50	6600	412	407.5	5.969		374.7
32	50	8000	440	436.3	5.98		400.2
33	50	8000	677	690.3	6.441		516.7
34	15	8000	677	690.3	6.441		516.7
35	15	8000	420	414.9	5.93		393.7

Table 5.7 Thermodynamic properties of system 3 during the charging period (continued)

36	15	8000	300	283.9	5.562		372.3
37	35	8000	677	690.3	6.441		516.7
38	0	101.3	298	298.3	6.86		0
39	35	8000	677	690.3	6.441		516.7
40	35	6000	460	458.7	6.114		382.6
41	60	3500	515.7	1050	2.725	0	242.2
42	60	3000	507	1726	4.061	0.4	520.6
43	36	3000	507	1008	2.645	0	224.6
44	24	3000	507	2803	6.185	1	964.5
45	24	2183	490	2781	6.268	0.99	917.9
46	24	2183	770	3459	7.382		1264
47	24	2183	762	3442	7.359		1253
48	7.314	332.5	318.7	1396	5.184	0.99	170.5
49	7.314	332.5	282.1	1258	4.727	0.99	169.3
50	7.314	130	249	1160	4.777	0.99	55.78
51	7.314	130	302	1370	5.549	0.99	35.82
52	5.486	130	302	1370	5.549	0.99	35.82
53	50	156.7	278	42.38	0.8148	0.6	35.58
54	50	400	299.8	64.95	0.8272	0.6	54.44
55	50	400	305	180	1.206	0.6	56.67
56	44.51	400	325	34.04	0.7233	0.4	11.54
57	44.51	400	303	-95.17	0.3155	0.4	3.85
58	44.51	160	298	-91.75	0.3282	0.4	3.477
59	5.486	400	340	1442	5.236	0.99	201
60	1.829	130	255	1204	4.952	0.99	47.78
61	13.06	101.3	276	12.08	0.04363		3.581
62	13.06	101.3	300	112.6	0.3928		0.02795
63	28.84	101.3	308	308.4	6.893		0.1652
64	28.84	101.3	255	255	6.703		3.458
65	6.856	101.3	278	20.49	0.07399		2.944
66	6.856	101.3	313	167	0.5702		1.528
67	24	2183	692	3287	7.147		1162
68	1.262	400	390	490.5	1.493		50.01
69	1.262	400	747	3430	8.12		1014
70	1.262	100	555	3038	8.153		613.1
71	1.262	100	371	410	1.283		32.31
72	193.8	101.3	288	288.2	6.825		0.1727
73	193.8	101.3	305	305.3	6.883		0.08149
74	24	250	420	2759	7.155		630.9
75	1573	200	392	498.9	1.515		51.83
76	1573	250	392	499	1.515		51.89

Table 5.7 Thermodynamic properties of system 3 during the charging period (continued)

77	524.4	250	392	499	1.515		51.89
78	524.4	250	392	499	1.515		51.89
79	524.4	250	392	499	1.515		51.89
80	70	200	385	469.2	1.439		44.92
81	17.4	200	385	469.2	1.439		44.92
82	52.6	200	385	469.2	1.439		44.92
83	49.6	200	390	490.4	1.494		49.81
84	30	200	384	465	1.428		43.96
85	30	200	384.3	466.2	1.431		44.25
86	1473	200	385	469.2	1.439		44.92
87	1523	200	385	469.2	1.439		44.92
88	1015	200	385	469.2	1.439		44.92
89	507.6	200	385	469.2	1.439		44.92
90	3.6	150	398	177	1.789		44.77
91	3.6	150	387	164.9	1.758		41.87
92	3.6	200	423	204.5	1.782		74.33
93	0.2955	200	423	126.6	0.187		70.46
94	0.01733	200	500	6850	58.04		1528
95	0.2773	200	500	107.1	3.839		25.464
96	3.304	200	350	131.5	1.717		57.52
97	531.5	400	298	297.6	6.464		0.6842
98	531.5	400	385	385.7	6.723		10.12
99	3.304	200	385	169.3	1.82		64.66
100	49.6	200	385	469.2	1.439		44.92
101	3	200	385	469.2	1.439		44.92
102	3	200	355	342.8	1.097		20.37
103	20.4	200	380.6	450.6	1.389		41.31
104	0.2	200	288	62.48	0.222		0.8182
105	0.2	200	350	321.8	1.038		17.13
106	0.1778	200	370	66.03	0.02187		60.58
107	0.0222	200	370	4967	53.68		944.7
108	8.982	5000	1000	1025	7.145		705
109	1.422	5000	1000	3964	7.578		1710
110	0.3103	5000	1000	14238	54.93		9842
111	10.29	5000	1000	1079	6.982		726.1
112	6.287	8000	1200	1015	7.197		970.1
113	2.952	8000	1200	4436	7.793		2118
114	12.95	8000	1200	1320	7.059		943.8
115	14.11	6000	1000	758.9	0.4852		613.5
116	4.217	6000	1000	3958	7.489		1731

Table 5.7 Thermodynamic properties of system 3 during the charging period (continued)

117	35.48	6000	1000	1080	6.928		743
118	6.287	4000	750	760.9	6.909		511.3
119	2.952	4000	750	3393	7.023		1305
120	12.95	4000	750	792.3	6.72		517.4
121	14.11	2000	790	504.4	0.4119		382
122	4.217	2000	790	3505	7.481		1281
123	35.48	2000	790	836.2	6.985		482.3
124	14.11	2000	520	203.3	0.173		219.3
125	4.217	2000	520	2895	6.532		953.1
126	35.48	2000	520	541	6.529		323.1
(CO:108,112,118), (H_2O: 109, 113, 116, 119, 122, 125), (H_2: 110), (N_2: 111,114, 117, 120, 123, 126), (CO_2: 115, 121, 124)							

In the second scenario, compressed air and heat transfer fluid are not divided into two streams at states 5 and 33. Similar to the first scenario, again average hourly solar radiation is assumed to be insufficient and biomass is to be added to the gasifier. Thermodynamic properties of the all stream points of this mechanism are given in Table 5.8.

Table 5.8 Thermodynamic properties of system 3 during the storing period

State	$\dot{m}_i$ (kg/s)	P_i (kPa)	T_i (K)	h_i (kJ/kg)	s_i (kJ/kgK)	x (kg/kg)	ex_{ph} (kJ/kg)
1	13	101.3	298	298.3	6.86		0
2	13	1250	631.6	640.8	6.906		328.7
3	13	1250	398.1	398	6.427		228.8
4	13	14420	819.4	850	6.479		665.1
5	13	14420	550	553.1	6.04		499
6	13	14420	550	553.1	6.04		499
7	13	14420	550	553.1	6.04		499
8	33.58	8000	1200	Combustion chamber 1 products: State 112-113-114			
9	33.58	4000	750	Expanded combustion chamber 1 products at HP turbine: State 118-119-120			
10	81.43	6000	1000	Combustion chamber 2 products: State 115-116-117			
11	81.43	2000	790	Expanded combustion chamber 2 products at LP turbine: State 121-122-123			
12	81.43	2000	520	Combustion chamber 2 products after leaving the heat exchanger 2: State 124-125-126			
13	38.14	101.3	298	298.3	6.86		0
14	38.14	101.3	380	381	7.105		9.656
15	38.14	101.3	470	472.6	7.321		36.8
16	0	101.3	298	298.3	6.86		0

Table 5.8 Thermodynamic properties of system 3 during the storing period (continued)

17	0	101.3	298	298.3	6.86		0
18	0	101.3	298	298.3	6.86		0
19	0	101.3	298	298.3	6.86		0
20	11.5	101.3	298	395.1	6.12		96.78
21	31.78	5000	1000	Gasifier products : State 108-109-110-111			
22	22.25	5000	1000	Gasifier products flows into the combustion chamber 1: State 108-109-110-111			
23	9.535	5000	1000	Gasifier products flows into the combustion chamber 2: State 108-109-110-111			
24	58.14	101.3	800	822.5	7.884		219.2
25	37.79	101.3	800	822.5	7.884		219.2
26	20.35	101.3	800	822.5	7.884		219.2
27	0.06729	101.3	800	822.5	7.884		219.2
28	20.28	101.3	800	822.5	7.884		219.2
29	20	101.3	298	298.3	6.86		0
30	58.14	101.3	418.8	412.3	7.184		17.35
31	50	6000	405	400.5	5.98		364.6
32	50	8000	440	436.3	5.98		400.2
33	50	8000	862	894.7	6.708		641.6
34	0	101.3	298	298.3	6.86		0
35	0	101.3	298	298.3	6.86		0
36	0	101.3	298	298.3	6.86		0
37	50	8000	862	894.7	6.708		641.6
38	0	101.3	298	298.3	6.86		0
39	50	8000	862	894.7	6.708		641.6
40	50	6000	405	400.5	5.98		364.6
41	60	3500	515.7	1050	2.725	0	242.2
42	60	3000	507	1726	4.061	0.4	520.6
43	36	3000	507	1008	2.645	0	224.6
44	24	3000	507	2803	6.185	1	964.5
45	24	2183	490	2781	6.268	0.99	917.9
46	24	2183	770	3459	7.382		1264
47	24	2183	762	3442	7.359		1253
48	7.314	332.5	318.7	1396	5.184	0.99	170.5
49	7.314	332.5	282.1	1258	4.727	0.99	169.3
50	7.314	130	249	1160	4.777	0.99	55.78
51	7.314	130	302	1370	5.549	0.99	35.82
52	5.486	130	302	1370	5.549	0.99	35.82
53	50	156.7	278	42.38	0.8148	0.6	35.58
54	50	400	299.8	64.95	0.8272	0.6	54.44
55	50	400	305	180	1.206	0.6	56.67

Table 5.8 Thermodynamic properties of system 3 during the storing period (continued)

56	44.51	400	325	34.04	0.7233	0.4	11.54
57	44.51	400	303	-95.17	0.3155	0.4	3.85
58	44.51	160	298	-91.75	0.3282	0.4	3.477
59	5.486	400	340	1442	5.236	0.99	201
60	1.829	130	255	1204	4.952	0.99	47.78
61	13.06	101.3	276	12.08	0.04363		3.581
62	13.06	101.3	300	112.6	0.3928		0.02795
63	28.84	101.3	308	308.4	6.893		0.1652
64	28.84	101.3	255	255	6.703		3.458
65	6.856	101.3	278	20.49	0.07399		2.944
66	6.856	101.3	313	167	0.5702		1.528
67	24	2183	692	3287	7.147		1162
68	1.262	400	390	490.5	1.493		50.01
69	1.262	400	747	3430	8.12		1014
70	1.262	100	555	3038	8.153		613.1
71	1.262	100	371	410	1.283		32.31
72	193.8	101.3	288	288.2	6.825		0.1727
73	193.8	101.3	305	305.3	6.883		0.08149
74	24	250	420	2759	7.155		630.9
75	1573	200	392	498.9	1.515		51.83
76	1573	250	392	499	1.515		51.89
77	524.4	250	392	499	1.515		51.89
78	524.4	250	392	499	1.515		51.89
79	524.4	250	392	499	1.515		51.89
80	70	200	385	469.2	1.439		44.92
81	17.4	200	385	469.2	1.439		44.92
82	52.6	200	385	469.2	1.439		44.92
83	49.6	200	390	490.4	1.494		49.81
84	30	200	384	465	1.428		43.96
85	30	200	384.3	466.2	1.431		44.25
86	1473	200	385	469.2	1.439		44.92
87	1523	200	385	469.2	1.439		44.92
88	1015	200	385	469.2	1.439		44.92
89	507.6	200	385	469.2	1.439		44.92
90	3.6	150	398	177	1.789		44.77
91	3.6	150	387	164.9	1.758		41.87
92	3.6	200	423	204.5	1.782		74.33
93	0.2955	200	423	126.6	0.187		70.46
94	0.01733	200	500	6850	58.04		1528
95	0.2773	200	500	107.1	3.839		25.464
96	3.304	200	350	131.5	1.717		57.52

Table 5.8 Thermodynamic properties of system 3 during the storing period (continued)

97	531.5	400	298	297.6	6.464		0.6842
98	531.5	400	385	385.7	6.723		10.12
99	3.304	200	385	169.3	1.82		64.66
100	49.6	200	385	469.2	1.439		44.92
101	3	200	385	469.2	1.439		44.92
102	3	200	355	342.8	1.097		20.37
103	20.4	200	380.6	450.6	1.389		41.31
104	0.2	200	288	62.48	0.222		0.8182
105	0.2	200	350	321.8	1.038		17.13
106	0.1778	200	370	66.03	0.02187		60.58
107	0.0222	200	370	4967	53.68		944.7
108	13.59	5000	1000	1025	7.145		705
109	2.151	5000	1000	3964	7.578		1710
110	0.4696	5000	1000	14238	54.93		9842
111	15.57	5000	1000	1079	6.982		726.1
112	9.514	8000	1200	1015	7.197		970.1
113	4.467	8000	1200	4436	7.793		2118
114	19.6	8000	1200	1320	7.059		943.8
115	21.36	6000	1000	758.9	0.4852		613.5
116	6.381	6000	1000	3958	7.489		1731
117	53.69	6000	1000	1080	6.928		743
118	9.514	4000	750	760.9	6.909		511.3
119	4.467	4000	750	3393	7.023		1305
120	19.6	4000	750	792.3	6.72		517.4
121	21.36	2000	790	504.4	0.4119		382
122	6.381	2000	790	3505	7.481		1281
123	53.69	2000	790	836.2	6.985		482.3
124	21.36	2000	520	203.3	0.173		219.3
125	6.381	2000	520	2895	6.532		953.1
126	53.69	2000	520	541	6.529		323.1

(CO:108,112,118), (H_2O: 109, 113, 116, 119, 122, 125), (H_2: 110), (N_2: 111,114, 117, 120, 123, 126), (CO_2: 115, 121, 124)

In the last scenario, flow stream at state (18) is released and compressed air which is stored in the underground cavern starts to discharge and connect to state (6), after passing through the packed bed storage system. Additionally, heat transfer fluid which is circulated in the solar-driven system, enters to the hot storage tank and receives the heat of the PCM and leaves the hot storage tank as heated at state (38). Thermodynamic properties of the all stream points of this mechanism are listed in Table 5.9.

Table 5.9 Thermodynamic properties of system 3 during the discharging period

State	$\dot{m}_i$ (kg/s)	P_i (kPa)	T_i (K)	h_i (kJ/kg)	s_i (kJ/kgK)	x (kg/kg)	ex_{ph} (kJ/kg)
1	15	101.3	298	298.3	6.86		0
2	15	1250	631.6	640.8	6.906		328.7
3	15	1250	398.1	398	6.427		228.8
4	15	14420	819.4	850	6.479		665.1
5	15	14420	550	553.1	6.04		499
6	15	14420	550	553.1	6.04		499
7	18	14420	525.9	526.8	5.991		487.3
8	36.15	8000	1200	Combustion chamber 1 products: State 112-113-114			
9	36.15	4000	750	Expanded combustion chamber 1 products at HP turbine: State 118-119-120			
10	88.51	6000	1000	Combustion chamber 2 products: State 115-116-117			
11	88.51	2000	790	Expanded combustion chamber 2 products at LP turbine: State 121-122-123			
12	88.51	2000	520	Combustion chamber 2 products after leaving the heat exchanger 2: State 124-125-126			
13	44.01	101.3	298	298.3	6.86		0
14	44.01	101.3	380	381	7.105		9.656
15	44.01	101.3	470	472.6	7.321		36.8
16	0	101.3	298	298.3	6.86		0
17	0	101.3	298	298.3	6.86		0
18	3	14420	283	251.9	5.285		422.9
19	3	14420	433	425.3	5.779		449.1
20	12.5	101.3	298	395.1	6.12		96.78
21	34.55	5000	1000	Gasifier products : State 108-109-110-111			
22	24.18	5000	1000	Gasifier products flows into the combustion chamber 1: State 108-109-110-111			
23	10.36	5000	1000	Gasifier products flows into the combustion chamber 2: State 108-109-110-111			
24	64.01	101.3	600	607.5	7.575		96.21
25	41.76	101.3	600	607.5	7.575		96.21
26	22.25	101.3	600	607.5	7.575		96.21
27	0.2039	101.3	600	607.5	7.575		96.21
28	22.05	101.3	600	607.5	7.575		96.21
29	20	101.3	298	298.3	6.86		0
30	64.01	101.3	416.3	417.8	7.197		18.89
31	50	7000	420	415.7	5.971		382.2
32	50	8000	440	436.3	5.98		400.2
33	50	8000	583	588.9	6.28		463.3
34	50	8000	583	588.9	6.28		463.3
35	0	101.3	298	298.3	6.86		0

Table 5.9 Thermodynamic properties of system 3 during the discharging period (continued)

36	0	101.3	298	298.3	6.86		0
37	0	101.3	298	298.3	6.86		0
38	50	8000	650	661	6.397		500.6
39	50	8000	650	661	6.397		500.6
40	50	7000	420	415.7	5.971		382.1
41	60	3500	515.7	1050	2.725	0	242.2
42	60	3000	507	1726	4.061	0.4	520.6
43	36	3000	507	1008	2.645	0	224.6
44	24	3000	507	2803	6.185	1	964.5
45	24	2183	490	2781	6.268	0.99	917.9
46	24	2183	770	3459	7.382		1264
47	24	2183	762	3442	7.359		1253
48	7.314	332.5	318.7	1396	5.184	0.99	170.5
49	7.314	332.5	282.1	1258	4.727	0.99	169.3
50	7.314	130	249	1160	4.777	0.99	55.78
51	7.314	130	302	1370	5.549	0.99	35.82
52	5.486	130	302	1370	5.549	0.99	35.82
53	50	156.7	278	42.38	0.8148	0.6	35.58
54	50	400	299.8	64.95	0.8272	0.6	54.44
55	50	400	305	180	1.206	0.6	56.67
56	44.51	400	325	34.04	0.7233	0.4	11.54
57	44.51	400	303	-95.17	0.3155	0.4	3.85
58	44.51	160	298	-91.75	0.3282	0.4	3.477
59	5.486	400	340	1442	5.236	0.99	201
60	1.829	130	255	1204	4.952	0.99	47.78
61	13.06	101.3	276	12.08	0.04363		3.581
62	13.06	101.3	300	112.6	0.3928		0.02795
63	28.84	101.3	308	308.4	6.893		0.1652
64	28.84	101.3	255	255	6.703		3.458
65	6.856	101.3	278	20.49	0.07399		2.944
66	6.856	101.3	313	167	0.5702		1.528
67	24	2183	692	3287	7.147		1162
68	1.262	400	390	490.5	1.493		50.01
69	1.262	400	747	3430	8.12		1014
70	1.262	100	555	3038	8.153		613.1
71	1.262	100	371	410	1.283		32.31
72	193.8	101.3	288	288.2	6.825		0.1727
73	193.8	101.3	305	305.3	6.883		0.08149
74	24	250	420	2759	7.155		630.9
75	1573	200	392	498.9	1.515		51.83

Table 5.9 Thermodynamic properties of system 3 during the discharging period (continued)

76	1573	250	392	499	1.515		51.89
77	524.4	250	392	499	1.515		51.89
78	524.4	250	392	499	1.515		51.89
79	524.4	250	392	499	1.515		51.89
80	70	200	385	469.2	1.439		44.92
81	17.4	200	385	469.2	1.439		44.92
82	52.6	200	385	469.2	1.439		44.92
83	49.6	200	390	490.4	1.494		49.81
84	30	200	384	465	1.428		43.96
85	30	200	384.3	466.2	1.431		44.25
86	1473	200	385	469.2	1.439		44.92
87	1523	200	385	469.2	1.439		44.92
88	1015	200	385	469.2	1.439		44.92
89	507.6	200	385	469.2	1.439		44.92
90	3.6	150	398	177	1.789		44.77
91	3.6	150	387	164.9	1.758		41.87
92	3.6	200	423	204.5	1.782		74.33
93	0.2955	200	423	126.6	0.187		70.46
94	0.01733	200	500	6850	58.04		1528
95	0.2773	200	500	107.1	3.839		25.464
96	3.304	200	350	131.5	1.717		57.52
97	531.5	400	298	297.6	6.464		0.6842
98	531.5	400	385	385.7	6.723		10.12
99	3.304	200	385	169.3	1.82		64.66
100	49.6	200	385	469.2	1.439		44.92
101	3	200	385	469.2	1.439		44.92
102	3	200	355	342.8	1.097		20.37
103	20.4	200	380.6	450.6	1.389		41.31
104	0.2	200	288	62.48	0.222		0.8182
105	0.2	200	350	321.8	1.038		17.13
106	0.1778	200	370	66.03	0.02187		60.58
107	0.0222	200	370	4967	53.68		944.7
108	14.77	5000	1000	1025	7.145		705
109	2.338	5000	1000	3964	7.578		1710
110	0.5104	5000	1000	14238	54.93		9842
111	16.92	5000	1000	1079	6.982		726.1
112	10.34	8000	1200	1015	7.197		970.1
113	4.855	8000	1200	4436	7.793		2118
114	21.31	8000	1200	1320	7.059		943.8
115	23.21	6000	1000	758.9	0.4852		613.5
116	6.936	6000	1000	3958	7.489		1731

Table 5.9 Thermodynamic properties of system 3 during the discharging period (continued)

117	58.36	6000	1000	1080	6.928		743
118	10.34	4000	750	760.9	6.909		511.3
119	4.855	4000	750	3393	7.023		1305
120	21.31	4000	750	792.3	6.72		517.4
121	23.21	2000	790	504.4	0.4119		382
122	6.936	2000	790	3505	7.481		1281
123	58.36	2000	790	836.2	6.985		482.3
124	23.21	2000	520	203.3	0.173		219.3
125	6.936	2000	520	2895	6.532		953.1
126	58.36	2000	520	541	6.529		323.1
(CO:108,112,118), (H_2O: 109, 113, 116, 119, 122, 125), (H_2: 110), (N_2: 111,114, 117, 120, 123, 126), (CO_2: 115, 121, 124)							

Figure 5.22 shows the entropy generation rates of main components in system 3. Entropy generation rates of these components get the same value in the all operating scenarios. Additionally, the all devices which are illustrated in Figure 5.22, have entropy generation rates below 2 kW/K. Also, entropy generation rates of direct-contact condenser and cooling tower are calculated as 4.093 kW/K and 17.55 kW/K, respectively.
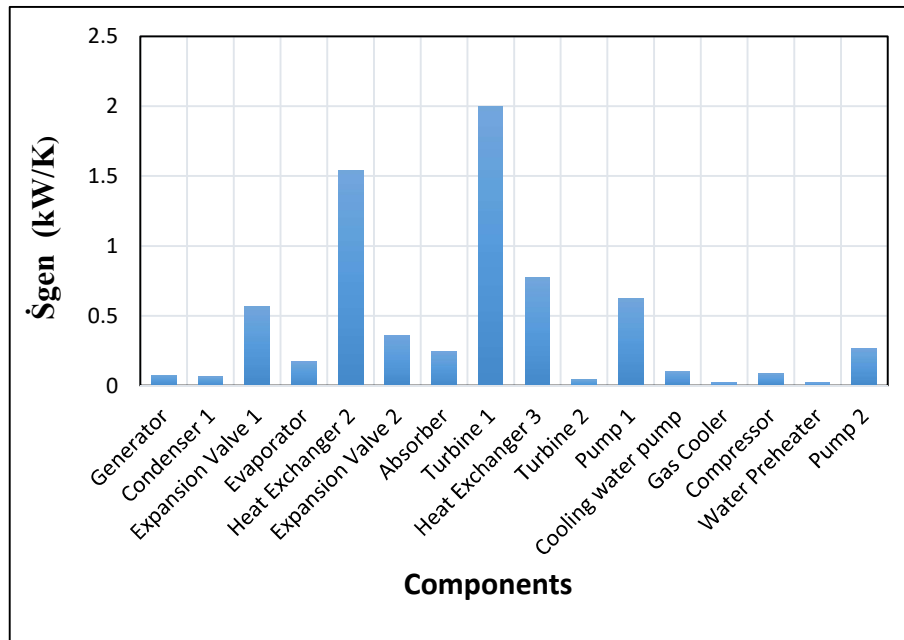
Figure 5.22 Entropy generation rates of main components in system 3
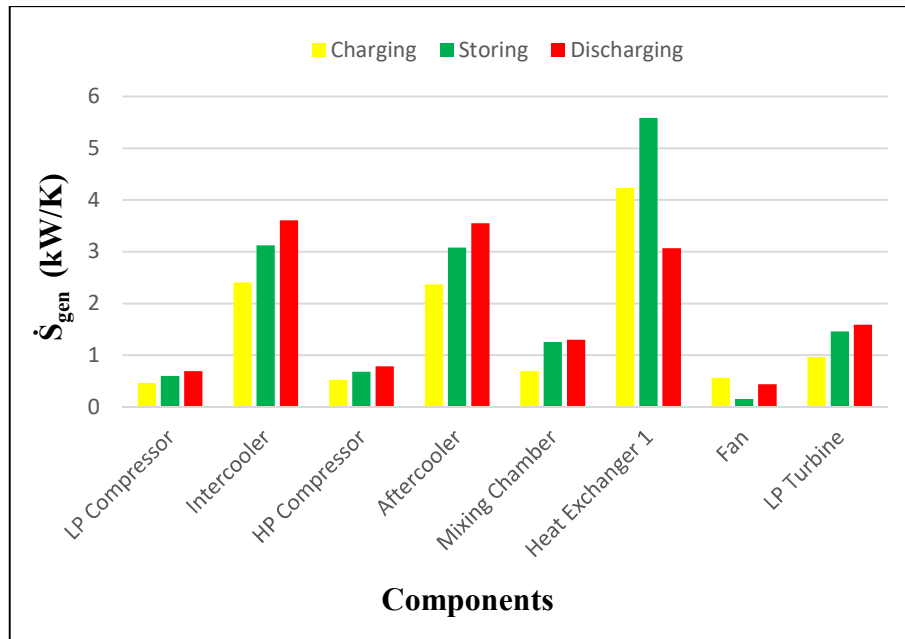
Figure 5.23 Entropy generation rates of some components in system 3 during the three different operating scenarios

Figure 5.23 illustrates how entropy generation rates of some components in system 3 change during the charging, storing and discharging periods. The highest entropy generation rate is determined to be 583.5 kW/K in the gasifier during the discharging period.
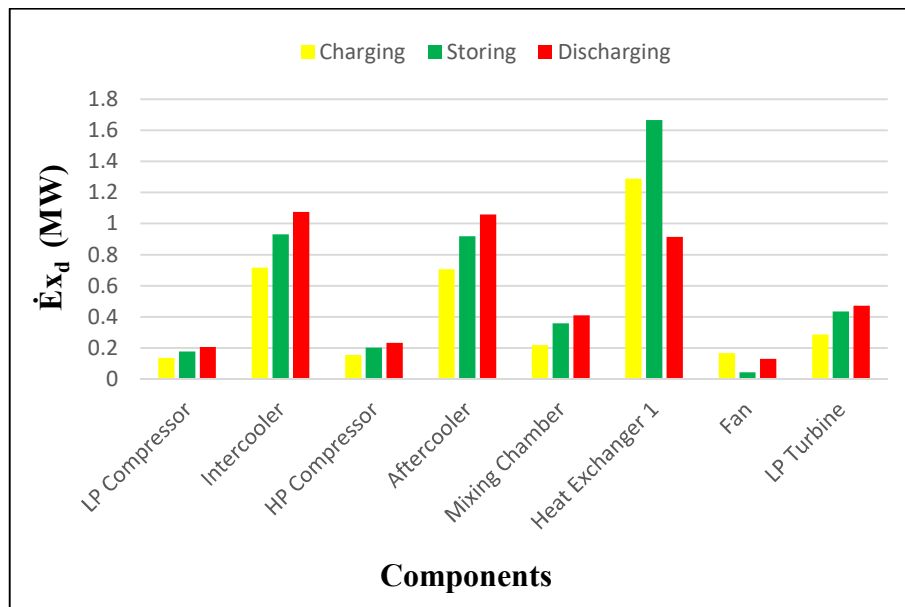
Figure 5.24 Exergy destruction rates of some components in system 3 during the three different operating scenarios

Figure 5.24 shows how exergy destruction rates of some components in system 3 change during the charging, storing and discharging periods. For the most part, the highest and lowest exergy destruction rates are observed during the discharging and charging periods, respectively.

While the inlet mass flow rate of biomass change, depending on this variation, the supplied mass flow rates of air to the gasifier and combustion chambers get different values which effect the overall energy efficiency of system 3 as shown in Figure 5.25. The highest and lowest overall energy efficiencies are determined during the charging and storing periods, respectively. While the inlet mass flow rate of biomass rises from 5 kg/s to 30 kg/s, overall energy efficiency of the proposed system for the charging period decreases from 67.04% to 31.81%.
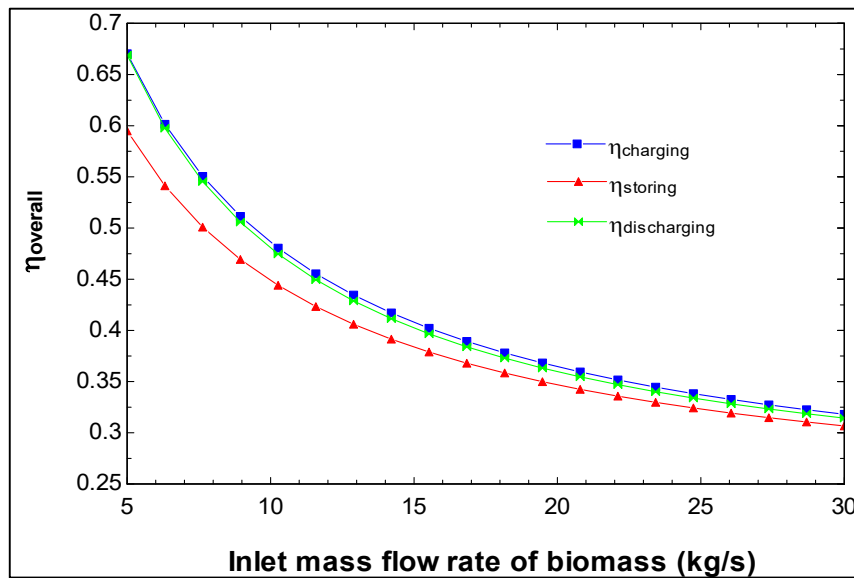
Figure 5.25 Effect of inlet mass flow rate of biomass on the overall energy efficiency of system 3 during the three different operating scenarios

Similar to the overall energy efficiency, the overall exergy efficiency of the designed system decreases, while the inlet mass flow rate of biomass rises. The highest and lowest overall exergy efficiencies are determined during the charging and storing periods, respectively. While inlet mass flow rate of biomass rises from 5 kg/s to 30 kg/s, overall exergy efficiency of the proposed system for the charging period decreases from 26.1% to 20.45% as shown in Figure 5.26.
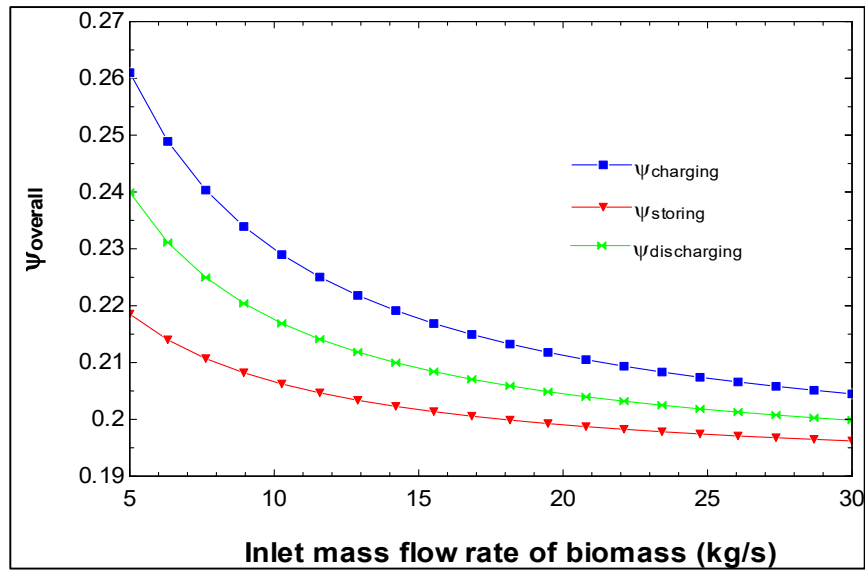
Figure 5.26 Effect of inlet mass flow rate of biomass on the overall exergy efficiency of system 3 during the three different operating scenarios

Figure 5.27 gives an information about how ambient temperature plays a role on the overall exergy efficiency of system 3 in the charging, storing and discharging periods. It can be clearly seen that when ambient temperature gets higher values, the overall exergy efficiency of the designed system slightly decreases. For the discharging period, while ambient temperature rises from 273 to 313 K, the overall exergy efficiency of the system decreases from 22.72% to 20.39%.
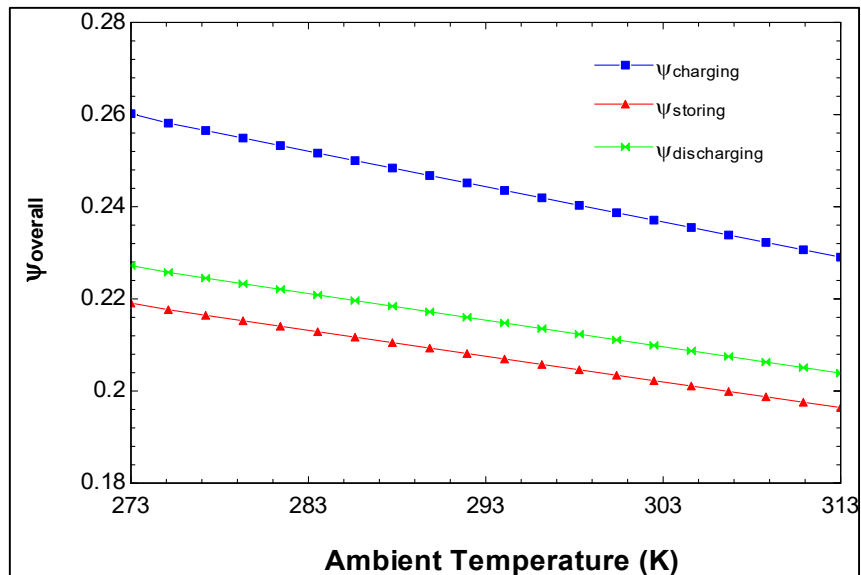
Figure 5.27 Effect of ambient temperature on the overall exergy efficiency of system 3 during the three different operating scenarios

The calculated parameters of the integrated system are given in Table 5.10, considering the assumptions. In the charging period at around 42.96 MW power can be generated from the proposed system. This number increases to 56.16 MW and 59.54 MW during the storing and discharging periods, respectively. The highest overall energy and exergy efficiencies are determined in the charging period with 55.15% and 24.05%, respectively.

Table 5.10 The calculated parameters used to evaluate the system 3

Parameter	Charging Period	Storing Period	Discharging Period
LP Compressor power input	3.425 MW	4.452 MW	5.137 MW
HP Compressor power input	4.520 MW	5.876 MW	6.780 MW
Compressor power input	0.1424 MW	0.1424 MW	0.1424 MW
Fan power input	1.441 MW	1.787 MW	1.032 MW
Solar heat input	12.7 MW	22.920 MW	7.628 MW
Wind power input	7.439 MW	7.439 MW	7.439 MW
Pump 1 power input	1.129 MW	1.129 MW	1.129 MW
Pump 2 power input	0.1016 MW	0.1016 MW	0.1016 MW
Cooling water pump power input	0.1123 MW	0.1223 MW	0.1223 MW
LP Turbine power output	14.146 MW	21.405 MW	23.266 MW
HP Turbine power output	11.582 MW	17.526 MW	19.050 MW
Wind Turbine system power output	3.526 MW	3.526 MW	3.526 MW
Turbine 1 power output	0.525 MW	0.525 MW	0.525 MW
Turbine 2 power output	0.494 MW	0.494 MW	0.494 MW
Turbine 3 power output	12.684 MW	12.684 MW	12.684 MW
Packed rock volume	274.8 m^3	274.8 m^3	274.8 m^3
Cavern volume	408.7 m^3	408.7 m^3	408.7 m^3
The number of collectors	298	298	298
Mass of the phase change material	240 tons	240 tons	240 tons
Heat losses of the underground cavern	Neglected	0.325 MW	Neglected
Overall energy efficiency	55.15%	42.45%	43.46%
Overall exergy efficiency	24.05%	20.47%	21.25%

5.4 System 4 Results

In this section, the results related to the hydrogen production from hydrogen sulfide are presented. Geothermal fluid mainly consists of steam with some percentage (from less than 1% and up to 15%) of non-condensable gases. For the present study, it is important to determine the amount of hydrogen sulfide which is released to atmosphere depending

on the inlet mass flow rate of the geothermal fluid. Through AMIS and electrolyzer units, hydrogen sulfide is decomposed to pure hydrogen and sulfur dimer in order to reduce the adverse effects of hydrogen sulfide and produce additional power supply by means of produced hydrogen. Figure 5.28 shows the obtained amounts of hydrogen sulfide and hydrogen depending on the inlet mass flow rate of the geothermal fluid for the different NCG compositions. As expected, while NCG composition gets higher values, obtained hydrogen sulfide and correspondingly hydrogen amounts increase. While inlet mass flow rate of the geothermal fluid is 60 kg/s, 0.7388 kg hydrogen sulfide and 0.0433 kg hydrogen emerge per second for 15% NCG composition.
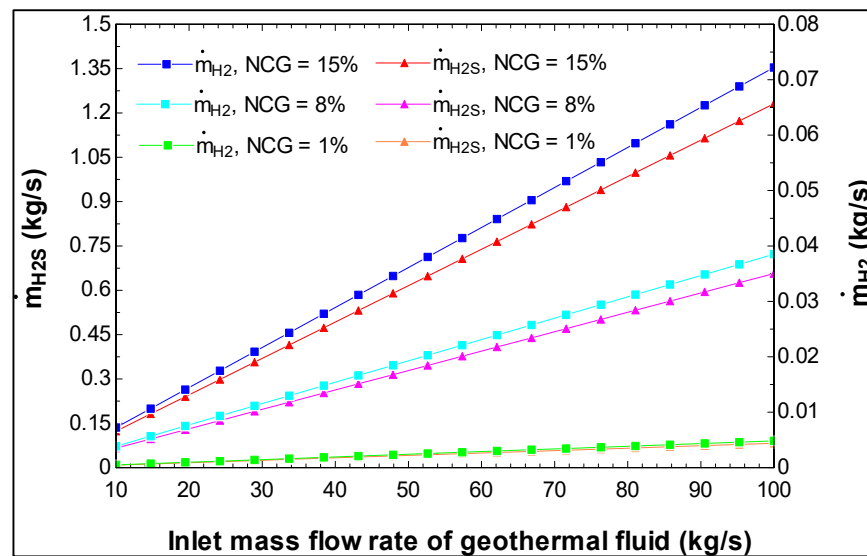
Figure 5.28 Obtained hydrogen sulfide and hydrogen amounts depending on the inlet mass flow rate of geothermal fluid

The required electrical work for the electrolysis process of hydrogen sulfide increases by the enhancement in the mass flow rate of hydrogen sulfide. The required electrical work is approximately 0.272 MW when the mass flow rate of hydrogen sulfide is 0.1 kg/s as shown in Figure 5.29. Also, the required electricity input increases, while the temperature of produced hydrogen rises.
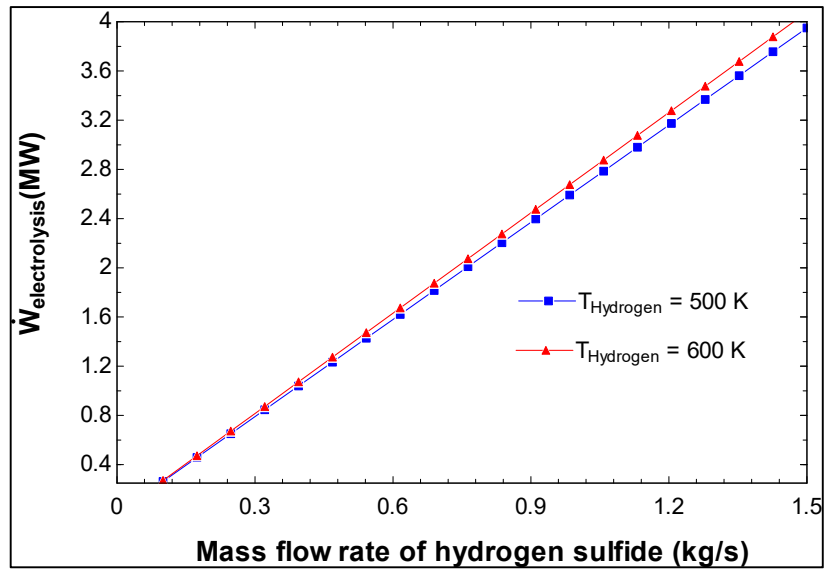
Figure 5.29 Effect of hydrogen sulfide mass flow rate on the required electricity input
for the electrolysis process

The required electrical work of the electrolysis process decreases while inlet temperature of hydrogen sulfide increases. The required electricity input is around 0.81 MW, while inlet temperature of hydrogen sulfide is 421 K as illustrated in Figure 5.30. As the temperature of the sulfur rises, the electricity demand becomes higher.
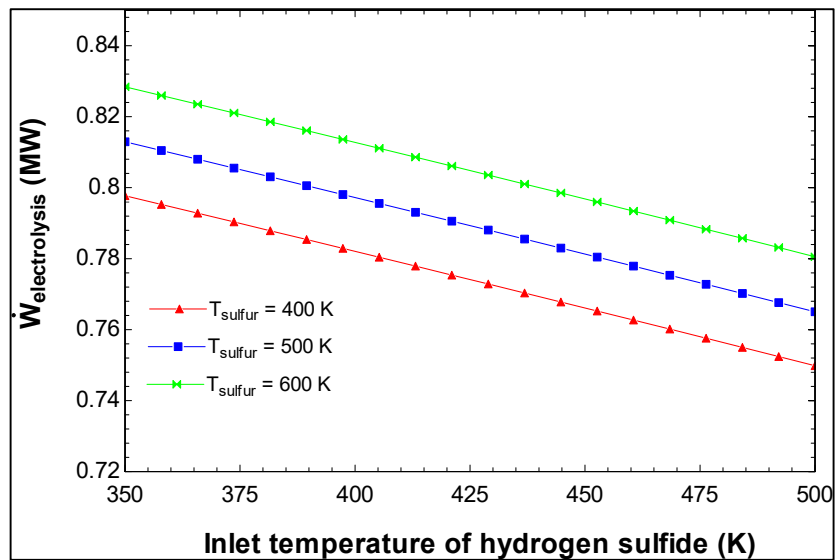

Figure 5.30 Effect of hydrogen sulfide inlet temperature on the required electricity input
for the electrolysis process
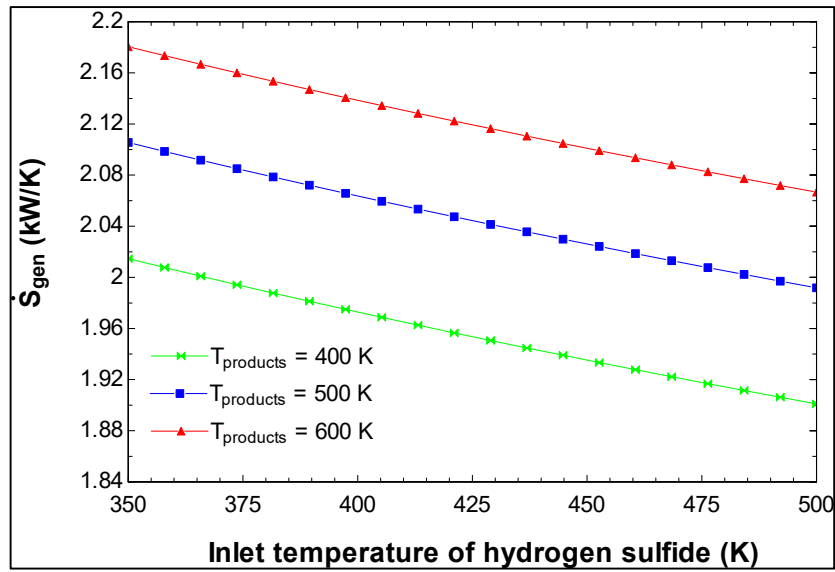
Figure 5.31 Effect of hydrogen sulfide inlet temperature on the entropy generation of electrolysis process

Figure 5.31 illustrates how entropy generation changes depending on the inlet temperature of hydrogen sulfide. It is obvious that, entropy generation has higher values at the lower temperatures of hydrogen sulfide. While inlet temperature of hydogen sulfide rises from 350 K to 500 K, entropy generation rate decreases from 2.015 kW/K to 1.901 kW/K.

In the designed system, hydrogen which is produced through the electrolysis process is sent to the fuel cell system in order to generate power by interacting with incoming oxygen stream. Figure 5.32 presents that how the amount of produced power changes depending on the mass flow rate of hydrogen sulfide. According to the figure, produced power rises from 0.852 MW to 12.79 MW, while the mass flow rate of hydrogen sulfide increases from 0.1 kg/s to 1.5 kg/s.
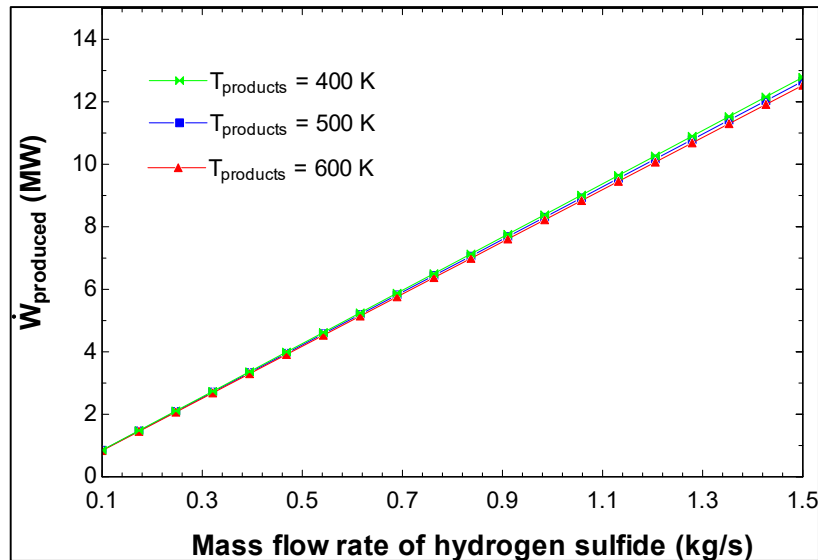
Figure 5.32 The amount of produced electrical power depending on the mass flow rate
of hydrogen sulfide

By considering the all useful outputs and total inputs the overall exergy efficiency of the
designed system can be defined. Figure 5.33 shows the effect of hydrogen sulfide inlet
temperature on the overall exergy efficiency of the designed system which includes an
electrolyzer and a fuel cell system. It can be clearly seen that, overall exergy efficiency
of the designed system rises, while inlet temperature of hydrogen sulfide rises. From the
figure can be inferred that, the overall exergy efficiency is 84.81%, when the inlet
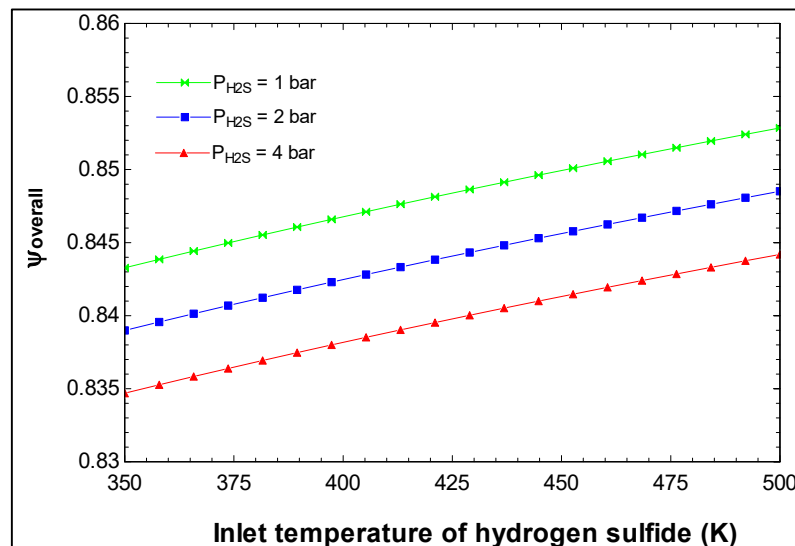temperature of hydrogen sulfide is about 421 K.

Figure 5.33 Effect of hydrogen sulfide inlet temperature on the overall exergy efficiency
of the designed system

Figure 5.34 illustrates how overall exergy efficiency of the designed system changes depending on the ambient temperature. It is clear that, it has a little impact on the overall efficiency. While ambient temperature rises from 280 K to 310 K, the efficiency value changes between 84.92% and 85.37%, by assuming the inlet temperature of hydrogen sulfide as 483 K.
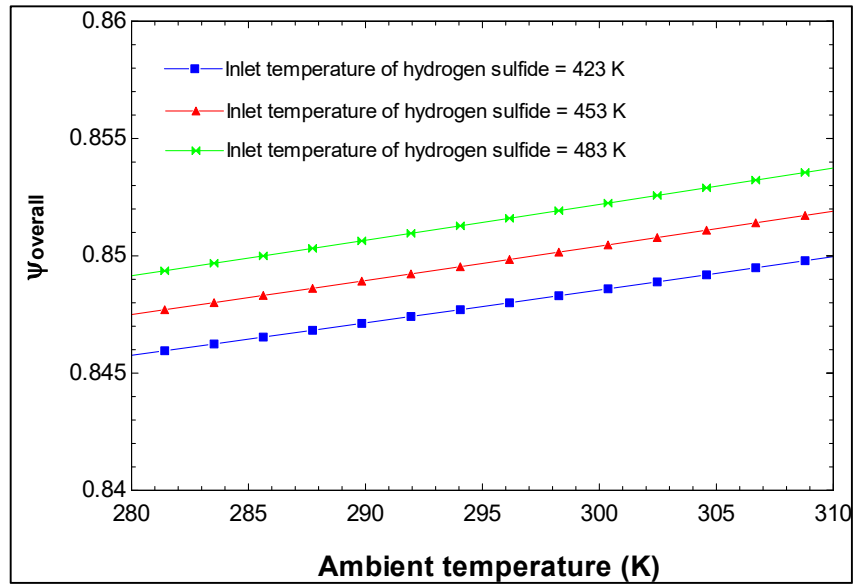

Figure 5.34 Effect of ambient temperature on the overall exergy efficiency of the designed system

Geothermal fluid is present with some percentages of non-condensable gases. In the present study non-condensable gases of the geothermal fluid are assumed as nitrogen, oxygen, methane, carbon dioxide and hydrogen sulfide. As expected, while mole percent of hydrogen sulfide increases among the non-condensable gases, more hydrogen sulfide is emitted and correspondingly more hydrogen can be generated through the electrolysis process as shown in Figure 5.35. While the mole percent of hydrogen sulfide rises from 3% to 21%, the amount of produced hydrogen increases from 26.75 g/s to 156 g/s, considering the inlet mass flow rate of the geothermal fluid as 120 kg/s.
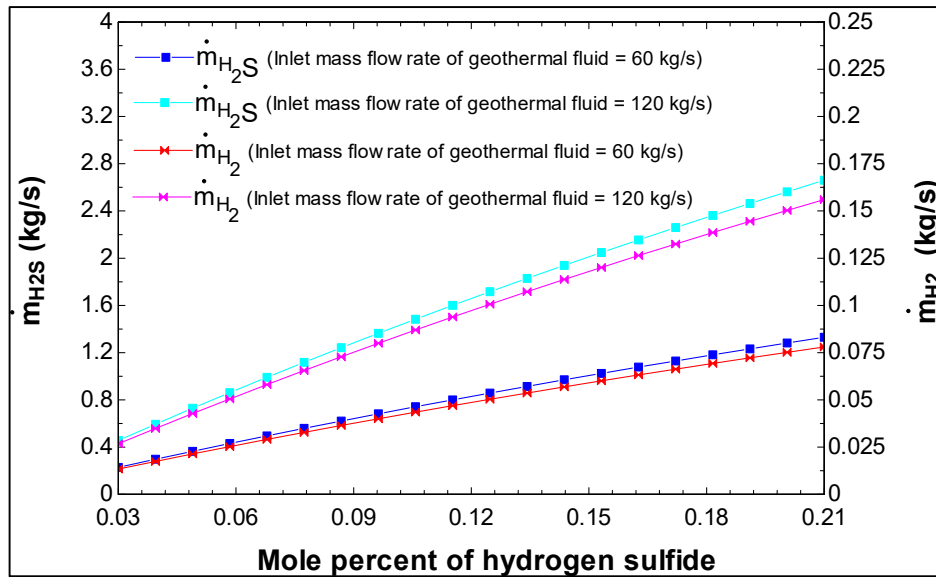
Figure 5.35 Effect of the mole percent of hydrogen sulfide on the amounts of produced
hydrogen sulfide and hydrogen

Thermodynamic properties of all stream points of the designed system are listed in Table
5.11.

Table 5.11 The thermodynamic properties of the designed system

State	$\dot{m}_i$ (kg/s)	P_i (kPa)	T_i (K)	h_i (kJ/kg)	s_i (kJ/kgK)	ex_{ph} (kJ/kg)
1	0.3	200	423	126.6	0.187	71.41
2	0.3	200	423	126.6	0.187	71.41
3	0.2815	200	500	107.1	3.839	25.59
4	0.0176	200	500	6850	58.04	1545
5	0.0176	200	500	6850	58.04	1545
6	0.0176	200	500	6850	58.04	1545
7	0.1408	100	298	-0.4316	0.002138	0
8	0.1584	150	350	321.8	1.038	17.08

5.5   Comparisons of the Proposed Systems

Three different types of renewable based multigeneration energy systems are already
analysed through energy and exergy approaches as well as electrolyzer and fuel cell units.
In this section, the results of each system are presented comparatively. First of all, the
overall energy efficiencies of the proposed systems are presented in Figure 5.36. The
highest energy efficiency value is determined in system 1 during the storing period with
67.95%. In addition, the lowest energy efficiency is observed in system 3 during the

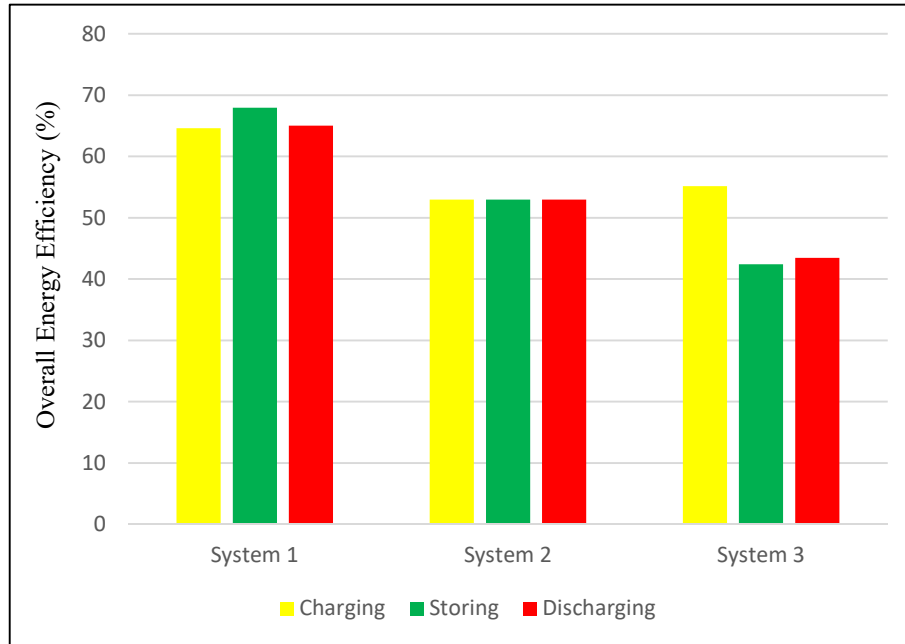storing period with 42.45%. These results are satisfactory for the renewable based systems.

Figure 5.36 Comparison of the overall energy efficiencies of the proposed systems

In Figure 5.37 illustrates the overall exergy efficiencies of the proposed systems. The highest exergy efficiency is calculated for system 1 during the storing period with 60.94% and the lowest efficiency value is determined in system 3 again during the storing period with 20.47%.
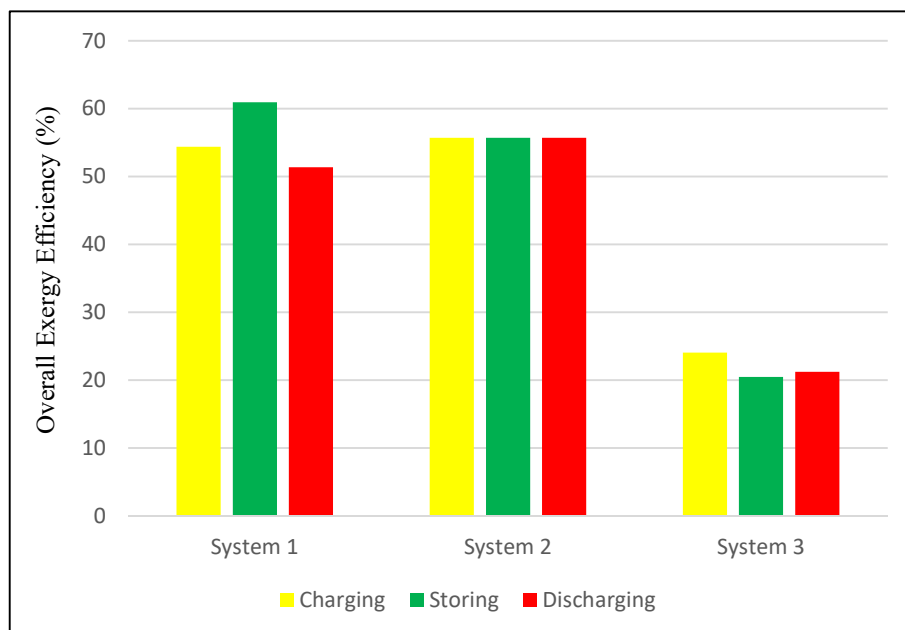

Figure 5.37 Comparison of the overall exergy efficiencies of the proposed systems

Figure 5.38 shows the total amount of produced power in the designed systems. According to the figure, the highest amount of power is produced in system 3 during the discharging period with 59.55 MW and the lowest amount of power is obtained from the system 1 during the discharging period with 14.26 MW.
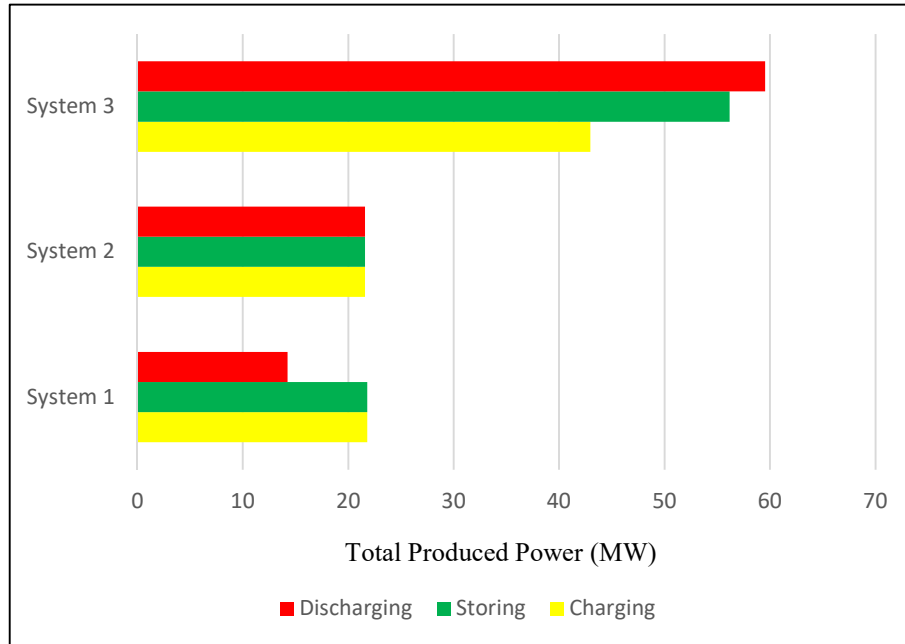

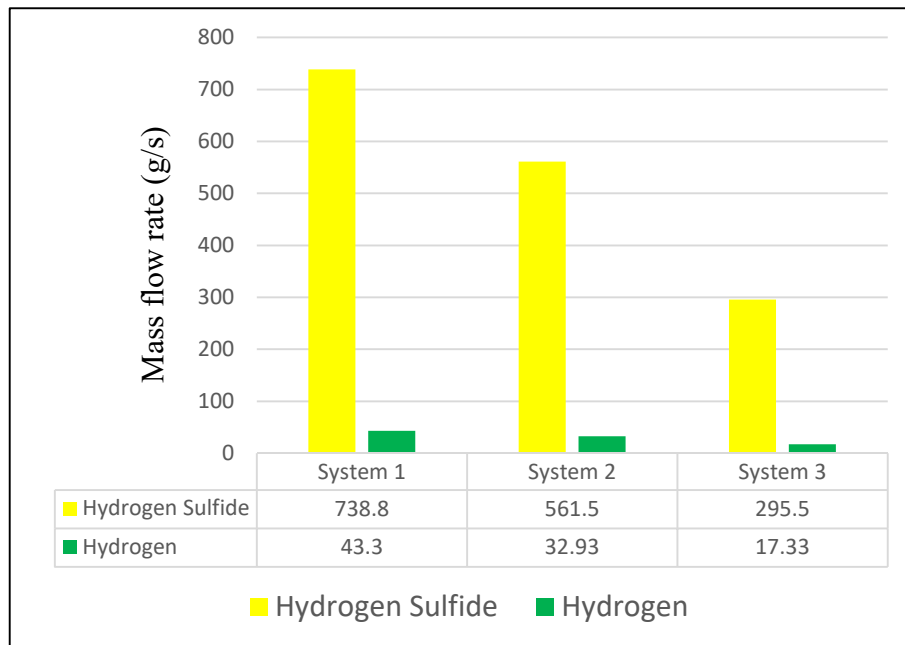Figure 5.38 Comparison of the total amount of produced power in the designed systems

Figure 5.39 Comparison of the obtained hydrogen sulfide and hydrogen amounts in the designed systems

Figure 5.39 shows the obtained amounts of hydrogen sulfide and hydrogen in the designed systems. From system 1, system 2 and system 3; hydrogen sulfide is emitted 738.8 g, 561.5 g and 295.5 g per second, respectively.

5.6 Concluding Remarks

The key findings of each system are summarized as follows.

5.6.1 System 1 Findings

The key findings related to system 1 can be summarized as follows:

- The highest entropy generation rate is determined in the cooling tower with 31.48 kW/K. On the other hand, all devices which are illustrated in Figure 5.1, have entropy generation rates below 1.21 kW/K.

- For the all 3 periods overall energy efficiency of the designed system increases, while the inlet mass flow rate of geothermal steam rises. The highest overall energy efficiency occurs in the storing period with 71.4% while the mass flow rate of the geothermal steam is about 200 kg/s.

- The overall exergy efficiency of the proposed system rises, while the inlet mass flow rate increases. The highest overall exergy efficiency of the system is calculated in the storing period as 71.94%, while the inlet mass flow rate of the geothermal steam is around 200 kg/s.

- The overall exergy efficiency of the integrated system decreases, while ambient temperature rises. In the charging period, the overall exergy efficiency changes between 60.36% and 50.2% when the ambient temperature rises from 273 to 313 K.

- There is a linear relation between the efficiencies and water inlet temperature, such that both energy and exergy efficiency of the PEM electrolyzer increases when the inlet temperature of the water rises. The energy and exergy efficiencies are approximately 82.9% and 83.4%, when inlet temperature of water is around 290 K. Furthermore, as the temperature of the electrolysis process products rises, both energy and exergy efficiency get lower values.

5.6.2 System 2 Findings

The key findings related to system 2 can be summarized as follows:

- The highest entropy generation rate is observed in the cooling tower with 81.13 kW/K.

- Inlet velocity of the wind is a significant criterion for the wind turbine designs. When inlet velocity of the wind gets higher values, the amount of produced electricity rises correspondingly. While inlet velocity of the air to the wind turbine is approximately 7.5 m/s, at around 71.2 kW power output can be obtained, considering the design parameters.

- With the increase in inlet velocity, the energy efficiency of the wind turbine first rises and then decreases after reaching the optimum velocity. The maximum energy efficiency is obtained from the wind turbine, when the outlet velocity of the wind is equal to one-third of the inlet velocity.

- Average hourly solar radiation is also a noteworthy design criterion for the solar assisted multigeneration systems. As expected, while average hourly solar radiation gets higher values, the geothermal steam temperature increases accordingly which provides us to produce more power from the system. While average hourly solar radiation is 2 MJ/m^{2}h, approximately 12.7 MW power is produced by turbine 2.

- As the ambient temperature changes from 273 K to 313 K, the energetic COP stays constant while exergetic COP rises from 0.0034 to 0.1682.

5.6.3 System 3 Findings

The key findings related to system 3 can be summarized as follows:

- There is an exponential relation between the convection heat transfer coefficient and the surface temperature of the charging pipe. While convection heat transfer coefficient has higher values, the surface temperature of the charging pipe increases. In addition, when the charging pipe length increases, the surface temperature of the charging pipe reaches up to 350 K for lower convection transfer coefficients.

- By increasing the packed bed system radius, the final temperature of the rock gets closer to its initial conditions. Therefore, it is important to minimize the radius of the packed bed system as far as possible in order to obtain higher rock temperatures. Additionally, three different kinds of rock are compared with each other. Results show that siltstone is the best option in terms of thermal properties. However, the physical properties and cycle life should be taken into account in the designing process of the system.

- To evaluate the underground cavern performance, heat losses from the underground cavern to the surrounded soil is an effective parameter. It is important to determine how the surrounded soil temperature changes regarding the ambient temperature. It is found that, beyond 2 m soil depth, soil temperature does not change significantly for the daily storage and also after at around 5 m soil depth, it does not change substantially when seasonal storage is considered. Therefore, soil behaves like an insulation material between the ambient and the cavern at higher depths.

- During the storing period, due to the mass and heat transfers from the underground cavern to the surrounded vicinity, the pressure of the compressed air decreases and therefore, air pressure which releases from the underground cavern in the discharging period would have lower values compared to inlet conditions. The energy efficiency of the underground cavern decreases from 70.32% to 67.40%, while outlet pressure of the compressed air changes between 10 MPa and 14.42 MPa.

- The effect of three different types of PCM on the energy and exergy efficiencies of the hot storage tank are examined. $LiNO_3$ exhibits the best performance and energy and exergy efficiencies of the hot storage tank reach to 82% and 84%, respectively, while the temperature of the PCM is 800 K at the end of the charging period.

- Effect of the equivalence ratio on the energy and exergy efficiencies of the gasifier is examined for each period. It is determined that, the optimal value of the equivalence ratio for the designed system is at around 0.32.

- The highest entropy generation rate is determined in the gasifier during the discharging period with 583,5 kW/K. For the most part, the highest and lowest

exergy destruction rates are observed during the discharging and charging periods, respectively.

- The highest and lowest overall energy efficiencies are determined during the charging and storing periods, respectively. While the inlet mass flow rate of biomass rises from 5 kg/s to 30 kg/s, overall energy efficiency of the proposed system for the charging period decreases from 67.04% to 31.81%.

5.6.4 System 4 Findings

The key findings related to the designed system can be summarized as follows:

- While NCG composition gets higher values, obtained hydrogen sulfide and correspondingly hydrogen amounts increase. While inlet mass flow rate of the geothermal fluid is 60 kg/s, 0.7388 kg hydrogen sulfide and 0.0433 kg hydrogen emerge per second for 15% NCG composition.

- The required electrical work for the electrolysis process of hydrogen sulfide increases by the enhancement in the mass flow rate of hydrogen sulfide. The required electrical work is approximately 0.272 MW when the mass flow rate of hydrogen sulfide is 0.1 kg/s.

- The required electrical work of the electrolysis process decreases while the inlet temperature of hydrogen sulfide increases. The required electricity input is around 0.81 MW, while the inlet temperature of hydrogen sulfide is 421 K.

- While inlet temperature of hydrogen sulfide rises from 350 K to 500 K, entropy generation rate decreases from 2.015 kW/K to 1.901 kW/K.

- The overall exergy efficiency of the designed system rises, while the inlet temperature of hydrogen sulfide rises. The overall exergy efficiency is 84.81%, when the inlet temperature of hydrogen sulfide is about 421 K.

- Ambient temperature has a little impact on the overall efficiency of the designed system. While ambient temperature rises from 280 K to 310 K, the efficiency value changes between 84.92% and 85.37%, by assuming the inlet temperature of hydrogen sulfide as 483 K.

5.6.5 Overall Findings

Three different types of renewable based multigeneration energy systems as well as electrolysis process of hydrogen sulfide are analysed and evaluated. Finally, the key findings related to the performed study are indicated in this part of the study. In system 1 geothermal and solar energy resources are utilized. System 2, is benefited from the geothermal and solar energy along with the wind energy. Also in system 3, 4 different types of renewable energy sources are used including geothermal, solar, wind and biomass. All three systems are designed to produce multiple useful commodities such as electricity, heating, cooling, domestic hot water and hydrogen. According to the obtained results, overall energy and exergy efficiencies for the studied systems can be reached up to 67.95% and 60.94%, respectively. These results are higher than of the many previous studies and make attractive to construct such environmentally benign energy systems for the future.

On the other hand, a detailed thermodynamic analysis is conducted related to the electrolysis process of hydrogen sulfide in geothermal power plants. According to the results, by adding the AMIS and electrolyzer units to the geothermal power plants, hydrogen sulfide emissions can be reduced 738.8 g/s, while the inlet mass flow rate of the geothermal fluid is 60 kg/s. In other words, approximately 23.29 kiloton hydrogen sulfide can be converted into hydrogen instead of releasing to the atmosphere, by considering the same inlet mass flow rate of the geothermal fluid. These results show that by applying this new technology in the geothermal power plants, negative effects of hydrogen sulfide on the environment can be abated substantially.

REFERENCES

[1]   Karapekmez, A. and Dincer, I., (2018). "Modelling of Hydrogen Production from Hydrogen Sulfide in Geothermal Power Plants", International Journal of Hydrogen Energy, 43: 10569-10579.

[2]   Al-Ali, M. and Dincer, I., (2014). "Energetic and Exergetic Studies of a Multigenerational Solar-Geothermal System", Applied Thermal Engineering, 71: 16-23.

[3]   Bicer, Y. and Dincer, I., (2016). "Development of a New Solar and Geothermal Based Combined System for Hydrogen Production", Solar Energy, 127: 269-284.

[4]   Akrami, E., Chitsaz, A., Nami, H. and Mahmoudi, S., (2017). "Energetic and Exergoeconomic Assessment of a Multigeneration Energy System Based on Indirect Use of Geothermal Energy", Energy, 124: 625-639.

[5]   Yuksel, Y., Ozturk, M. and Dincer,I., (2018). "Energetic and Exergetic Performance Evaluations of a Geothermal Power Plant Based Integrated System for Hydrogen Production", International Journal of Hydrogen Energy, 43: 78-90.

[6]   Barbour, E., Mignard, D., Ding, Y. and Li, Y., (2015). "Adiabatic Compressed Air Energy Storage with Packed Bed Thermal Energy Storage", Applied Energy, 155: 804-815.

[7]   Houssainy, S., Janbozorgi, M., Ip, P. and Kavehpour, P., (2018). "Thermodynamic Analysis of a High Temperature Hybrid Compressed Air Energy Storage (HTH-CAES) System", Renewable Energy, 115: 1043-1054.

[8]   Zhao, P., Jiangfeng, W. and Dai, Y., (2015). " Thermodynamic Analysis of an Integrated Energy System Based on Compressed Air Energy Storage (CAES) System and Kalina Cycle", Energy Conversion and Management, 98: 161-172.

[9]   Arabkoohsar, A., Machado, L., Farzaneh-Gord, M. and Koury, R.N.N., (2015). "The First and Second Law Analysis of a Grid Connected Photovoltaic Plant Equipped with a Compressed Air Energy Storage Unit", Energy, 87: 520-539.

[10]   Ortega-Fernandez, I., Zavattoni, S.A., Rodriguez-Aseguinolaza, J., D'Aguanno, B. and Barbato, M.C., (2017). "Analysis of an Integrated Packed Bed Thermal Energy Storage System for Heat Recovery in Compressed Air Energy Storage Technology", Applied Energy, 205: 280-293.

[11]   Reverberi, A.P., Klemes, J.J., Varbanov, P.S. and Fabiano, B., (2016). "A Review on Hydrogen Production from Hydrogen Sulphide by Chemical and Photochemical Methods", Journal of Cleaner Production, 136: 72-80.

[12]   Guldal, N.O., Figen, H.E. and Baykara, S.Z., (2017). "Production of Hydrogen from Hydrogen Sulfide with Perovskite Type Catalysts: $LaMO_3$", Chemical Engineering Journal, 313: 1354-1363.

[13]   Zaman, J. and Chakma, A., (1995). "Production of Hydrogen and Sulfur from Hydrogen Sulfide", Fuel Processing Technology, 41(2): 159-198.

[14]   Mbah, J.C., (2008). "Endurance Materials for Hydrogen Sulfide Splitting in Electrolytic Cell", PhD thesis, University of South Florida, USA.

[15]   International Energy Agency (IEA), World Energy Outlook 2016, https://www.iea.org/weo/, 04 September 2018.

[16]   Rand, D.A.J. and Dell, R.M., (2007). Hydrogen Energy: Challenges and Prospects, Royal Society of Chemistry, UK.

[17]   Wikipedia, https://en.wikipedia.org/wiki/Energy_density, 27 May 2017.

[18]   International Energy Agency (IEA), World Energy Outlook 2015, http://dx.doi.org/10.1787/weo-2014-en, 12 April 2018.

[19]   Kyriakopoulos, G.L. and Arabatzis, G., (2016). "Electrical Energy Storage Systems in Electricity Generation: Energy Policies, Innovative Technologies, and Regulatory Regimes", Renewable&Sustainable Energy Reviews, 56: 1044-1067.

[20]   DOE International Energy Storage Database, http://www.energystorageexchange.org/, 14 April 2018.

[21]   Luo, X., Wang, J., Dooner, M. and Clarke, J., (2015). "Overview of Current Development in Electrical Energy Storage Technologies and the Application Potential in Power System Operation", Applied Energy, 137: 511-536.

[22]   Chen, H., Cong, T.N., Yang, W., Tan, C., Li, Y. and Ding,Y., (2009). "Progress in Electrical Energy Storage System", Progress in Natural Science, 19: 291-312.

[23]   Dincer, I. and Zamfirescu, C., (2012). "Renewable Energy-Based Multigeneration Systems", International Journal of Energy Research, 36: 1403-1415.

[24]   Renato, S., Domenico, G., Claudia, T. and Carlo,T., (2017). "Modelling of Hydrogen Sulfide Dispersion From Geothermal Power Plants of Tuscany (Italy) ", Science of the Total Environment, 583: 408-420.

[25]   World Health Organization (WHO), (2003). Hydrogen Sulfide: Human Health Aspects, Concise International Chemical Assessment Document 53, Geneva.

[26]   Chamorro, C., Mondejar, M., Ramos, R. and Villamanan, M., (2012). "World Geothermal Power Production Status: Energy, Environmental and Economic Study of High Enthalpy Technologies", Energy, 42: 10-18.

[27]   Yaws, C., (1999). Chemical Properties Handbook: Physical, Thermodynamic, Environmental, Transport, Safety and Health Related Properties for Organic and Inorganic Chemicals, McGraw-Hill, USA.

[28] Demirel, Y., (2015). Energy: Production, Conversion, Storage, Conservation, and Coupling, Second Edition, Springer, Germany.

[29] Prabir, B., (2010). Biomass Gasification and Pyrolysis : Practical Design, Elsevier, USA.

[30] Baldacci, A., Mannari, M. and Sansone, F., (2005). "Greening of Geothermal Power: An Innovative Technology for Abatement of Hydrogen Sulfphide and Mercury Emission", World Geothermal Congress 2005, 24-29 April 2005, Antalya.

[31] Dincer, I. and Rosen, M., (2013). Exergy: Energy, Environment and Sustainable Development, Second Edition, Elsevier, USA.

[32] Cengel, Y., (1994). Heat Transfer: A Practical Approach, Second Edition, McGraw-Hill, USA.

[33] Eppelbaum, L., Kutasov, I. and Pilchin, A., (2014). Applied Geothermics, Springer, Germany.

[34] Coscia, K., Nelle, S., Elliot, T. and Neti, S., (2013). "Thermophysical Properties of $LiNO_3$- $NaNO_3$- KNO_3 mixtures for use in concentrated solar power", Journal of Solar Energy Engineering, 135.

[35] Ptasinski, K., (2016). Efficiency of Biomass Energy: An Exergy Approach to Biofuels, Power, and Biorefineries, Wiley, USA.

[36] Hosseini, M., Dincer, I. and Rosen, M., (2012). "Steam and Air Fed Biomass Gasification: Comparisons Based on Energy and Exergy", International Journal of Hydrogen Energy, 37: 16446-16452.

[37] Szargut, J., (2005). Exergy Method: Technical and Ecological Applications, WIT Press, UK.

[38] Kreith, F. and Goswami, D.Y., (2018). Handbook of Energy Efficiency and Renewable Energy, Second Edition, CRC Press, USA.

[39] Peralta, O., Castro, T., Duron, M., Salcido, A., Murillo, A., g, Gonzalez, R. and Marquez, C., (2013). "H_2S Emissions from Cerro Prieto Geothermal Power Plant, Mexico, and Air Pollutants Measurements in the Area", International Journal of Geothermal Research and Its Applications, 46: 55-65.

CURRICULUM VITAE

PERSONAL INFORMATION

Name Surname	: Aras KARAPEKMEZ
Date of birth and place	: 22/08/1991 – Beyoglu/Istanbul
Foreign Languages	: English, German
E-mail	: araskarapekmez@hotmail.com

EDUCATION

Degree	Department	University	Date of Graduation
Master	Mechanical Engineering	Yildiz Technical University	2018
Undergraduate	Mechanical Engineering	Yildiz Technical University	2014

PUBLISHMENTS

Papers

1. Karapekmez, A. and Dincer, I., (2018). "Modelling of Hydrogen Production from Hydrogen Sulfide in Geothermal Power Plants", International Journal of Hydrogen Energy, 43: 10569-10579.

Conference Papers

1. Karapekmez, A., Dincer, I. and Javani, N., (2018). "Thermodynamic Study of an Integrated System with Compressed Air and Heat Storage Units", 14th International Conference on Energy Storage, 25-28 April 2018, Adana.
2. Karapekmez, A. and Dincer, I., (2018). "Thermodynamic Analysis of a Novel Solar and Geothermal Based Combined System for Hydrogen Production", 10th International Exergy, Energy and Environment Symposium, 1-4 July 2018, Katowice.